Coherent Radio-over-Fiber Links with Increased Spectral Efficiency

Amir Abbas Sardarzadeh

Thesis submitted to the University of Ottawa
in partial fulfillment of the requirements for the degree of
Master of Applied Science

School of Electrical Engineering and Computer Science
Faculty of Engineering
University of Ottawa

December 2025

Abstract

This thesis advances radio-over-fiber (RoF) links by jointly improving spectral use, phase-noise tolerance, and hardware simplicity. We develop and experimentally validate three complementary architectures, each paired with a tailored digital signal-processing (DSP) algorithm.

First, we propose a cascaded intensity/phase-modulation (IM/PM) coherent RoF architecture in which four independent microwave vector signals are power-multiplexed in pairs, modulated on an optical carrier, and then polarization-multiplexed with an unmodulated optical carrier from the same laser used for modulation. After coherent detection, the DSP algorithm recovers the IM/PM signals, demultiplexes the power-multiplexed pairs, and mitigates polarization rotation, unstable offset frequency, and phase noise, achieving low error-vector magnitude (EVM) at modest received optical powers. This structure leverages both intensity and phase together with power-multiplexing to use the optical spectrum more efficiently and address limitations of prior RoF systems.

Second, we introduce a transmitter based on a dual-drive Mach–Zehnder modulator (DD-MZM) for coherent RoF links that phase-modulates two power-multiplexed signal pairs on a single optical carrier via two RF ports of the modulator. A joint DSP algorithm cancels shared phase noise and unstable offset frequency, enabling independent recovery of digital signals on multi-GHz RF carriers and delivering up to 4× per-carrier spectral efficiency using only one optical wavelength and polarization.

Third, to reduce cost and power by avoiding an external local oscillator, we design a self-coherent, direct-detection RoF link that employs a single-sideband (SSB) pilot as an in-band reference for optical-phase retrieval. The corresponding DSP algorithm cancels AWG-induced phase noise, enabling the simultaneous demodulation of two RF signals. Experiments show constellations with low EVM at sub-milliwatt received powers across representative symbol rates, indicating robustness to dispersion and front-end impairments such as phase noise and in-phase and quadrature (I/Q) imbalances.

Collectively, these results show that power-multiplexing combined with a tailored DSP algorithm yields higher per-carrier spectral efficiency and improved phase-noise tolerance while simplifying hardware, offering a scalable path to compact, low-cost RoF front ends and clear opportunities for future RoF systems.

List of Publications

Published:

[1] **A. A. Sardarzadeh**, P. Li, and J. Yao, "Investigating power multiplexing for coherent microwave photonic links," in *Proc. International Topical Meeting on Microwave Photonics (MWP)*, Pisa, Italy, 2024, pp. 1–4.

Manuscripts (in preparation):

[1] **A. A. Sardarzadeh**, L. Huang, P. Li, and J. Yao, "Power Multiplexing in Coherent Microwave Photonic Links: A Strategy for Data Rate Expansion," *manuscript in preparation* (2025).

[2] **A. A. Sardarzadeh** and J. Yao, "Novel High Spectral Efficiency Microwave Photonic Link Based on Self-Coherent Detection," *manuscript in preparation* (2025).

Acknowledgments

I owe my deepest gratitude to my supervisor, **Professor Jianping Yao**, for his unwavering support, guidance, and patience throughout my master's studies. During a particularly difficult period when I underwent back surgeries, his encouragement and flexibility made it possible for me to continue and complete this work. I am profoundly grateful.

My heartfelt thanks also go to **my parents in Iran**, whose daily emotional support, love, and prayers sustained me across the distance. Their faith in me has been my greatest strength.

Table of Contents

List of Figures

List of Tables

List of Abbreviations

ADC	Analog-to-Digital Converter
AI	Artificial Intelligence
AM	Amplitude modulation
ASE	Amplified Spontaneous Emission
AWG	Arbitrary Waveform Generator
BER	Bit Error Rate
BPF	Band-Pass Filter
CD	Chromatic Dispersion
CW	Continuous Wave
DD-MZM	Dual-drive Mach–Zehnder Modulator
DSO	Digital Storage Oscilloscope
DSP	Digital Signal Processing
EDFA	Erbium-Doped Fiber Amplifier
EVM	Error Vector Magnitude
FEC	Forward Error Correction
FIR	Finite Impulse Response
FWM	Four-Wave Mixing
IM	Intensity Modulation
IM/DD	Intensity-Modulation/Direct-Detection
IM/PM	Intensity/Phase Modulation
I/Q	In-phase/Quadrature
ISI	Intersymbol Interference
KK	Kramers–Kronig

LD	Laser Diode
LO	Local Oscillator
LPF	Low-Pass Filter
ML	Machine Learning
MZM	Mach–Zehnder Modulator
OBPF	Optical Band-Pass Filter
PC	Polarization Controller
PBC	Polarization Beam Combiner
PD	Photodiode
PDM	Polarization-Division Multiplexing
PDL	Polarization-Dependent Loss
PM	Phase Modulation
QAM	Quadrature Amplitude Modulation
QPSK	Quadrature Phase-Shift Keying
RF	Radio Frequency
RoF	Radio-over-Fiber
SBS	Stimulated Brillouin Scattering
SIC	Successive Interference Cancellation
SMF	Single-Mode Fiber
SNR	Signal-to-Noise Ratio
SPM	Self-Phase Modulation
SRS	Stimulated Raman Scattering
SSB	Single-Sideband
SVR	Support Vector Regression
WDM	Wavelength-Division Multiplexing

Chapter 1 Introduction

1.1 Background and Motivation

The evolution of communication systems has been driven by a persistent push for higher data rates, greater capacity, and improved efficiency [1],[2]. From early telegraphy and telephony to today's high-speed digital networks, rising traffic demand, combined with advances in modulation, coding, and networking, has propelled this progression [1],[2]. A decisive inflection point occurred in the 1970s with the advent of optical-fiber communication, which enabled orders-of-magnitude increases in bandwidth and low-loss transmission, fundamentally reshaping the global telecommunications infrastructure [3],[4].

Optical-fiber communication transmits information by modulating data on light and guiding it through low-loss glass or plastic fibers [1],[2]. The theoretical foundations were articulated in 1966 by Kao and Hockham, who quantified the loss requirements and feasibility of dielectric-fiber waveguides for long-distance links [5]. Practical deployment became viable after the 1970 demonstration of low-loss silica fibers at Corning and the emergence of reliable semiconductor light sources capable of continuous operation at (or near) room temperature [1],[2]. These breakthroughs enabled the first field trials and early commercial systems in the late 1970s, typically around the digital signal 3's rate (~45 Mb/s) over spans on the order of 10 km without repeaters [3],[6].

The subsequent decades witnessed remarkable advancements in optical communication technology. The development of single-mode fibers [6], erbium-doped fiber amplifiers (EDFAs) [7], wavelength division multiplexing (WDM) [8], and coherent detection techniques have progressively increased the capacity and reach of optical networks [9]. Modern optical communication systems can transmit data at rates exceeding 100 Tbps over transoceanic distances [10], while research demonstrations approach the petabit scale [11],[12].

Within this broader context, radio-over-fiber (RoF) has matured as a key microwave-photonics technique that transports radio frequency (RF) signals over optical fiber, combining fiber's low loss and vast bandwidth with the flexibility of wireless access. Foundational reviews highlight RoF's benefits for broadband access and its role in 5G and beyond [13]-[15].

Early RoF deployments largely used intensity modulation with direct detection (IM/DD) for cost and simplicity, but IM/DD suffers dispersion-induced power fading and limited spectral efficiency over practical fiber distances [13],[16]. Single-sideband (SSB) optical modulation is a well-established mitigation that suppresses chromatic-dispersion fading and improves spectral use [16],[17]. Capacity scaling has also been achieved by multiplexing across wavelengths and polarization [18],[19].

A major step-change came with coherent RoF links, which recover amplitude and phase, enabling high-order formats and substantially better sensitivity than IM/DD. Experiments report ~20 dB receiver-sensitivity improvements for coherent microwave-photonics/RoF links over comparable IM/DD baselines, along with DSP methods that manage laser phase noise [3],[20],[21].

Despite its advantages, coherent detection in RoF systems presents significant challenges. The phase noise and frequency instability originating from the transmitter and local oscillator (LO) lasers pose a significant challenge. The system is highly sensitive to these phase fluctuations, leading to a severe degradation in performance that is particularly acute for higher-order modulation schemes. Additionally, traditional coherent detection systems require complex optical front-ends with components such as optical hybrids and balanced photodetectors, leading to increased cost, size, and power consumption [22],[23].

The complexity and cost associated with coherent detection have motivated research into alternative approaches that can achieve high spectral efficiency while maintaining system simplicity. One promising direction is the development of digital signal processing (DSP) techniques to mitigate phase noise and enhance system performance. As demonstrated by Chen et al., "The phase noise which is introduced by both the transmitter and LO laser sources can be, in principle, completely eliminated by summing the squared magnitudes of the in-phase and quadrature (I/Q) components from the coherent receiver" [24]. This DSP-based approach to phase noise cancellation represents a significant advancement in making coherent detection more practical for RoF applications [24]-[30].

One remaining innovative approach to enhancing spectral efficiency in RoF systems is power multiplexing [31],[32], which enables the transmission of multiple signals at different power levels on the same optical and RF carrier. This technique, inspired by the non-orthogonal multiple access (NOMA) principle used in wireless communications, offers a promising pathway to increase data capacity and the number of users without requiring additional optical wavelengths or polarization states. While prior studies have demonstrated the feasibility of integrating power multiplexing within IM/DD configurations [33]-[35], efforts to coherently detect NOMA signals represent a novel avenue for future research.

More recently, self-coherent detection has emerged as an alternative approach that combines the advantages of coherent detection with the simplicity of direct detection [36],[37]. In self-coherent systems, a pilot carrier or tone derived from the same laser source as the data-carrying signal is transmitted along with the modulated signals [38]-[44]. This pilot carrier serves as a self-reference at the receiver, enabling the recovery of both amplitude and phase information without requiring a separate local oscillator. This approach, which can simplify receiver design by using a single polarization state for both the pilot carrier and data signals, offers a promising balance between spectral efficiency and system complexity.

The convergence of these advanced techniques, coherent detection, digital signal processing, power multiplexing, and self-coherent detection, presents exciting opportunities for the development of high-capacity, spectrally efficient RoF systems. However, realizing the full potential of these approaches requires addressing several key challenges, including phase noise mitigation, reducing system complexity, ensuring cost-effectiveness, and employing DSP methods to recover signals. These challenges serve as the motivation for this thesis research, which aims to develop novel techniques for enhancing the spectral efficiency of coherent RoF links while addressing practical implementation considerations.

The relentless demand for higher data rates in both wireless and optical communication systems necessitates continuous innovation in microwave photonic (MWP) technologies. As wireless networks evolve toward 5G and beyond, the backhaul and fronthaul infrastructure must support unprecedented data capacities with high reliability and low latency. Coherent RoF links with enhanced spectral efficiency offer a promising solution to these challenges, potentially enabling the seamless integration of optical and wireless networks in future communication systems. This thesis contributes to this important field by proposing and demonstrating novel approaches to increase the spectral efficiency of coherent RoF links through power multiplexing and self-coherent detection techniques.

1.2 Problem Statement and Thesis Objectives

Problem Statement: Despite the significant advancements in optical communication technologies, RoF systems face critical challenges that limit their widespread deployment in next-generation communication networks [13]-[15]. The primary challenge is achieving high spectral efficiency while maintaining system simplicity, reliability, and cost-effectiveness [13]. This challenge becomes increasingly important as the demand for bandwidth-intensive applications continues to grow exponentially, particularly with the emergence of 5G and beyond wireless networks [13],[14].

As indicated before, traditional RoF systems based on IM/DD offer simplicity and low cost but suffer from limited spectral efficiency [9],[13]. These systems can only detect the intensity of the optical signals, which restricts the use of advanced modulation formats that leverage both amplitude and phase dimensions [29]. Additionally, IM/DD systems are susceptible to chromatic dispersion-induced power fading, which further limits their transmission performance over longer distances [16],[17].

Coherent detection has emerged as a promising solution to enhance spectral efficiency in RoF systems by enabling the recovery of both amplitude and phase information by employing a LO at the receiver [21] and using polarization diversity as a way to increase spectral efficiency. However, conventional coherent detection approaches without a DSP unit introduce several significant challenges:

1. Phase noise sensitivity: A primary limitation is the system's vulnerability to phase instability. This issue, which includes combined phase noise and frequency drift from the transmitter and LO lasers, can severely compromise performance [24].

2. System complexity and cost: The reliance of traditional coherent detection on complex hardware, like 90° optical hybrids and balanced photodetectors, drives up the system's size, cost, and power draw. This complexity ultimately limits its practicality and appeal for real-world applications.[29].

3. Local oscillator requirements: The need for a separate local oscillator at the receiver adds complexity, cost, and stability challenges [9].

These challenges highlight the need for innovative approaches that can achieve high spectral efficiency in RoF systems while addressing the limitations of both IM/DD and conventional coherent detection techniques. Specifically, there is a critical need for:

1. Effective methods, such as digital signal processing techniques or hardware-based solutions, to mitigate phase noise in coherent detection systems [20],[21].

2. Advanced modulation and multiplexing techniques, such as power multiplexing and self-coherent detection, to increase spectral efficiency without significantly increasing system complexity [33]-[35],[46].

3. Approaches that can leverage both amplitude, phase, polarization, and power dimensions as degrees of freedom for signal transmission [28].

4. Solutions that simplify the system and reduce costs by eliminating the need for a separate local oscillator at the receiver [36]-[40].

Addressing these challenges requires a multifaceted approach that combines advanced modulation techniques, innovative multiplexing strategies, and sophisticated digital signal processing algorithms. This thesis aims to contribute to this important field by proposing and demonstrating novel approaches to increase the spectral efficiency of coherent RoF links while maintaining practical implementation considerations.

Thesis Objectives: The primary objective of this thesis is to develop and demonstrate novel techniques for increasing the spectral efficiency of coherent RoF links. Specifically, this research focuses on three key contributions:

1. Intensity-Phase Modulation with Power Multiplexing: To develop a coherent RoF link that employs power multiplexing with both intensity and phase modulation, incorporating a digital phase noise cancellation technique. This approach aims to increase data capacity by transmitting multiple signals at different power levels on the same optical and RF carrier, while effectively mitigating phase noise through digital signal processing.

2. Dual-drive Mach-Zehnder Modulator (DD-MZM) architecture-based RoF link with Power Multiplexing: To design and implement a RoF link employing power multiplexing using a DD-MZM to quadruple data rate on a single RF carrier. This objective involves leveraging the DD-MZM's dual-drive capability to modulate two independent pairs of power-multiplexed signals on one polarization state, along with developing a DSP algorithm to cancel joint phase noise from free-running lasers and unstable frequency offsets.

3. Self-Coherent Detection: To demonstrate a self-coherent RoF link that eliminates the need for a local oscillator while maintaining high spectral efficiency. This objective involves modulating a single-sideband (SSB) pilot tone and multiple microwave vector signals onto a single RF carrier using a DD-MZM, and developing a DSP algorithm to recover the transmitted signals while canceling phase noise from the laser and arbitrary waveform generator.

To achieve these objectives, the thesis addresses the following specific goals:

1.Design and implement experimental setups for each of the three proposed approaches, including appropriate optical and electrical components, modulation schemes, and detection techniques.

2.Develop and optimize digital signal processing algorithms for phase noise cancellation, signal recovery, and power demultiplexing in each of the proposed systems.

3.Experimentally evaluate the performance of each approach in terms of key metrics such as error vector magnitude (EVM), bit error rate (BER), and spectral efficiency at various optical power levels and transmission distances.

4.Compare the proposed approaches with traditional coherent detection and direct detection systems in terms of performance, complexity, and cost-effectiveness.

5.Identify the advantages, limitations, and potential applications of each approach, providing insights for future research and development in the field of high spectral efficiency RoF systems.

Through these objectives, this thesis aims to advance in microwave photonic technologies by integrating novel modulation architectures, power multiplexing techniques, and robust DSP algorithms. The proposed frameworks are expected to enhance spectral efficiency, scalability, cost-effectiveness, and simplicity, addressing critical needs for 5G and future high-capacity communication networks.

The research presented in this thesis is particularly relevant in the context of the growing demand for high-capacity, high-speed communication systems. By developing techniques that increase spectral efficiency while maintaining practical implementation considerations, this work contributes to the broader goal of enabling seamless integration of optical and wireless networks in future communication infrastructures.

1.3 Outline of the Thesis

This thesis is organized into five chapters that systematically present the research on coherent RoF links with increased spectral efficiency. Each chapter builds upon the previous ones to provide a comprehensive exploration of the proposed techniques, their theoretical foundations, experimental implementations, and performance evaluations. The following outline provides an overview of the content and structure of the thesis:

- **Chapter 1: Introduction**

The current chapter introduces the research context, motivation, and objectives of the thesis. It provides a historical perspective on optical communication systems and RoF technology, highlighting the importance of spectral efficiency in modern communication networks. The chapter presents the key challenges in existing RoF systems and articulates the specific objectives of the thesis research, setting the stage for the subsequent chapters.

- **Chapter 2: Theoretical Overview**

Chapter 2 establishes the theoretical foundation for the research presented in this thesis. It begins with an explanation of the fundamental principles of RoF systems, including signal generation, modulation, transmission, and detection. The chapter then delves into coherent detection principles, exploring the theoretical advantages and challenges of coherent detection in RoF applications. Various multiplexing techniques for enhancing spectral efficiency are discussed, with particular emphasis on power multiplexing and polarization multiplexing. The chapter concludes with an overview of relevant mathematical tools and signal processing techniques that are essential for understanding the proposed approaches.

- **Chapter 3: Power Multiplexing in Coherent Microwave Photonic Links**

Chapter 3 presents the first major contribution of the thesis: power multiplexing in coherent MWP links. The chapter introduces the concept of power multiplexing in coherent detection and explains how it can be leveraged to increase data capacity without requiring additional optical wavelengths. Two system architectures are presented and analyzed in detail:

First, a system architecture based on intensity-modulation and phase-modulation (IM/PM) is described, including its architecture, operational principles, and digital signal processing algorithm. Experimental results demonstrating the transmission of four power-multiplexed vector signals (two 16QAM and two QPSK) at a carrier frequency of 5 GHz are presented and discussed.

Second, a system architecture using a dual-drive Mach-Zehnder modulator (DD-MZM) is introduced, highlighting its advantages in terms of implementation simplicity and performance. The chapter details the experimental setup, DSP algorithm, and performance evaluation of this approach, demonstrating its capability up to 4× per-carrier spectral efficiency. The chapter concludes with a summary of the key findings and a comparison of the two power multiplexing approaches.

- **Chapter 4: Self-Coherent Detection for High Spectral Efficiency RoF Links**

Chapter 4 focuses on the second major contribution of the thesis: self-coherent detection for high spectral efficiency RoF links. The chapter begins with an overview of self-coherent detection principles and a survey of various self-coherent detection approaches, including Stokes Vector Receivers and Kramers-Kronig (KK) detection methods.

The proposed DD-MZM-based self-coherent detection system is then presented in detail, including its architecture, operational principles, and advantages over traditional coherent detection systems. The chapter explains how the system modulates two independent microwave vector signals along with a single-sideband pilot carrier on a single RF and optical carrier, enabling direct detection at the receiver while maintaining high spectral efficiency.

The DSP algorithms for signal recovery and phase noise cancellation are described, followed by a comprehensive presentation of experimental results. The system's performance is evaluated in terms of EVM, BER, and constellation quality at various optical power levels. The chapter concludes with a discussion of the advantages and potential applications of the proposed self-coherent detection approach.

- **Chapter 5: Conclusion and Future Work:**

The final chapter summarizes the key contributions and findings of the thesis, highlighting how the proposed approaches address the challenges identified in the introduction. The research contributions are contextualized within the broader field of MWP technologies and their potential impact on future communication systems is discussed.

The chapter also acknowledges the limitations and challenges encountered during the research, including phase noise issues and phase coherency. These limitations are analyzed to provide insights for future improvements and research directions.

Finally, the chapter outlines promising avenues for future research, including the potential application of machine learning techniques in communication systems to further enhance performance, adaptability, and robustness of coherent RoF links.

Chapter 2 Theoretical Overview

2.1 Fundamentals of Radio-over-Fiber Systems

RoF technology represents a convergence of wireless and optical communication systems, where RF signals are transmitted over optical fiber links. This integration leverages the complementary strengths of both domains: the mobility and flexibility of wireless communications and the high bandwidth, low loss, and immunity to electromagnetic interference of optical fiber transmission. As wireless networks evolve toward higher data rates and increased coverage, RoF systems have emerged as a promising solution for the distribution of RF signals in various applications, including cellular networks, broadband wireless access, and radar systems [47]-[50].

2.1.1 Basic Principles and Architecture

The fundamental principle of RoF technology involves the modulation of RF signals on optical carrier for transmission over optical fiber and their subsequent reconversion to RF signals at the receiver. A typical RoF system consists of three main components: a central station, optical fiber links, and multiple remote antenna units [13],[51].

The central station houses the equipment for signal generation, processing, and control. It typically includes RF signal generators, optical transmitters (lasers), and optical modulators. The optical fiber links serve as the transmission medium, connecting the central station to the remote antenna units. These links can span distances ranging from a few meters to several hundred kilometers, depending on the application requirements. The RAUs are responsible for the optical-to-electrical conversion and wireless transmission of RF signals. They include photodetectors, RF amplifiers, antennas, and signal processing units like filters [48].

This architecture offers several advantages over traditional RF distribution systems. By centralizing the complex and expensive signal processing equipment at the central station, the remote antenna units can be simplified, resulting in reduced cost, size, and power consumption. This centralization also facilitates the implementation of advanced signal processing techniques, such as beamforming and MIMO (Multiple-Input Multiple-Output), which can enhance the performance of the wireless network [14],[35].

2.1.2 Signal Generation and Modulation Techniques

In RoF systems, the generation and modulation of optical signals carrying RF information can be achieved through various techniques, each with its own advantages and limitations. The choice of techniques depends on factors such as the required bandwidth, transmission distance, and system complexity or cost [48],[51].

Direct Modulation: Direct modulation is the simplest approach, where the RF signal directly modulates the intensity of the light emitted by a semiconductor laser. The laser's bias current is varied according to the RF signal, resulting in corresponding variations in the optical output power. This technique is cost-effective and straightforward to implement, but suffers from limitations in bandwidth and transmission distance due to frequency chirp (unwanted frequency modulation) and dispersion effects [13],[14].

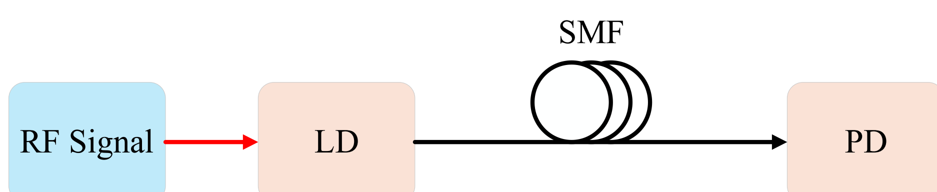

Fig 2.1 An RoF link with direct modulation [14].

External Modulation: External modulation addresses the limitations of direct modulation by using a continuous-wave (CW) laser as the light source and an external modulator to impose the RF signal onto the optical carrier [52]-[54]. The most used external modulators in RoF systems are Phase modulators (PM), intensity modulators (IM), and Polarization modulators [52],[53].

Phase Modulation (PM): The phase of the optical carrier is modulated in accordance with the RF signal, while the amplitude remains constant. PM is achieved by changing the refractive index of the fiber by applying an electrical voltage to it, like the RF signal [54],[55]. Since direct detection can't detect the phase change, and only detects the intensity of light [56], for phase modulation, we need another type of receiver, like coherent detectors, as shown in Figs. 2.2 and 2.3, which will be explained later in detail.

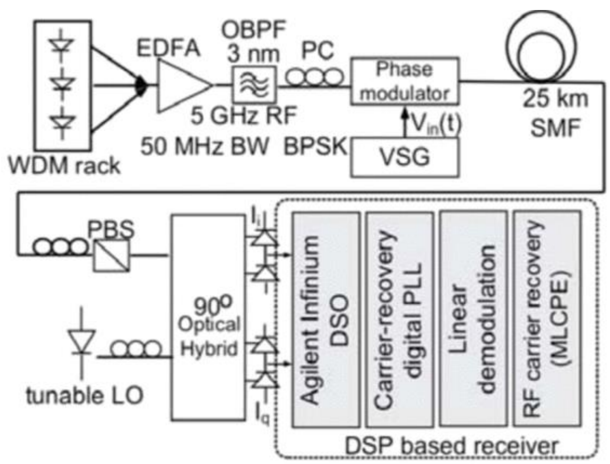

Fig 2.2 The experimental setup for a phase-modulated RoF link. DSO: digital storage oscilloscope, EDFA: Erbium-doped fiber amplifier, LO: local oscillator, OBPF: optical band-pass filter, PBS: polarization beam splitter, PC: polarization controller, SMF: single-mode fiber, VSG: vector signal generator, WDM: wavelength division multiplexing **[57]**.

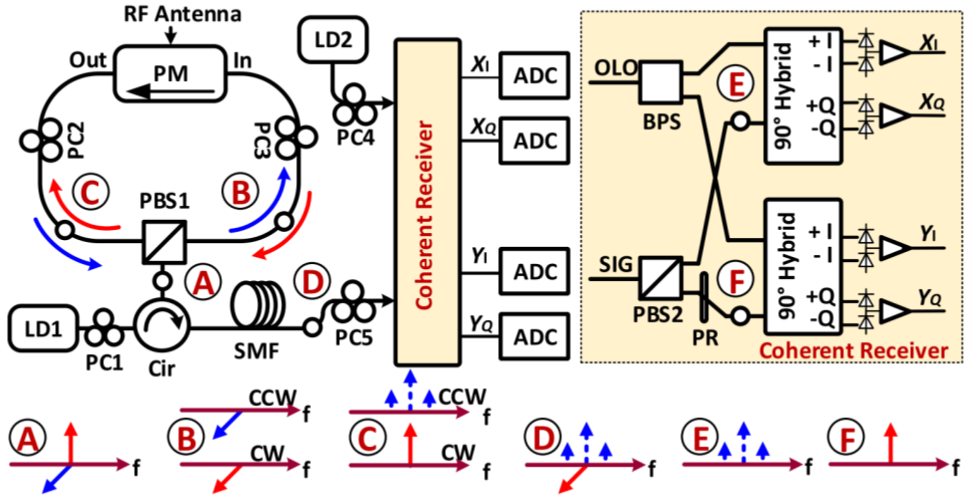

Fig 2.3 The architecture of the polarization and phase diversity coherent receiver. LD: laser diode, Cir: circulator, PM: phase modulator, PBS: beam power splitter, PR: polarization rotator; DSP, digital signal processor; SIG, signal; LO: local oscillator **[58]**.

For Intensity modulation shown in Fig. 2.4, Mach-Zehnder modulators (MZMs) are utilized, which operate based on the principle of interference between two optical paths, or in other words, two PMs. The incoming light is split into two paths, and an electric field (corresponding to the RF signal) is applied to one or both paths, inducing a phase shift. When the two paths recombine, the phase difference results in intensity modulation of the output light [52],[53]. The transfer function of an MZM can be expressed as [59]:

$$E_{out}(t) = E_{in}(t) \cdot cos\left[\pi \frac{V(t)}{2V_{\pi}}\right] \tag{2-1}$$

where $E_{out}(t)$ is the output optical field, $E_{in}(t)$ is the input optical field, $V(t)$ is the applied voltage (RF signal), and V_{π} is the half-wave voltage of the modulator.

Electroabsorption modulators exploit the Franz-Keldysh effect or the quantum-confined Stark effect, where the application of an electric field changes the absorption coefficient of a semiconductor material. The RF signal modulates the absorption of the material, resulting in intensity modulation of the transmitted light. EAMs offer advantages such as compact size, low power consumption, and potential for integration with semiconductor lasers [60]-[63].

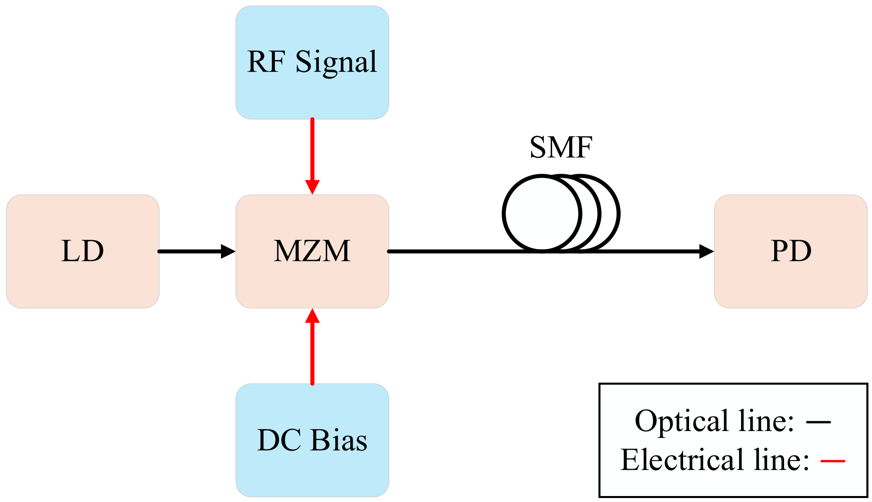

Fig 2.4 An RoF link with external modulation.

2.1.3 Transmission Characteristics and Impairments

The transmission of RF signals over optical fiber in RoF systems is subject to various impairments that can degrade the quality of the received signal. Understanding these impairments is crucial for designing robust and high-performance RoF systems [3],[25].

Fiber Attenuation: ptical fiber attenuation refers to the reduction in optical power as the signal propagates through the fiber. It is primarily caused by absorption and scattering mechanisms within the fiber material. The attenuation coefficient (α) is typically expressed in dB/km and varies with wavelength. For standard single-mode fiber (SMF), the attenuation is approximately 0.2 dB/km at 1550 nm, which is the preferred wavelength for long-distance transmission due to its low attenuation [3],[4]. The optical power after propagation through a fiber of length L can be calculated as:

$$P_{out} = P_{in} \cdot 10^{\left(-\frac{\alpha L}{10}\right)} \tag{2-2}$$

where P_{out} is the output optical power, P_{in} is the input optical power, α is the attenuation coefficient in dB/km, and L is the fiber length in km.

Chromatic Dispersion (CD): Chromatic dispersion is a phenomenon where different wavelength components of the optical signal travel at different velocities, leading to pulse broadening and intersymbol interference (ISI). In intensity-modulated RoF systems, chromatic dispersion can cause power fading, severely limiting the system's bandwidth and transmission distance [16],[17].

The dispersion-induced power fading can be characterized by the following expression:

$$H(f) = cos^2\left(\pi \frac{LD\lambda^2 f^2}{c}\right) \tag{2-3}$$

where $H(f)$ is the power transfer function, L is the fiber length, D is the dispersion parameter, λ is the wavelength, f is the RF frequency, and c is the speed of light.

Polarization Mode Dispersion (PMD): Polarization mode dispersion arises from the birefringence of optical fibers, where the two orthogonal polarization components of the optical signal travel at different velocities. This differential group delay can lead to pulse broadening and signal distortion, particularly in high-bit-rate systems and coherent detection schemes [64]-[66].

Nonlinear Effects: At high optical power levels, nonlinear effects in the fiber can become significant, introducing additional impairments. These effects include [67]-[72]:

1) Self-Phase Modulation: The intensity-dependent refractive index of the fiber causes the optical signal to modulate its own phase, leading to spectral broadening [67],[72].

2) Cross-Phase Modulation (XPM): In wavelength-division multiplexed (WDM) systems, the intensity variations of one channel can modulate the phase of other channels [67][67],[69].

3) Four-Wave Mixing (FWM): The interaction of multiple wavelength components generates new wavelength components, causing crosstalk and power depletion [68],[73].

4) Stimulated Brillouin Scattering (SBS) and **Stimulated Raman Scattering (SRS)**: These scattering processes can transfer power from the signal to other wavelengths, limiting the maximum optical power that can be launched into the fiber [70],[71].

Noise Sources: Various noise sources contribute to the degradation of the signal-to-noise ratio (SNR) in RoF systems [74],[75]:

1) Relative Intensity Noise: Fluctuations in the laser's output power, typically characterized by the RIN parameter in dB/Hz [76].

2) Shot Noise: Quantum noise arising from the discrete nature of photons and electrons, proportional to the photocurrent [75].

3) Thermal Noise: Electronic noise generated by the random thermal motion of charge carriers in the receiver circuitry [15].

4) Amplified Spontaneous Emission (ASE) Noise: In systems employing optical amplifiers, ASE noise is introduced by the amplification process [77].

5) Phase noise: Random fluctuations of the optical and electrical carrier phase originating from the transmitter laser, the LO laser, and any RF synthesizers used for up and downconversion. In coherent RoF, the detected phase is the difference between the phase noise and LO phases; for independent Lorentzian lasers, the effective (beat) linewidth is the sum [78]-[80]:

$$\Delta\varphi = \varphi_s - \varphi_{LO}$$
$$\Delta\omega = \omega_s - \omega_{LO} \tag{2-4}$$

where $\Delta\varphi$ is the phase noise seen at the coherent receiver, and $\Delta\omega$ is the unstable offset frequency between the transmitter laser and the LO, which is also translated to a microwave signal. We will explain ways to mitigate the phase noise later [24],[81].

2.1.4 Direct Detection vs. Coherent Detection Approaches

RoF systems can employ different detection techniques at the receiver to convert the optical signal back to the RF domain. The two main approaches are direct detection and coherent detection, each with its own characteristics and applications [13],[14],[82], and three other ways to detect signals.

1) Direct Detection: Direct detection is the simplest and most widely used approach in RoF systems. In this scheme, a photodetector (typically a PIN photodiode or an avalanche photodiode) directly converts the optical power into an electrical current proportional to the incident power. The photocurrent is given by [75]:

$$I_{ph}(t) \ = \ R \ . \ P(t) = R \ . \ \left|E(t)\right|^2 \tag{2-5}$$

where $I_{ph}(t)$ is the photocurrent, R is the responsivity of the photodetector, and $P(t)$ is the optical power.

Direct detection is well-suited for capturing the intensity information of optical signals, but it cannot recover phase information. It offers advantages such as simplicity, low cost, and robustness, but suffers from limited sensitivity and susceptibility to dispersion-induced power fading [16],[75]

2) Coherent Detection: Coherent detection involves mixing the received optical signal with a LO laser before photodetection. This process enables the recovery of both amplitude and phase information, allowing for more advanced modulation formats and improved receiver sensitivity [3],[28]-[30],[83].

In a coherent receiver shown in Fig. 2.5, the photocurrent is proportional to the product of the electric fields of the received signal and the local oscillator. To be able to calculate the photocurrent, we first need to know the electrical fields at the output of the 90º optical hybrid [81]:

$$\begin{bmatrix} E_a(t) & E_b(t) & E_c(t) & E_d(t) \end{bmatrix} = \begin{bmatrix} E_s(t) & E_{LO}(t) \end{bmatrix} \begin{bmatrix} 1 & 1 & 1 & 1 \\ 1 & e^{j\pi} & e^{j\frac{\pi}{2}} & e^{-j\frac{\pi}{2}} \end{bmatrix} \tag{2-6}$$

where $E_s(t)$ is the electric field of the received signal, and $E_{LO}(t)$ is the electric field of the local oscillator. The photocurrents obtained after balanced photodetectors are:

$$\begin{aligned} X_I(t) &= \frac{1}{2} R\left[E_a(t)E_a^*(t) - E_b(t)E_b^*(t)\right] \\ X_Q(t) &= \frac{1}{2} R\left[E_c(t)E_c^*(t) - E_d(t)E_d^*(t)\right] \end{aligned} \tag{2-7}$$

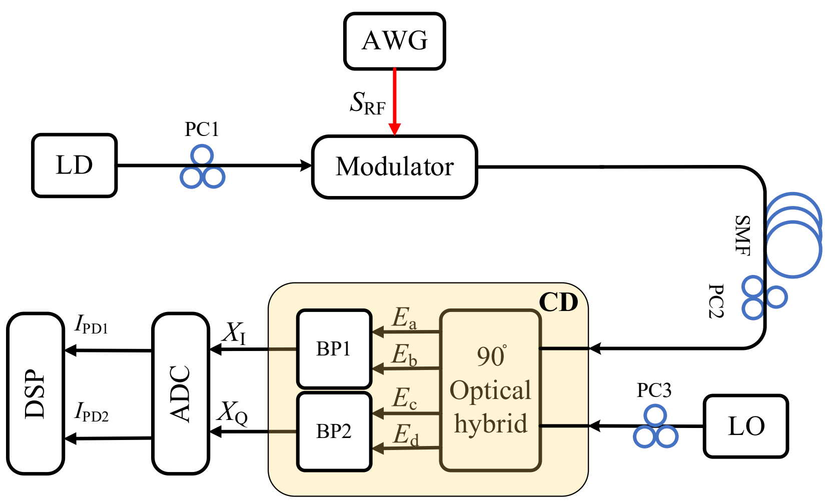

Fig 2.5 The schematic of an MWP link: ADC: analog-to-digital converter, AWG: arbitrary waveform generator, BP: balanced photodetector, CD: coherent detector, LO: local oscillator, PC: polarization controller, SMF: single-mode fiber.

Coherent detection offers several advantages over direct detection, including [9],[84]-[86]:

Improved Receiver Sensitivity: Coherent detection can approach the quantum limit of sensitivity, providing a significant advantage over direct detection, especially in power-limited scenarios [3],[82].

Phase Recovery: The ability to recover phase information of the optical signal enables the use of advanced multilevel modulation formats, such as detecting multiple RF signals (phase modulated QPSK + Intensity modulated 16QAM) on a single optical and RF carrier, thereby increasing spectral efficiency [58],[84].

Frequency Selectivity: Coherent detection provides inherent frequency selectivity, facilitating the implementation of WDM without requiring optical filters [86].

Resilience to Dispersion: The phase information recovered through coherent detection enables digital compensation of chromatic dispersion and polarization mode dispersion [85].

However, coherent detection also introduces challenges such as increased complexity, sensitivity to phase noise, and the need for sophisticated digital signal processing algorithms [9],[83].

3) Self-Coherent Detection: Self-coherent detection represents a middle ground between direct detection and coherent detection. In this approach, a portion of the transmitter laser output is used as a reference signal (pilot tone or carrier) and transmitted along with the modulated signal. At the receiver, the reference signal serves as a local oscillator, enabling the recovery of phase information without requiring a separate laser source [41],[87],[88].

Self-coherent detection can be implemented in various configurations, including:

a) Pilot Tone Assisted Detection: A pilot tone derived from the transmitter laser is transmitted alongside the modulated signal, typically in the same polarization state as the modulated optical signal [36],[37].

b) **KK Detection:** Like previous configurations, a pilot tone is also transmitted with the signal, and based on the KK relations, this technique enables the recovery of phase information from a single-sideband signal with a strong carrier component [38]-[42].

c) **Stokes Vector Receiver (SVR):** This approach uses the Stokes parameters to represent the polarization state of the optical signal, enabling the recovery of both amplitude and phase information through direct detection of multiple polarization components. In this method, the pilot tone is also transmitted to the receiver [43],[44],[89].

Self-coherent detection offers a compromise between the simplicity of direct detection and the performance of coherent detection, making it an attractive option for certain RoF applications where cost and complexity are critical considerations [87],[88].

In conclusion, the choice between direct detection, coherent detection, and self-coherent detection in RoF systems depends on various factors, including the required performance, system complexity, cost constraints, and specific application requirements. As RoF technology continues to evolve, advanced detection techniques and hybrid approaches are being developed to address the growing demands for higher data rates, increased spectral efficiency, and improved system performance.

2.2 Coherent Detection Principles

Coherent detection represents a fundamental paradigm shift in optical communication systems, offering significant advantages over conventional direct detection methods. By preserving both the amplitude and phase information of the optical signal, coherent detection enables higher receiver sensitivity, improved spectral efficiency, and enhanced resilience to transmission impairments. This section explores the theoretical foundations of coherent detection, its implementation techniques, and its application in RoF systems.

2.2.1 Theoretical Foundations of Coherent Detection

Coherent detection in optical communications is based on the principle of optical field mixing, where the received optical signal is combined with a LO laser before photodetection, as shown in Fig. 2.6. This mixing process, when added with DSP techniques, enables the conversion of the optical field information, such as amplitude, phase, and polarization, into the electrical domain.

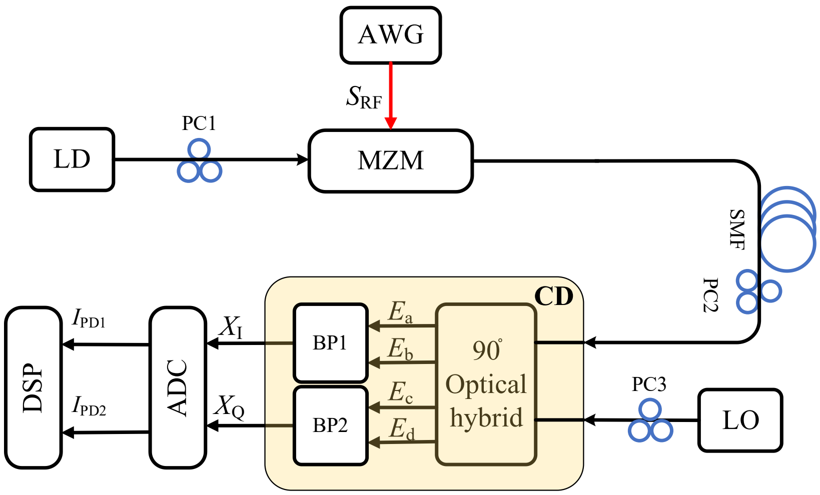

Fig 2.6 A coherent MWP link.

Optical Field Representation: To understand coherent detection, it is essential to consider the mathematical representation of optical fields. The optical field at the output of the transmitter can be described as a complex-valued function [24]:

$$E_s(t) = E_s.\cos\left(\pi \frac{S_{RF}}{2V_\pi} + \frac{\pi}{4}\right).\exp\left(\omega_c t + \varphi(t)\right) \tag{2-8}$$

where E_s is the constant amplitude and the S_{RF} is the RF signal, which is intensity modulated, ω_c is the angular frequency of the optical carrier, and $\varphi(t)$ is the phase noise generated by the laser diode, V_π is the half-wave voltage of the MZM.

Similarly, the optical field at the output of the LO is

$$E_{LO}(t) = E_{LO}.\exp\left(\omega_{LO} t + \varphi_{LO}(t)\right) \tag{2-9}$$

where E_{LO} is the constant amplitude, ω_{LO} is the angular frequency of the optical carrier, and $\varphi_{LO}(t)$ is the phase noise generated by the LO.

The optical signal from the transmitter and the light wave from the LO laser source are co-polarized and are combined in a 90° optical hybrid. At the four outputs of the 90° optical hybrid, we have:

$$\begin{aligned} E_a(t) &= E_s(t) + E_{LO}(t) \\ E_b(t) &= E_s(t) - E_{LO}(t) \\ E_c(t) &= E_s(t) + j.E_{LO}(t) \\ E_d(t) &= E_s(t) - j.E_{LO}(t) \end{aligned} \tag{2-10}$$

and then the photocurrents after the balanced photodetector are as written:

$$\begin{aligned} I_{PD1} &= \frac{1}{2} R\left(E_a(t).E_a^*(t) - E_b(t).E_b^*(t)\right) \\ &\propto R.E_s.E_{LO}.\cos\left[\frac{\pi S_{RF1}}{2V_\pi} + \frac{\pi}{4}\right] \cdot \cos\left[\Delta\omega.t + \varphi(t) - \varphi_{LO}(t)\right] \end{aligned} \tag{2-11}$$

$$\begin{aligned} I_{PD2} &= \frac{1}{2} R\left(E_c(t).E_c^*(t) - E_d(t).E_d^*(t)\right) \\ &\propto R.E_s.E_{LO}.\cos\left[\frac{\pi S_{RF1}}{2V_\pi} + \frac{\pi}{4}\right] \cdot \sin\left[\Delta\omega.t + \varphi(t) - \varphi_{LO}(t)\right] \end{aligned} \tag{2-12}$$

where $\Delta\omega = \omega_s - \omega_{LO}$ is the unstable frequency offset between the optical carrier and LO. These I_{PD1} and I_{PD2} components preserve the full information content of the optical field, enabling the recovery of both amplitude and phase modulation.

2.2.2 **Phase and Polarization Diversity Techniques**

To fully use the capacity of light by a coherent detector, both the phase and polarization states must be considered. This is achieved through diversity techniques.

Phase Diversity: Phase diversity involves the simultaneous detection of both the (I/Q) components of the optical signal. This is typically implemented using a 90° optical hybrid, which combines the signal and local oscillator with different phase relationships [58].

Polarization Diversity: Polarization provides an additional degree of freedom in optical-fiber transmission, as illustrated in Fig. 2.7. By simultaneously modulating the two orthogonal polarization states, a technique known as polarization-division multiplexing, we can convey two independent data streams, effectively doubling both the data rate and the spectral efficiency [25].

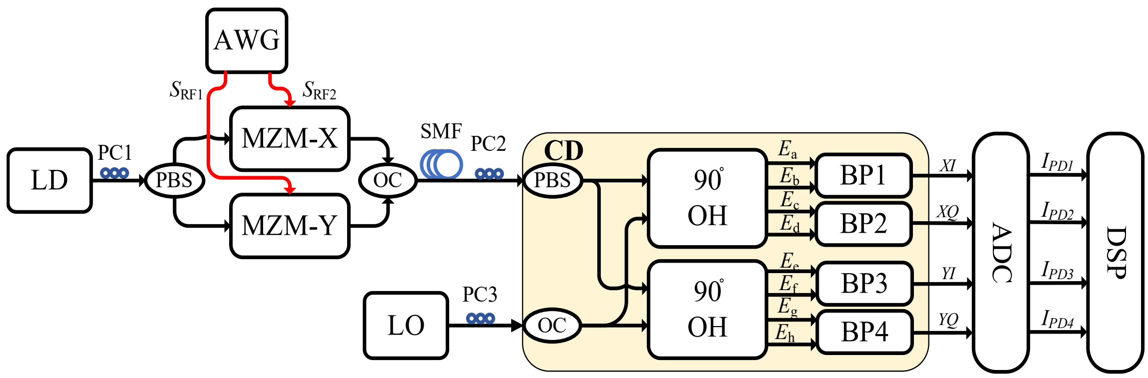

Fig 2.7 A coherent MWP link with phase and polarization diversity.

A typical polarization diversity receiver splits the received signal and local oscillator into their orthogonal polarization components ($\vec{x}$ and $\vec{y}$) and processes each component independently using phase diversity detection.

As illustrated in Fig. 2.7, a coherent receiver with two orthogonal polarizations produces four electrical channels: the I/Q components of both orthogonal polarization states. Once digitized, these four signals are jointly processed in the DSP block to reconstruct the data on each polarization.

The Critical Role of Beat Notes in Coherent Detection: In coherent detection systems, the beat note between LO and the transmitter laser is not merely a technical detail but the fundamental mechanism that enables phase-sensitive detection. This beat note serves as the carrier of phase information, translating the optical phase variations into detectable electrical signals. Without this beat note, the phase information would be lost during photodetection, as conventional photodetectors respond only to the intensity of light, not its phase.

The beat note in coherent detection systems is generated when the optical field of the incoming optical signal interferes with the optical field of the LO at the receiver. This interference produces a photocurrent with a component oscillating at the difference frequency between the two optical sources. This difference frequency component, known as the beat note, carries both the phase information and the same phase noise of the original optical signal, but at a frequency that can be processed by conventional electronic circuits. This will be used to recover the PM signal and cancel the phase noise.

2.2.3 Digital Signal Processing for Coherent Detection

The full potential of coherent detection is realized through sophisticated DSP algorithms that compensate for various impairments and extract the transmitted information from the received signal [21],[90],[91].

Front-End Correction: The first stage of DSP in a coherent receiver typically involves correcting for imperfections in the analog front-end, including [21],[90]:

I/Q Imbalance Compensation: I/Q imbalance arises because the in-phase and quadrature branches rarely have identical gain or a perfect 90° phase split, so a portion of the signal's "image" (its complex conjugate) leaks into the desired baseband and distorts the constellation. Digital compensation measures the mismatch, typically via short pilot symbols or a low-overhead decision-directed algorithm, then applies a simple, widely linear filter that subtracts the estimated conjugate component, simultaneously equalizing the gain and restoring the correct quadrature relationship [92].

Digital Spectral Filtering: Once the signal is in the DSP domain, we can excise *any* unwanted spectral components, DC, spurs, or out-of-band noise, by applying an ideal rectangular ("brickwall”) filter: transform to the frequency domain, zero the bins outside the desired band, and transform back, leaving only the information-bearing spectrum [21],[91].

Timing-skew correction: It removes the fractional-symbol misalignment that builds up between parallel branches, such as the two polarization tributaries or multiple analog-to-digital converter (ADC) lanes, when clock paths, cables, or package traces differ in length. The DSP continuously estimates the relative delay (e.g., via cross-correlation on training sequences or decision-directed metrics) and then realigns the streams by inserting or discarding samples for coarse adjustment and applying fractional-delay finite impulse responce filters for fine adjustment, so that all paths arrive sample-synchronous before subsequent MIMO equalization [90],[92].

Chromatic Dispersion Compensation: Chromatic dispersion is a purely phase-modulating impairment: frequency components of an optical waveform accumulate different propagation delays, so the impulse broadens without any change in amplitude. In the frequency domain, a single-mode fiber is well modelled by the quadratic transfer function [9]:

$$H_{CD}(\omega) = \exp\left(-j\frac{\beta_2 L}{2}\omega^2\right) \tag{2-13}$$

where L is the fibre length and β_2 is the group-velocity-dispersion coefficient (units $s^2\ m^{-1}$). Many system engineers prefer the dispersion parameter D expressed in $(\frac{ps}{nm.km})$; the two are related by $\beta_2 = -(\lambda^2 D)/(2\pi c)$, so substituting D flips the sign in the exponent. Because the magnitude of H_{CD} is unity, compensation only needs to reverse this phase.

Digital signal processing does that efficiently in the frequency domain. A block of samples is first transformed with a fast-Fourier-transform; each spectral bin is then multiplied by the inverse phase filter:

$$H_{CD}^{-1}(\omega) = \exp\left(+j\frac{\beta_2 L}{2}\omega^2\right) \tag{2-14}$$

An inverse fast-Fourier-transform returns the equalized waveform to the time domain. With overlap-save or overlap-add framing, this $O(N.\log(N))$ procedure restores the original pulse shape even after many hundreds of kilometres, making frequency-domain equalisation the standard approach for chromatic dispersion compensation in coherent optical receivers [93],[94].

Polarization Demultiplexing and PMD Compensation: In systems employing polarization division multiplexing, the received signal contains a mixture of the two transmitted polarization components due to polarization mode dispersion and polarization-dependent loss. Polarization demultiplexing aims to separate these components and recover the original transmitted signals [95],[96].

A common approach is the Constant Modulus Algorithm or its variants, which adaptively adjust a 2×2 MIMO (Multiple-Input Multiple-Output) filter to minimize a cost function based on the expected properties of the transmitted signals [96]-[98].

Carrier Recovery: In a coherent receiver, we need the LO to "turn" at exactly the same phase as the laser that sent the signal; otherwise, every point in the constellation keeps sliding around. Digital carrier-recovery logic, therefore, does two jobs [22],[80]:

1. Remove the bulk frequency mistake: The incoming samples are first analyzed to measure the average difference in laser frequency Δf. Once that spacing is known, the receiver rotates every sample by $-\Delta f\ t \cdot 2\pi$, pulling the whole signal back to its proper center frequency [99].

2. Touch up the remaining phase wobble: Even after the coarse fix, the two lasers still drift a little from symbol to symbol after sampling. A lightweight tracking loop smooths the phase noise in real

time and subtracts them, so the constellation points stay still, and decisions can be made cleanly [100].

By breaking the task into a better correction by fine tracking, the receiver quickly locks to any transmitter without adding noticeable complexity [22],[80].

Equalization and Symbol Detection: After the carrier is steady, the receiver still needs to remove any residual smearing between symbols and determine which bits were sent. A short, adaptive digital filter, called the feed-forward equalizer, learns the fiber's impulse response in real time and cancels the ISI it causes. Once the samples are corrected or compensated, each point is compared with the ideal locations of the chosen constellation (QPSK, 16QAM, etc.) and assigned to the nearest one, turning waveforms back into data symbols. Finally, a forward-error-correction decoder (for example, Reed-Solomon, Low-Density Parity-Check, or turbo coding) corrects the few symbol errors that remain, delivering an error-free bit stream to the higher layers [101],[102].

2.2.4 **Phase-Noise Cancellation**

Lasers are never perfectly monochromatic**;** their narrow linewidth broadens the optical carrier and shows up in the electrical domain as phase noise, a slow, random rotation or distortion of every constellation point. If left unchecked, this phase noise increases the BER. Modern coherent receivers maintain the constellation's stability using one of the following digital techniques [22], [78], as shown in Table 2.1.

By selecting the method that best matches the modulation format, laser quality, and system cost, designers can all but eliminate phase noise and recover an error-free bit stream without burdening the rest of the digital signal-processing chain [22].

Table 2.1 Techniques to cancel phase noise.

Technique	Core Principle	Advantages & Applications
Feed-forward carrier recovery	Measure phase directly from the raw samples before any decisions are made. For QPSK, the classic Viterbi–Viterbi algorithm raises the signal to the 4th power, which strips away the data and leaves only the phase drift. Averaging over a short window gives a clean estimate that is subtracted from each sample [100],[103].	M-PSK formats with modest laser linewidths.
Decision-directed tracking	First, make a "best guess" of each symbol, then compare the guess with the actual sample; the angle between them is the residual phase error. A running average of that error is used to nudge the constellation back into place [83],[100],[104].	Higher-order QAM (e.g., 16- or 64-QAM), where feed-forward methods are less effective.
Pilot-aided compensation	Periodically insert known symbols (pilots) into the data stream. Because the receiver already knows what those pilots should look like, it can measure the phase error very accurately, even when lasers are noisy, and interpolate the result to the data that lies between pilots [105]-[107].	Very high spectral efficiencies and systems with exceptionally wide laser linewidths.
Digital phase noise cancellation	In some RoF links, the in-phase (I) and quadrature (Q) outputs are squared and added: $\lvert I\rvert^2 + \lvert Q\rvert^2$. The phase terms cancel out mathematically, so the result is immune to laser noise. This novel property, as demonstrated in [80], enables system designers to utilize inexpensive, free-running lasers without compromising performance, as shown in [24]-[30].	It can cancel phase noise and unstable frequency offset between LD and LO.
Self-homodyne detection	Transmit a small unmodulated slice of the transmitter laser (a "pilot tone") along with the data, either on the orthogonal polarization or at a slight frequency offset. At the receiver, that tone serves as an optical reference, so any phase wander is common-mode and cancels out automatically [108].	Links where an extra optical channel is acceptable and absolute simplicity at the DSP stage is desirable.

2.2.5 Coherent Detection in RoF Applications

Coherent detection unlocks a set of capabilities that are difficult or impossible to realize with the simpler IM/DD approach traditionally used in RoF. By beating the received optical field with a LO laser and digitizing both in-phase and quadrature components, the receiver keeps full knowledge of the signal's amplitude and phase. This single architectural change drives the four main benefits outlined below [109].

First, the system has vastly better sensitivity because the LO supplies most of the optical power that reaches the photodiodes, allowing it to work with only a few photons from the remote transmitter. Practical coherent RoF links already achieve sensitivities within ~3 dB of the quantum limit at gigabit-per-second data rates [109],[110]. That headroom translates directly into longer fiber runs or fewer in-line EDFAs in applications such as campus-wide distributed antenna systems [111].

Second, support for spectrally efficient modulation. With phase information intact, the link can carry both multiple RF signals or even single-sideband subcarrier multiplexing. Spectral efficiencies of ≥ 6 bits/s/Hz have been demonstrated over tens of kilometers without resorting to dense WDM grids [112].

Third, digital immunity to dispersion. The receiver's DSP unit can calculate and apply the exact inverse of chromatic dispersion and first-order polarization-mode dispersion. That software-defined compensation keeps broadband RF signals in spec after 50 km or more of standard single-mode fiber, eliminating the need for expensive dispersion-compensating modules [85],[113].

Fourth, inherent frequency selectivity allows sharp digital filters to isolate individual sub-bands or WDM channels without the need for optical add-drop components. This simplifies remote-unit design and enables flexible spectrum slicing for multi-band 5G front-haul [85].

These advantages come with trade-offs. Coherent front-ends need balanced photodiodes, polarization-diversity hybrids, high-speed ADCs, and a non-trivial amount of DSP horsepower. They are also sensitive to LO and transmitter phase noise, so they either rely on narrow-linewidth lasers or on sophisticated phase-tracking algorithms as described in this chapter. Managing polarization adds another layer of control circuitry [114].

Recent research is closing those gaps. "Low-complexity" coherent receivers use single-ended photodiodes and digital polarization multiplexing to cut parts count by half [95],[115]. Blind-phase-search kernels now run in real time on ASICs drawing <1 W, allowing the use of inexpensive 1 MHz-linewidth lasers [116]. Self-coherent and pilot-tone schemes further simplify the LO by transmitting a copy of the carrier alongside the data, while monolithic indium-phosphide or silicon-photonics chips integrate hybrids, modulators, and detectors on a few square millimeters of die area [79],[117],[118].

In summary, coherent detection provides RoF links with quantum-limited sensitivity, high spectral efficiency [119], and digital resilience to fiber impairments, features that align directly with emerging needs such as multi-band 5G/6G front-haul and large-venue distributed antenna systems. Although the approach is more expensive than direct detection today, rapid progress in integrated photonics and DSP is pushing coherent RoF toward practical, cost-effective deployment.

2.3 Multiplexing Techniques for High Spectral Efficiency

Multiplexing techniques are fundamental to modern communication systems, enabling the efficient utilization of available resources by allowing multiple signals to share the same transmission medium. In the context of RoF systems, these techniques are crucial for achieving high spectral efficiency and meeting the growing demand for bandwidth-intensive applications. This section examines various multiplexing approaches employed in RoF systems, with a particular emphasis on power multiplexing and NOMA principles [120]-[123].

2.3.1 Wavelength Division Multiplexing (WDM)

Wavelength division multiplexing is a technique that combines multiple optical carriers at different wavelengths onto a single optical fiber. Each wavelength carries an independent data stream, effectively creating parallel channels within the same physical medium [121],[122].

Principles of WDM: The fundamental principle of WDM is based on the property that optical signals at different wavelengths can propagate through the same fiber with minimal interference. The optical spectrum is divided into multiple channels, each centered at a specific wavelength and separated by a guard band to prevent crosstalk. The capacity of a WDM system can be expressed as:

$$C = N \times B \tag{2-15}$$

where C is the total capacity, N is the number of wavelength channels, and B is the data rate per channel.

In RoF applications, WDM enables the transmission of multiple RF signals over a single fiber by assigning each signal to a different optical wavelength [124],[125]. This approach is particularly valuable in scenarios such as:

Cellular Backhaul: Multiple base stations can share the same fiber infrastructure, with each station assigned a dedicated wavelength [125],[126].

Distributed Antenna Systems: Different areas or sectors within a building or campus can be served by separate wavelengths, simplifying routing and reducing interference [124].

Multi-Service Networks: Different services (e.g., cellular, Wi-Fi, Radio, Television, and satellite broadcasts) can be allocated to different wavelengths, allowing for independent optimization and management [49],[127].

While WDM significantly increases the capacity of RoF systems, it also introduces challenges such as the need for multiple laser sources or high-speed modulators, wavelength-selective components, and management of nonlinear effects at high optical powers. These factors contribute to increased system complexity and cost, particularly for Dense-WDM and Ultra Dense-WDM implementations [128],[129].

2.3.2 Polarization Division Multiplexing (PDM)

Polarization division multiplexing leverages the vector nature of light to transmit two independent data streams on orthogonal polarization states of the same optical carrier. This technique effectively doubles the spectral efficiency without requiring additional bandwidth [91],[98],[130].

Principles of PDM: Light, as an electromagnetic wave, has two orthogonal polarization components that can propagate independently through an ideal medium. In PDM, these two polarization states (typically referred to as X and Y, or horizontal and vertical) are used as separate channels for data transmission [130],[131]. The electric field of a PDM signal can be represented as [3]:

$$E(t)=\left[E_x(t) \quad , \quad E_y(t)\right]^T \tag{2-20}$$

where $E_x(t)$ and $E_y(t)$ are the field components carrying independent data streams.

PDM Implementation: A typical PDM transmitter consists of [96],[98],[132]:

1) Two independent modulators for the X and Y polarization components

2) A polarization beam combiner (PBC) to merge the modulated signals

3) Polarization-maintaining components to preserve the orthogonality

At the receiver, a polarization diversity scheme is employed to recover both polarization components as shown in Fig. 2.7 [96],[98]:

1. A polarization beam splitter (PBS) separates the received signal into two orthogonal components.

2. Each component is processed independently, and the DSP unit is used to recover signals in each polarization.

Challenges in PDM: While PDM offers significant advantages in terms of spectral efficiency, it faces several challenges [65]:

Polarization Mode Dispersion: Different propagation velocities for the two polarization components lead to differential group delay and signal distortion.

Polarization-Dependent Loss: Unequal attenuation of the polarization components affects the signal-to-noise ratio and increases the bit error rate [133].

PDM in RoF Systems: In RoF applications, PDM can be employed to double the capacity of a single wavelength channel. For example, two independent RF signals can be transmitted on orthogonal polarization states, effectively doubling the spectral efficiency. This approach is particularly valuable in scenarios where wavelength resources are limited or expensive [19],[132].

PDM can also be combined with other multiplexing techniques, such as WDM, to further increase the system capacity. For instance, a PDM-WDM system with N wavelengths can support $2N$ independent RF signals, making it an attractive solution for high-density deployments [117].

2.3.3 **Power Multiplexing and NOMA Principles**

Power multiplexing, based on the principles of NOMA, represents a paradigm shift in multiplexing techniques. Unlike traditional orthogonal approaches, where resources are exclusively allocated to users, NOMA allows multiple users to share the same time, frequency, and spatial resources, with separation achieved in the power domain [122],[123],[134].

Fundamentals of Power Domain NOMA: The core principle of power domain NOMA is the allocation of different power levels to different users or signals, enabling their superposition in the same resource block. At the receiver, successive interference cancellation (SIC) is employed to sequentially decode and subtract the signals, starting from the strongest one [32],[134].

In a basic two-user NOMA scenario, the transmitted signal can be expressed as:

$$S_{total} = \alpha_1 S_1 + \alpha_2 S_2 \tag{2-21}$$

where S_{total} is the power multiplexed signal, S_1 and S_2 are the signals for users 1 and 2, and α_1 and α_2 are their allocated powers.

The power allocation is typically designed to ensure that the stronger signal is received by the user with better channel conditions (such as less attenuation, interference, or noise, e.g.), while the weaker signal is received by the user with worse channel conditions. This approach, known as "power-domain user multiplexing," ensures that both users can achieve satisfactory performance. In other words, for a specified signal with definite power, the user with a higher signal-to-noise-ratio (SNR) will be considered the strong user, and the user with a lower SNR will be considered the weak user [122],[135].

Successive Interference Cancellation (SIC): SIC is the key enabling technology for NOMA, allowing the receiver to separate the superimposed signals. The SIC process involves the following steps [136]:

1. Decode the strongest signal (highest power) while treating other signals as noise
2. Reconstruct the strongest signal using the decoded information
3. Subtract the reconstructed signal from the received signal
4. Repeat the process for the next strongest signal

Mathematically, for a two-user scenario, the SIC process can be described as follows:

For user 1 (stronger user) [1],[137]:

$$y_1 = h\left[\alpha_1 S_1 + \alpha_2 S_2\right] + n \tag{2-22}$$

S_1 is decoded, while $\alpha_2 S_2$ is treated as noise. h is the channel impulse response and n is the noise.

Theoretical Capacity of NOMA: From an information theory perspective, NOMA can achieve the capacity region of the broadcast channel, making it theoretically optimal in terms of spectral efficiency. For a two-user scenario, the achievable rates are [138],[139]:

$$\begin{aligned} R_1 &= \log_2\left(1 + \frac{\alpha_1^2}{\alpha_2^2 + \sigma^2}\right) \\ R_2 &= \log_2\left(1 + \frac{\alpha_2^2}{\sigma^2}\right) \end{aligned} \tag{2-23}$$

where σ^2 is the noise power. The sum rate of NOMA is [140]:

$$R_{sum} = R_1 + R_2 = \log_2\left(1 + \frac{\alpha_1^2 + \alpha_2^2}{\sigma^2}\right) \tag{2-24}$$

which is equivalent to the capacity of a single-user system with the same total power, demonstrating the spectral efficiency of NOMA [141].

Power Multiplexing in RoF Systems: The application of power multiplexing and NOMA principles in RoF systems offers various advantages for increasing spectral and system efficiency. By allowing multiple RF signals to share the same optical carrier, time slot, and frequency band, power multiplexing enables more efficient and simplified utilization of available resources [46], [142],[143].

In a power-multiplexed RoF system, multiple RF signals with different power levels are combined and used to modulate an optical carrier. At the receiver, after optical-to-electrical conversion, SIC is employed to sequentially recover the individual RF signals [46].

The implementation of power multiplexing in RoF systems can take various forms:

Direct Power Multiplexing: Multiple RF signals with different power levels are directly combined in the electrical domain before optical modulation [143].

Optical Power Allocation: Power allocation is performed in the optical domain, with different optical modulation indices assigned to each signal [46].

2.4 Relevant Mathematical Tools and Signal Processing

The implementation of advanced RoF systems, particularly those employing coherent detection and sophisticated multiplexing techniques, relies heavily on mathematical tools and signal processing algorithms. This section examines the fundamental mathematical frameworks and signal processing techniques that facilitate the analysis, design, and optimization of high spectral efficiency RoF systems [9],[22].

2.4.1 Signal Representation and Analysis

High spectral efficiency in RoF link systems is underpinned by advanced mathematical models and signal processing techniques. This section reviews the key theoretical tools used to analyze and enhance RoF links, focusing on digital signal processing for coherent detection, phase noise modeling and cancellation, power-domain multiplexing with successive interference cancellation, frequency-domain equalization, and modulation methods (Intensity modulation + Phase modulation, QPSK, 16QAM) in MWP. The emphasis is on the theoretical foundations rather than implementation details [22],[131].

Digital Signal Processing for Coherent RoF Links: Coherent detection in RoF systems employs an LO laser at the receiver to mix with the incoming optical signal, enabling the recovery of both amplitude and phase information. In a typical coherent receiver, the signal and LO are combined in a 90° optical hybrid and detected with balanced photodiodes, producing two I/Q electrical outputs that carry the complex envelope of the transmitted microwave signal. These baseband I/Q signals are then processed by a DSP unit to retrieve the data. The DSP algorithms perform critical tasks such as carrier frequency offset correction, channel equalization, and carrier phase recovery. For example, in a high-efficiency coherent RoF link, a DSP algorithm can eliminate the phase noise and frequency offset introduced by two free-running lasers at the transmitter and receiver. This allows the successful recovery of advanced modulation signals like multilevel modulation (IM+PM) that would otherwise be distorted by laser instability. Generally, DSP in coherent RoF links ensures high-fidelity signal reconstruction by compensating optical link impairments in the digital domain. Modern research demonstrations implement DSP pipelines that handle multiple impairment compensation steps in tandem – for instance, mitigating laser phase noise while simultaneously demultiplexing multiplexed signals – to maintain signal integrity in high spectral efficiency links [9],[22],[83],[93].

Phase Noise Modeling and Joint Phase Noise Cancellation: Phase noise in RoF systems originates from the narrow linewidth and frequency fluctuations of lasers. It is typically modeled as a stochastic phase perturbation superimposed on the optical carrier phase. Mathematically, the optical field of a transmitter laser can be expressed as $E_s(t) = \sqrt{P_s}\exp[j(\omega_c t + \phi_c(t))]$, where $\sqrt{P_s}$ is the laser power, ω_c the optical carrier frequency, and $\phi_c(t)$ a random phase noise process. Similarly [24]-[30], the LO laser produces $E_{LO}(t) = \sqrt{P_{LO}}\exp[j(\omega_{LO} t + \phi_{LO}(t))]$, with $\phi_{LO}(t)$ describing the LO's phase noise. In a coherent RoF link, the received signal's phase is impacted by the joint phase noise of both the transmitter and LO lasers, effectively the difference $\phi_c(t) - \phi_{LO}(t)$ contributes a time-varying phase error. This joint phase noise causes constellation rotation and must be tracked and corrected by the receiver's DSP. Advanced RoF systems employ digital phase noise cancellation algorithms to estimate and remove this random phase drift. One common approach is pilot-aided or data-aided phase estimation, where an unmodulated optical pilot tone or a known reference symbol is sent along with the data to measure the instantaneous phase error. Alternatively, blind algorithms (e.g., phase recovery via Costas loops or signal fourth-power methods) exploit the properties of the modulation to infer the phase [144]. In either case, the DSP effectively generates an equal and opposite phase rotation to derotate the received signal. In recent works, Li *et al.* demonstrate [25]-[27] a joint phase noise cancellation algorithm that accounts for both laser sources, mitigating the combined phase noise and any slowly varying frequency offset between them. By applying such algorithms, multiple multiplexed signals can be recovered free of common phase perturbations, obviating the need for optical phase-locked loops. Chen and Yao's coherent RoF experiments [24],[28]-[30] are a case in point: using free-running lasers for transmitter and LO, they relied on DSP-based phase noise cancellation to successfully recover QPSK and 16QAM signals without optical locking. Thus, robust mathematical modeling of phase noise as a Wiener process (random walk) and the development of phase tracking algorithms are indispensable tools for coherent RoF systems.

Power Multiplexing and Successive Interference Cancellation: To further increase spectral efficiency, RoF systems can employ power-domain multiplexing, a principle borrowed from NOMA. In power multiplexing, multiple independent microwave signals are transmitted over the same optical carrier or frequency channel by assigning them different power levels. Mathematically, if two signals $S_1(t)$ and $S_2(t)$ share a channel, the transmitted composite signal can be written (in baseband form) as $x(t) = \alpha_1 S_1(t) + \alpha_2 S_2(t)$, where α_1, α_2 are power allocation coefficients (with $\alpha_1 + \alpha_2 = 1$ for normalization). The receiver distinguishes the layered signals based on their power disparity. The theoretical foundation for separating these superposed signals is successive interference cancellation (SIC). In SIC, the receiver first decodes the strongest (highest power) signal while treating any weaker co-channel signals as noise. Once the strongest data stream is obtained, its contribution is digitally subtracted from the composite received signal, yielding a residual in which the next signal becomes the strongest. The receiver then decodes the next signal, and this process continues sequentially. This sequential cancellation scheme can be represented algorithmically as: $\hat{S}_1 = \mathcal{D}(x)$ (decode strongest), then $x' = x - \alpha_1 \hat{S}_1$ (subtract estimated interference), and $\hat{S}_2 = \mathcal{D}(x')$ (decode next), and so on [144]. By leveraging SIC, the overlapping signals become decodable despite not being orthogonal, thereby expanding throughput within a given bandwidth. Recent RoF studies have applied power multiplexing in the optical domain by Li *et al.* [46] where they modulate two microwave vector signals on orthogonal optical polarizations and then adjust their power ratio via a polarization combiner to achieve the desired power allocation. At the coherent receiver, a DSP algorithm (implementing SIC logic) successfully demultiplexes the two signals, resulting in improved error vector magnitudes thanks to the optimized power split. Importantly, this power multiplexing/SIC approach relies on the theoretical guarantee that if the power ratios are chosen appropriately, each signal can be retrieved with interference from the others largely canceled. The concept, initially developed in wireless communications theory, is thus a powerful tool in microwave photonic links to push spectral efficiency beyond the orthogonal multiplexing limit [145]-[147].

Chapter 3 Power Multiplexing in Coherent Microwave Photonic Links

3.1 Concept of Power Multiplexing in Coherent Detection

The relentless growth in data traffic and the increasing demand for high-speed wireless communication systems have driven researchers to explore innovative techniques to enhance spectral efficiency in RoF systems. Among these techniques, power multiplexing in coherent microwave photonic links has emerged as a promising approach to significantly increase data transmission rates without requiring additional optical wavelengths or bandwidth [32],[123].

Power multiplexing, inspired by NOMA principles, enables the simultaneous transmission of multiple data streams over a single channel by assigning them distinct power levels. This technique enables the receiver to distinguish between signals based on their power ratios, thereby increasing the spectral efficiency of the system. When combined with coherent detection, power multiplexing offers a powerful solution to address the growing bandwidth demands of modern communication networks.

Coherent detection represents a significant advancement over traditional IM/DD systems. By utilizing a LO at the receiver, coherent detection enables the recovery of both amplitude and phase information from the optical signal, effectively doubling the amount of information that can be transmitted [22]. This capability is particularly valuable in microwave photonic links, where preserving phase information is crucial for multilevel modulation formats, such as PM added to IM.

A fundamental aspect of coherent detection is the generation of a beat note between the transmitted optical signal and the local oscillator, since we will have access to both sidebands. This beat note, which occurs when two optical waves with slightly different frequencies interfere, is essential for extracting the phase information from the optical signal. The proper detection and processing of this beat note are critical for the successful implementation of coherent detection systems, as it directly impacts the system's ability to recover the transmitted information accurately [22],[83].

In this chapter, we explore two innovative approaches to implementing power multiplexing in coherent microwave photonic links. The first approach utilizes orthogonal polarization to separate the modulated signal from an unmodulated optical carrier, which serves as a reference for extracting the beat note at the receiver. The second approach employs a digital filter technique to capture the beat note after detection, eliminating the need for precise optical path length matching between channels.

Both approaches demonstrate the potential of power multiplexing in coherent microwave photonic links to significantly enhance spectral efficiency and data transmission rates. By examining these techniques in detail, we gain valuable insights into the design considerations and performance characteristics of advanced microwave photonic systems for next-generation communication networks.

The remainder of this chapter is organized as follows: Section 3.2 presents the system architecture of a power-multiplexed intensity-phase modulation (IM/PM) system, which utilizes orthogonal polarization for coherent detection. Section 3.3 describes an alternative system architecture based on a DD-MZM, which employs digital filtering for beat note extraction. Finally, Section 3.4 provides a summary of the key findings and insights gained from the investigation of these power multiplexing techniques in coherent microwave photonic links.

3.2 System Architecture of an IM/PM system

3.2.1 System Architecture

The first approach to implementing power-multiplexing in a microwave photonic link, which we utilize orthogonal polarization to separate the modulated signal from an unmodulated optical carrier. This technique, demonstrated in our first experimental work, provides an elegant solution for generating and extracting the beat note necessary for coherent detection.

In this approach, a continuous wave (CW) light is generated by a laser source and then split into two channels. Channel 1 carries approximately 90% of the optical power and undergoes modulation, while Channel 2 carries the remaining 10% and remains unmodulated, serving as a reference for beat note extraction at the receiver. The system architecture is illustrated in Fig. 3.1, which shows the transmitter and receiver setup optimized for handling high-throughput microwave signals over a standard SMF.

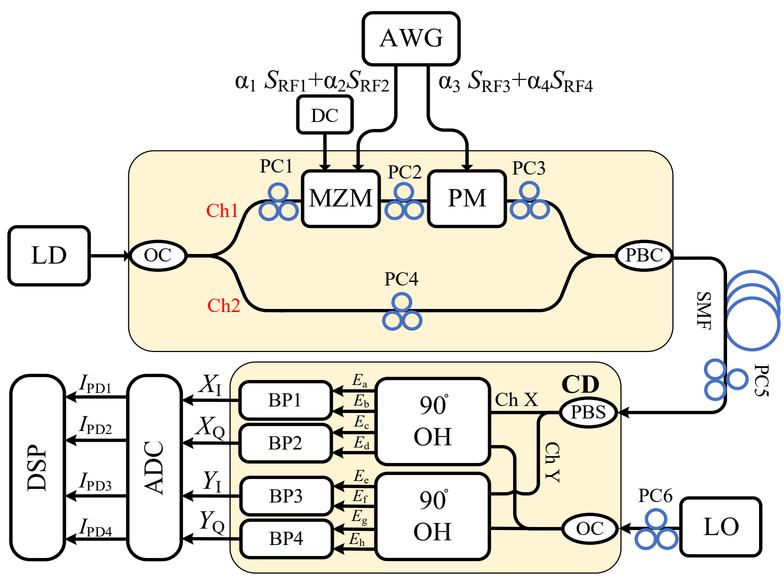

Fig 3.1 The schematic of the first proposed RoF link: ADC: analog-to-digital converter (implemented by the built-in ADCs of the digital storage oscilloscope used for waveform acquisition), AWG: arbitrary wave generator, BP: balanced photodetector, DSP: digital signal processing, LO: local oscillator, MZM: Mach-Zehnder modulator, OC: optical coupler, PBC: polarization beam combiner, PBS: polarization beam splitter, OH: optical hybrid, PC: polarization controller, PM: phase modulator, SMF: single-mode fiber.

At the transmitter, the light in Channel 1 undergoes cascaded modulation processes. First, it is amplitude-modulated by an MZM, and then phase-modulated by a PM. Two power-multiplexed microwave signals, generated by an AWG, are applied to the RF ports of the modulators. Meanwhile, the light in Channel 2 remains unmodulated, preserving its original phase and amplitude characteristics. Following modulation, the light waves from both channels are polarization multiplexed by a PBC. This polarization multiplexing is a key feature of the system, as it allows the modulated signal and the unmodulated reference to be transmitted over the same fiber without interfering with each other. The orthogonal polarization states ensure that the two signals can be separated at the receiver without crosstalk. Upon reception, the light waves are first polarization-demultiplexed by a polarization beam splitter (PBS) incorporated inside a polarization- and phase-diversity coherent optical receiver. This receiver manages the orthogonally polarized light waves from Channel X (modulated) and Channel Y (unmodulated reference). Each channel's light wave is directed to a 90° optical hybrid, where it interferes with a local oscillator (LO) signal. The optical hybrids facilitate the balanced detection of incoming signals, outputting four channels: XI, XQ, YI, and YQ, which represent the in-phase and quadrature components of the two orthogonally polarized signals. These four analog electrical waveforms (XI, XQ, YI, and YQ) are digitized by the built-in ADCs of a multi-channel digital storage oscilloscope (DSO). The captured samples are stored and then transferred to the DSP workstation for offline post-processing, where phase-noise cancellation and signal recovery are performed (i.e., the experiment is not implemented in real time).

Mathematical Model for Beat Note Extraction: The optical field at the output of the transmitter can be expressed as:

$$E(t)=\vec{X}\begin{bmatrix}\sqrt{P_{s-c1}L_{c1}}.\cos\left(\frac{\alpha_1\cdot\pi S_{RF1}(t)+\alpha_2\cdot\pi S_{RF2}(t)}{2V_{\pi IM}}+\frac{\pi}{4}\right)\\ \cdot\exp\left(j\left(\omega_c t+\varphi_{c1}(t)+\frac{\alpha_3\cdot\pi S_{RF3}(t)+\alpha_4\cdot\pi S_{RF4}(t)}{2V_{\pi PM}}\right)\right)\end{bmatrix} + \vec{Y}\left[\sqrt{P_{s-c2}L_{c2}}\exp\left(j\left(\omega_c t+\varphi_{c1}(t)+\varphi_{c2}(t)\right)\right)\right] \tag{3-1}$$

where $\vec{X}$ and $\vec{Y}$ represent the polarization states for each channel, P_{s-c1} and P_{s-c2} are the optical powers entering Channels 1 and 2, L_{C1} and L_{C2} account for the link losses, $\varphi_{C1}(t)$ and $\varphi_{C2}(t)$ are the transmitter laser source phase noise terms for each channel, $V_{\pi IM}$ and $V_{\pi PM}$ are the half-wave voltages of the MZM and PM, $S_{RF1}(t)$ through $S_{RF4}(t)$ signify the microwave vector signals, ω_c is the light wave's angular frequency, and α_1 through α_4 are the power multiplexing coefficients.

At the receiver, the LO field is given by:

$$\mathrm{E}_{LO}(t)=\sqrt{P_{LO}}\exp\left(j\left(\omega_{LO}t+\varphi_{LO}(t)\right)\right) \tag{3-2}$$

where P_{LO} is the power of the LO, ω_{LO} is its angular frequency, and $\varphi_{LO}(t)$ is its phase noise term.

The output of 90° optical hybrid is as follow:

$$\begin{bmatrix}\mathrm{E}_a(t) & \mathrm{E}_b(t) & \mathrm{E}_c(t) & \mathrm{E}_d(t)\\ \mathrm{E}_e(t) & \mathrm{E}_f(t) & \mathrm{E}_g(t) & \mathrm{E}_h(t)\end{bmatrix}=\sqrt{L_h}\begin{bmatrix}\sqrt{L_f}\mathrm{E}_x(t) & \mathrm{E}_{LO}(t)\frac{e^{j\varphi_x}}{\sqrt{2}}\\ \sqrt{L_f}\mathrm{E}_y(t) & \mathrm{E}_{LO}(t)\frac{e^{j\varphi_y}}{\sqrt{2}}\end{bmatrix}\cdot\begin{bmatrix}1 & 1 & 1 & 1\\ 1 & e^{j\pi} & e^{j\frac{\pi}{2}} & e^{-j\frac{\pi}{2}}\end{bmatrix} \tag{3-3}$$

here, L_h and L_f are the link losses attributable to the two 90° optical hybrids and the SMF, respectively. The phase terms φ_x and φ_y arise due to the polarization mismatch between the signal and the LO laser source light wave.

After photodetection, the outputs of the balanced photodetectors can be expressed as:

$$I_{PD1} = \frac{1}{2} R\left(E_a(t).E_a^*(t) - E_b(t).E_b^*(t)\right)$$

$$= 2RL_h \begin{bmatrix} \sqrt{2P_{LO}P_{s-c1}L_{c1}L_f} \cos\left[\frac{\alpha_1 \cdot \pi S_{RF1}(t) + \alpha_2 \cdot \pi S_{RF2}(t)}{2V_{\pi IM}} + \frac{\pi}{4}\right] \cdot \\ \cos\left[\Delta\omega t + \varphi_{c1}(t) - \varphi_{LO}(t) - \varphi_x + \frac{\alpha_3 \cdot \pi S_{RF3}(t) + \alpha_4 \cdot \pi S_{RF4}(t)}{2V_{\pi PM}}\right] \end{bmatrix} \quad (3\text{-}4)$$

$$I_{PD2} = \frac{1}{2} R\left(E_c(t).E_c^*(t) - E_d(t).E_d^*(t)\right) =$$

$$= 2RL_h \begin{bmatrix} \sqrt{2P_{LO}P_{s-c1}L_{c1}L_f} \cos\left[\frac{\alpha_1 \cdot \pi S_{RF1}(t) + \alpha_2 \cdot \pi S_{RF2}(t)}{2V_{\pi IM}} + \frac{\pi}{4}\right] \cdot \\ \sin\left[\Delta\omega t + \varphi_{c1}(t) - \varphi_{LO}(t) - \varphi_x + \frac{\alpha_3 \cdot \pi S_{RF3}(t) + \alpha_4 \cdot \pi S_{RF4}(t)}{2V_{\pi PM}}\right] \end{bmatrix} \quad (3\text{-}5)$$

$$I_{PD3} = 2RL_h \sqrt{2P_{s-c2}P_{LO}L_f L_{c2}} \cos\left[\Delta\omega t + \varphi_{c2}(t) - \varphi_{LO}(t) - \varphi_y\right] \quad (3\text{-}6)$$

$$I_{PD4} = 2RL_h \sqrt{2P_{s-c2}P_{LO}L_f L_{sc2}} \sin\left[\Delta\omega t + \varphi_{c2}(t) - \varphi_{LO}(t) - \varphi_y\right] \quad (3\text{-}7)$$

where R is the responsivity of the photodetectors.

The Digital signal-processing method to extract IM power-multiplexed signals is as follows:

$$I_{IM} = I_{PD1}^2 + I_{PD2}^2 =$$

$$= 4R^2 L_h^2 L_f P_{s-c1} P_{LO} L_{c1} \cdot \left(\cos\left[\frac{\alpha_1.\pi S_{RF1}(t) + \alpha_2.\pi S_{RF2}(t)}{2V_{\pi IM}} + \frac{\pi}{4}\right]\right)^2 \quad (3\text{-}8)$$

$$\approx 4R^2 L_h^2 L_f P_{s-c1} P_{LO} L_{c1} \left\{1 - \left[\frac{\pi\left(\alpha_1 \cdot \pi S_{RF1}(t) + \alpha_2 \cdot \pi S_{RF2}(t)\right)}{V_{\pi IM}}\right]\right\}$$

In practice, non-idealities in the modulation stages introduce IM/PM crosstalk at the coherent receiver. Equation (3-8) exploits the quadratic (square-law) operation enabled by the coherent I/Q outputs: since the I and Q branches are ideally in quadrature (90° phase shift), the combination $I_{PD1}^2 + I_{PD2}^2$ removes the phase-dependent terms (via the identity $cos^2(\cdot) + sin^2(\cdot) = 1$ and therefore suppresses the influence of the PM-induced phase term on the recovered IM component.

thus, both power-multiplexed signals are achieved, power-demultiplexing will also be explained later.

For PM-power-multiplexed signals, the DSP method is

$$I_{PM} = \tan^{-1}\left\{\frac{I_{PD2}\times I_{PD3}-I_{PD1}\times I_{PD4}}{I_{PD1}\times I_{PD3}+I_{PD2}\times I_{PD4}}\right\} = \tan^{-1}\left\{\frac{\sin\left[\begin{array}{l}\frac{\pi\left(\alpha_3\cdot\pi S_{RF3}(t)+\alpha_4\cdot\pi S_{RF4}(t)\right)}{V_{\pi PM}}\\ +\varphi_{c1}(t)-\varphi_{c2}(t)-\varphi_x+\varphi_y\end{array}\right]}{\cos\left[\begin{array}{l}\frac{\pi\left(\alpha_3\cdot\pi S_{RF3}(t)+\alpha_4\cdot\pi S_{RF4}(t)\right)}{V_{\pi PM}}\\ +\varphi_{c1}(t)-\varphi_{c2}(t)-\varphi_x+\varphi_y\end{array}\right]}\right\}$$

(3-9)

$$= \frac{\pi\left(\alpha_3\cdot\pi S_{RF3}(t)+\alpha_4\cdot\pi S_{RF4}(t)\right)}{V_{\pi PM}}+\varphi(t)$$

where $\varphi(t)$ is

$$\varphi(t)=\varphi_{c1}(t)-\varphi_{c2}(t)-\varphi_x+\varphi_y \tag{3-10}$$

and we can filter out the $\frac{\pi(\alpha_3 S_{RF3}(t)+\alpha_4 S_{RF4}(t))}{V_{\pi PM}}$, if its central frequency is higher than $\varphi(t)$. It is worth noting, while writing these equations, The harmonics due to the non-linearity of the modulators should not be ignored. After detection in the DSP unit, the harmonics should be filtered out due to the nonlinear property of squaring in (3-12) and inverse tangent in (3-13).

Interpretation of (3-9): It recovers the PM component by forming a phase estimate through a cross-combination of the coherent outputs from the two polarizations (e.g., XI, XQ, YI, and YQ). This structure is equivalent to extracting the phase of a complex quantity and therefore leverages the 90° I/Q relationship in both polarizations. Importantly, the “arctangent + cross-product” form cancels common amplitude factors, which mitigates the impact of residual IM leakage on the PM recovery. The unmodulated orthogonal polarization provides an effective reference, so the resulting output isolates the PM term plus the slowly varying phase term

The Critical Importance of Channel Length Matching: A crucial aspect of this orthogonal polarization approach is that the length difference in the fiber between Channels 1 and 2 must be carefully controlled to avoid phase mismatches at the receiver. This requirement stems from the fact that the DSP algorithm for signal recovery assumes that the beat notes in XI and YI are in-phase and have a 90° phase shift with respect to the beat notes from XQ and YQ.

If there is a significant length difference between the two channels, the phase relationship between the beat notes will be disrupted, leading to impaired signal recovery. This is because the phase of the optical carrier evolves as it propagates through the fiber, and any difference in path length will result in a phase difference between the two channels.

In our experimental implementation, we ensured that Channels 1 and 2 had precisely matched lengths to maintain the required phase relationship between the beat notes. When precise length matching was not feasible, we employed a variable optical delay line on Channel 2 to adjust the phase relationship and ensure proper beat note alignment.

This requirement for precise channel length matching represents a significant implementation challenge for the orthogonal polarization approach. It necessitates careful fiber measurements and potentially the use of additional components for phase adjustment, adding complexity to the system.

Now that both power-multiplexed AM and PM signals are achieved, we continue onward by explaining power demultiplexing and SIC. In brief, power multiplexing involves the simultaneous transmission of multiple data streams over a single channel by assigning them distinct power levels, as shown by their coefficients α_1, α_2, α_3 and α_4 in (3-4) and $\alpha_1 + \alpha_2 = 1$ & $\alpha_3 + \alpha_4 = 1$, allowing a receiver to differentiate between them based on these power ratios. Now, the signal processing technique in which overlapping signals are sequentially decoded, starting from the strongest signal, is called SIC; after decoding, each signal is subtracted from the received combination, facilitating the decoding of the second strongest signal. An interpretation of what SIC looks like is presented in Fig.3.2. Note that Fig. 3.2 is a conceptual illustration of the SIC principle (commonly used in wireless/NOMA literature) and is included only for explanation. In the experimental RoF setup presented in this thesis, no antenna and no over-the-air wireless link are used; SIC is applied digitally in the offline DSP to separate the power-multiplexed streams from the oscilloscope-captured waveforms.

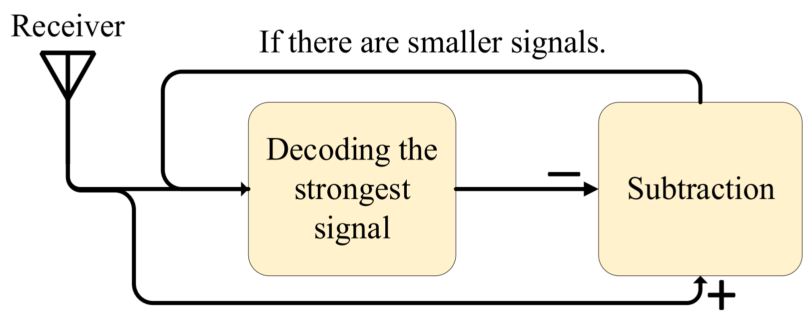

Fig 3.2 Successive interference cancellation (SIC) demodulation principle (conceptual illustration for explanation; not the experimental setup; no antenna/over-the-air link is used).

For example, for two QPSK, the constellation diagram is shown in Fig.3. As can be seen in Fig.3.3, the strongest signal is decoded first. Then, the weak signals can be decoded, but while decoding any signal, the weaker signals are detected as an interference.

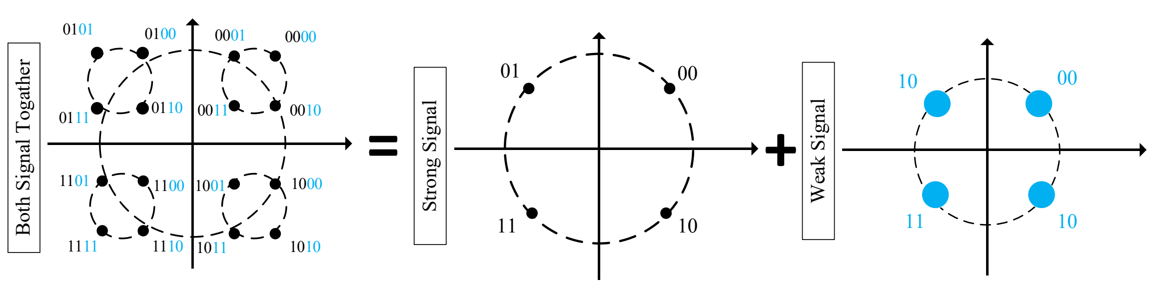

Fig 3.3 Constellation diagram of two power-multiplexed QPSKs.

3.2.2 Experimental Results

To validate the proposed high spectral efficiency power-multiplexed coherent MPL, a comprehensive experimental was constructed. A tunable laser source (Agilent N7714A) operating at 1550.00 nm and an output power of 16 dBm. The laser output was divided into two channels by an OC with a splitting ratio of 90:10 for channels 1 and 2, respectively. The optical signal was first routed through PC1 to a Mach-Zehnder modulator (MZM, Optilab 40 GHz Analog Modulator and insertion loss of 5 dB) biased at the quadrature point for amplitude modulation of the power-multiplexed microwave signal generated by an Arbitrary Wave Generator (Keysight M8195A) at a carrier frequency of 5 GHz. Then, the AM signal underwent phase modulation via a phase modulator (PM, Thorlabs 40 GHz High-speed electro-optic phase modulator and insertion loss of 4 dB) after passing PC2. The modulated signal is then directed through PC3 to a PBC. The PBC facilitated PDM of the modulated signal with the unmodulated light from Channel 2, which had been orthogonally aligned using polarization controllers (PC4). The experiment initially transmitted two pairs of power multiplexed QPSK signals, followed by a combination of 16QAM and QPSK signals. The symbol rate for each digital modulation was set at 0.5 Gbaud/s, resulting in bit rates of 2 Gb/s for the 16QAM and 1 Gb/s for the QPSK signals, which culminated in total system bit rates of 4 Gb/s and 6 Gb/s for the two scenarios, respectively. The optical signals were then transmitted over a 10 km SMF to a coherent receiver (Keysight N4391A). A second laser (from Agilent N7714A, via another port), tuned to 1550.01 nm with an output power of 16 dBm, serves as the local oscillator (LO) and is sent to the receiver via PC6. Due to the wavelength difference between the transmitter laser and the LO, a beat note is created, and its frequency is approximately 1.25 GHz, resulting in a frequency shift to the PMD microwave signals. All four IQ signals at the receiver's output are sent to a digital storage oscilloscope (DSO: Keysight DSOZ504A) with an 80 GSample/s sampling rate. These signals were subsequently processed using developed DSP algorithms to recover the microwave vector signals and cancel out phase noises from both the optical carrier and the LO, ensuring high fidelity in signal reconstruction and analysis.

All the I/Q signals are shown in Fig.3.4 (a-j); the modulated signals are on the X polarization, and the Y polarization state is only used to extract the beat note for the DSP algorithm. From Fig.3.4 (a), and Fig.3.4 (b), it can be understood that there are harmonics at 9 and 11 GHz, so we have filtered out all the noises and harmonics, as can be seen in Figure 3.4 (e), and all the noises have been filtered out from the beat note as shown in Fig.3.4 (f). After the DSP algorithm, the AM and PM signals also have harmonics since it is an inherent property of squaring and tangent inverse to have harmonics, and all these harmonics are visible in Fig.3.4 (g), and Fig.3.4 (h). and we have filtered them out at Fig.3.4 (i), and Fig.3.4 (j).

The recovered constellation diagrams of power-multiplexed signals after recovery and phase noise cancellation are shown in Fig. 3.5. All Fig. 3.5 (1) show the IM signals, and all Fig. 3.5 (2) show the PM signals.

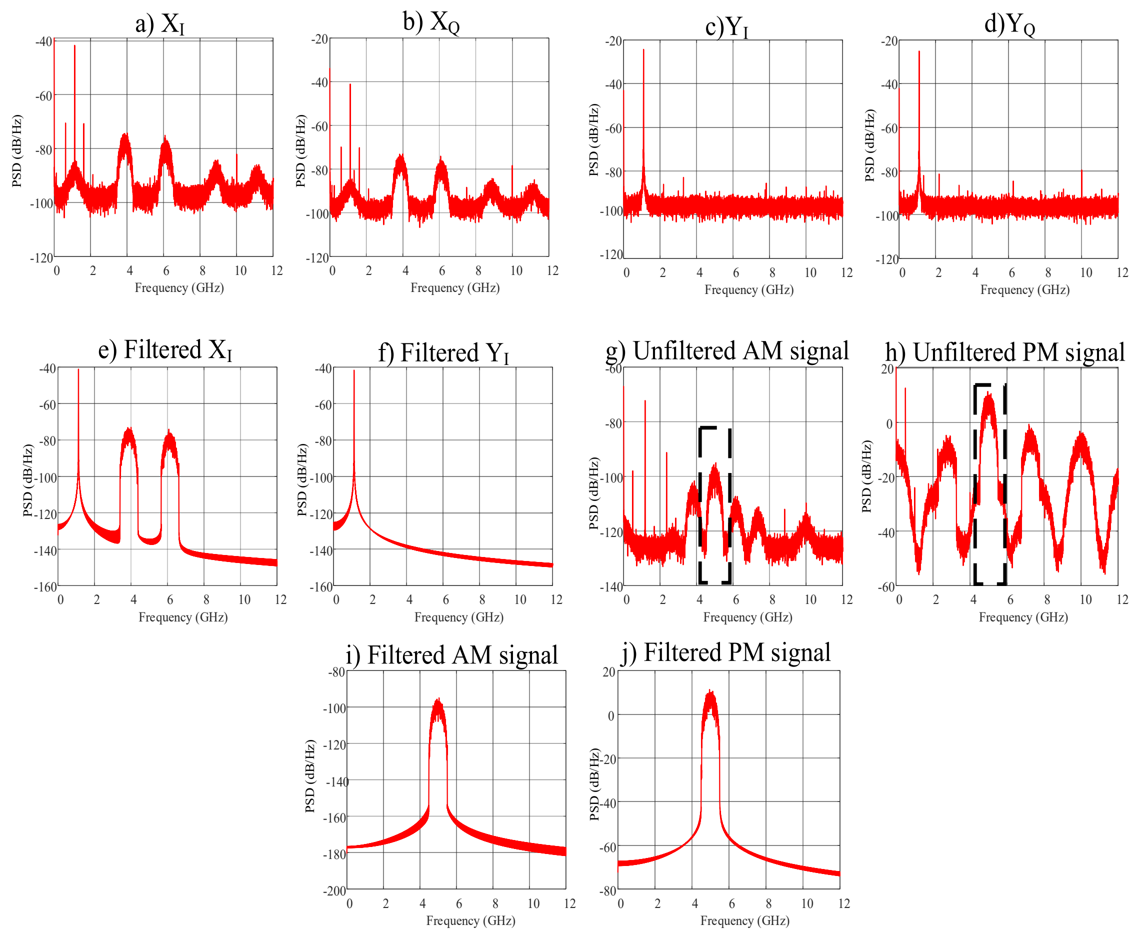

Fig 3.4 a) $\boldsymbol{X_I}$ after detection, b) $\boldsymbol{X_Q}$, c) $\boldsymbol{Y_I}$, d) $\boldsymbol{Y_Q}$, e) $\boldsymbol{X_I}$, only the beat note and the signal, f) $\boldsymbol{Y_I}$, only the beat note. g) AM-power-multiplexed signal after the DSP algorithm, h) PM-power-multiplexed signal after the DSP algorithm, i) AM-power-multiplexed signal after filtering, and j) PM-power-multiplexed signal after filtering.

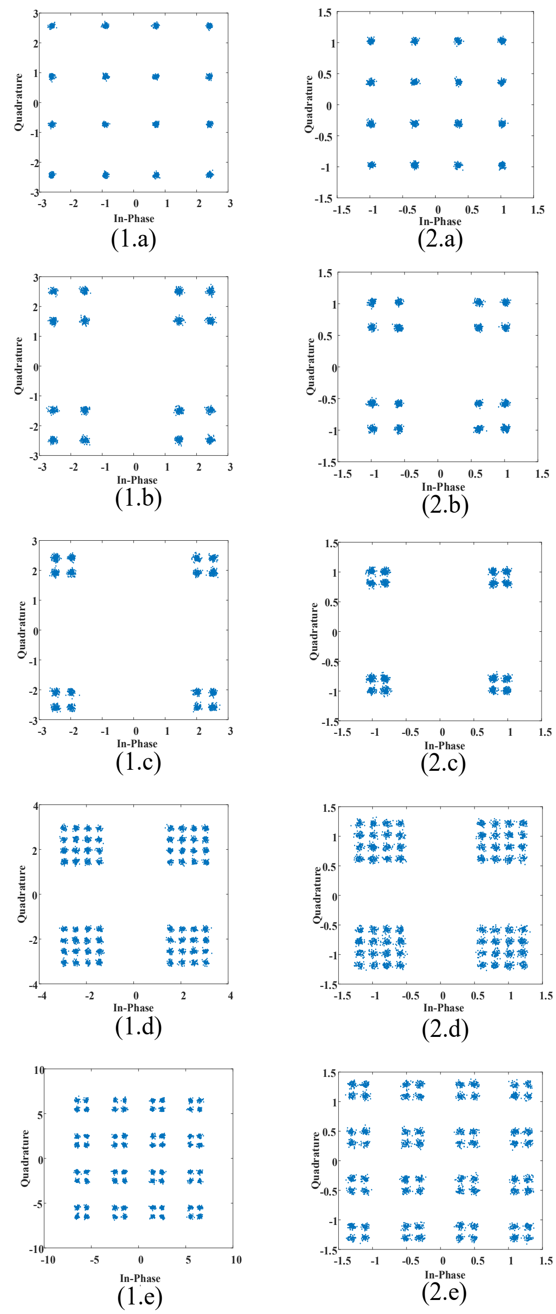

Fig 3.5 Constellation diagram of the recovered AM (at left) and PM (at right) power-multiplexed signals at the optical received power of -2 dBm. 1. a and 2. a) 0.66×QPSK+0.33×QPSK (power ratio 3 dB), 1. b and 2. b) 0.76×QPSK+0.24×QPSK (power ratio 5 dB), 1. c and 2. c) 0.84×QPSK+0.16×QPSK (power ratio 7 dB), 1.d and 2.d) 0.16×16QAM+0.84×QPSK (power ratio is 7 dB), 1. e and 2. e) 0.16×QPSK+0.84×16QAM (power ratio is 7dB).

As explained, SIC is used to separate the power-multiplexed signals, where the stronger signal is decoded first and subtracted from the power-multiplexed signal. The procedure is then repeated for the second strongest signal.

To further evaluate the system's performance, the EVMs for the four recovered QPSK microwave signals at different power allocation ratios are measured and shown in the Fig. 3.6 for both AM and PM received signals. It can be seen that the EVM performance of the strong QPSK gradually improves with the increase in the power allocation ratio for the strong signal, as the interference from the weak signal decreases. The optimal power allocation ratio for both QPSKs yields the best trade-off in EVM performance between the two signals, as shown in Fig. 7, where the EVM values for MZM Signals are approximately 2.8%, and for PM signals, they are approximately 3.2%.

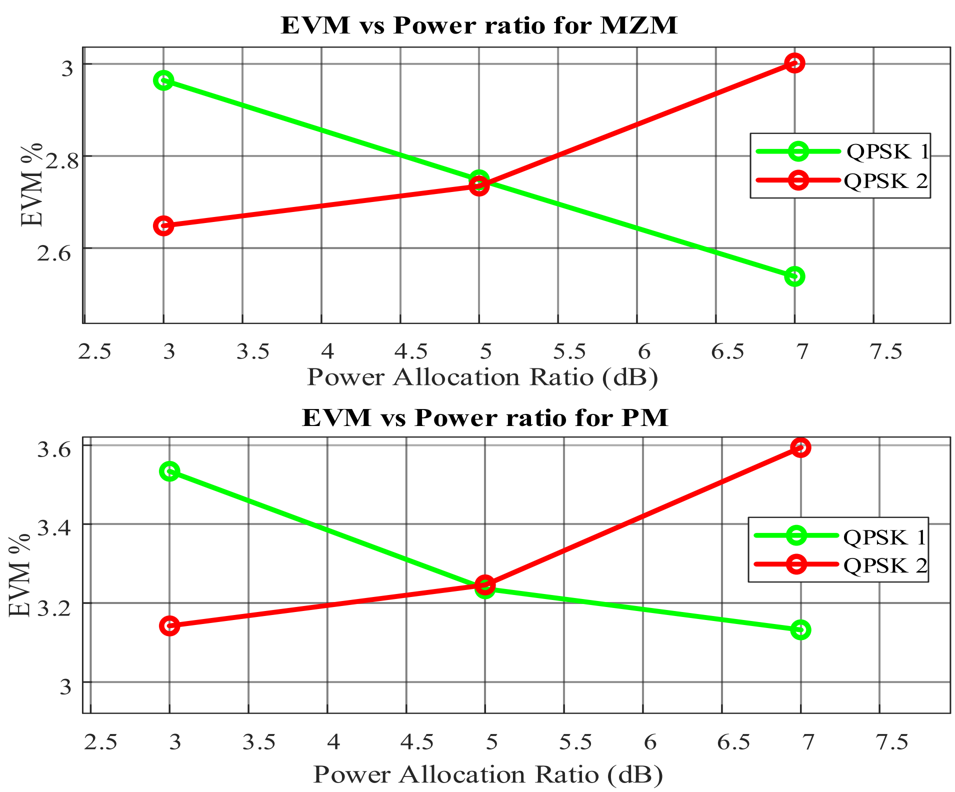

Fig 3.6 Measured EVM for 2QPSK modulated by MZM and PM, and optical received power fixed at -2dBm.

The measured EVM of recovered AM and PM signals at different received optical power levels is shown in Figs. 3.7 and 3.8.

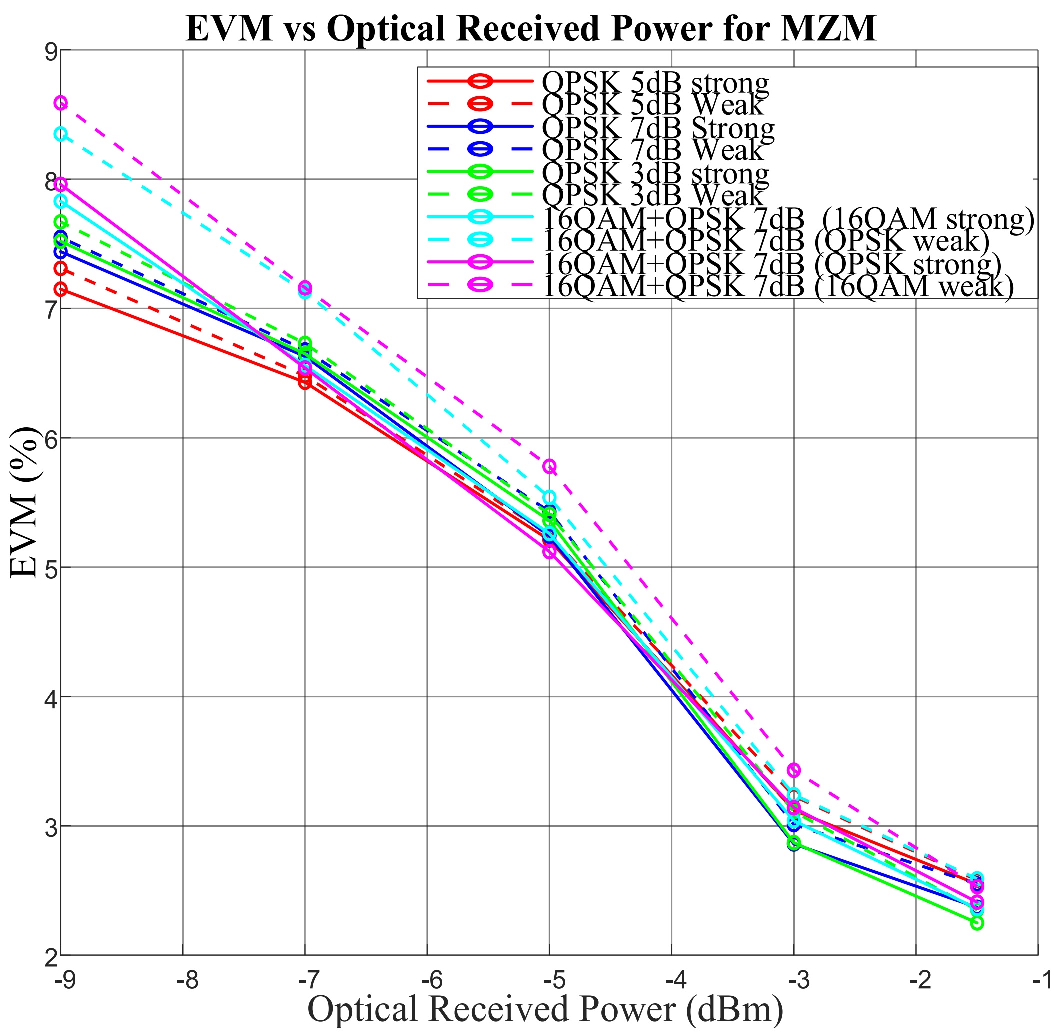

Fig 3.7 Measured EVMs of the AM received microwave vector signals.

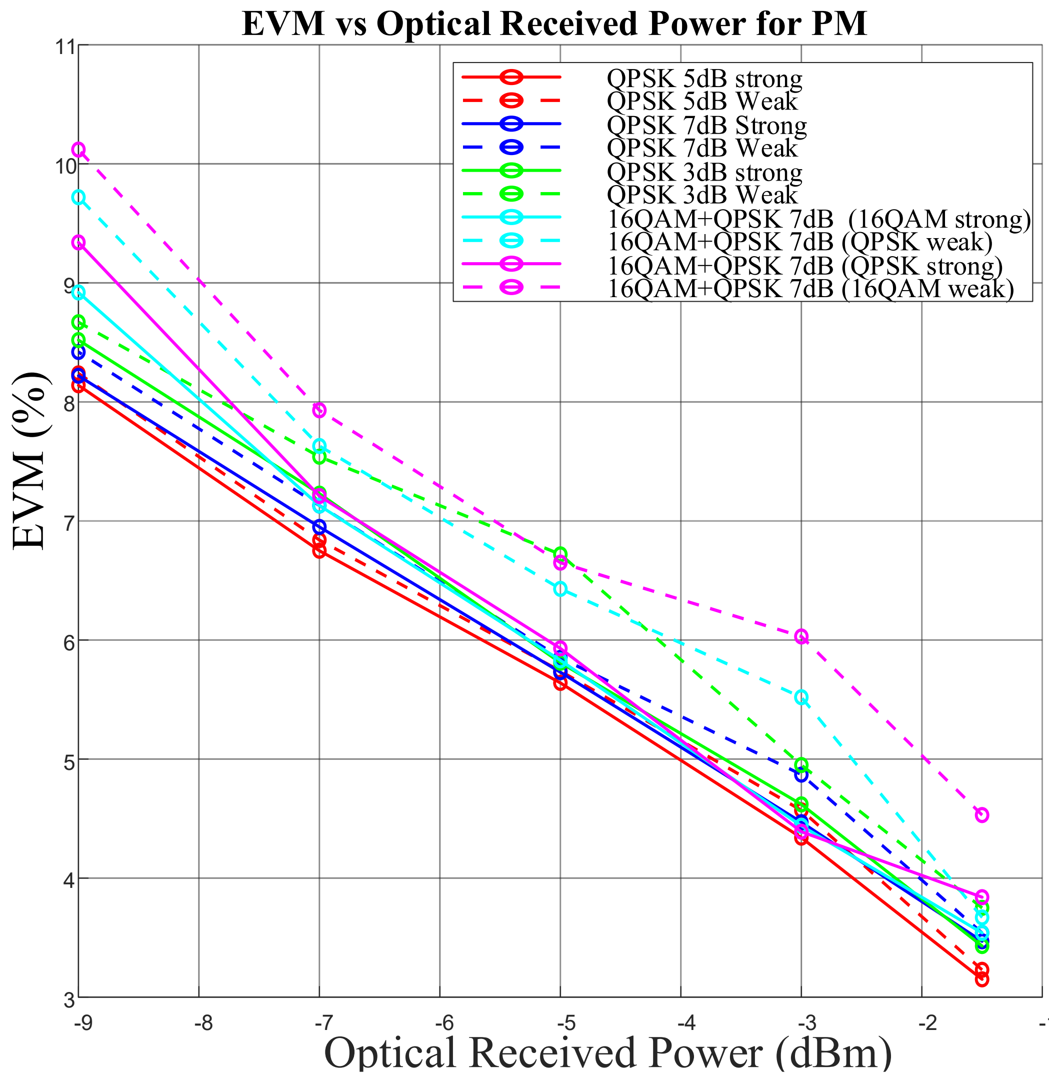

Fig 3.8 Measured EVMs of the PM received microwave vector signals.

Calculated bit error rates (BER) are shown in Fig. 3.9 and 3.10.

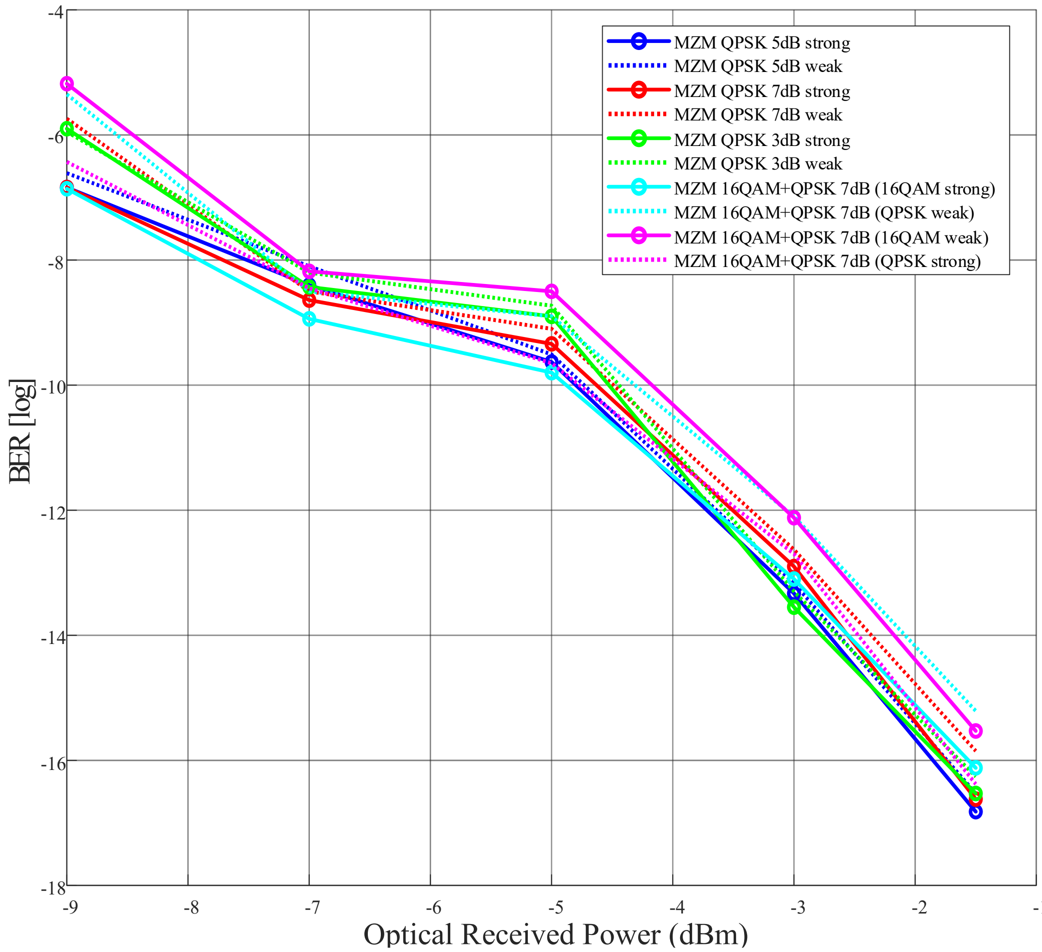

Fig 3.9 Calculated BER of AM signals.

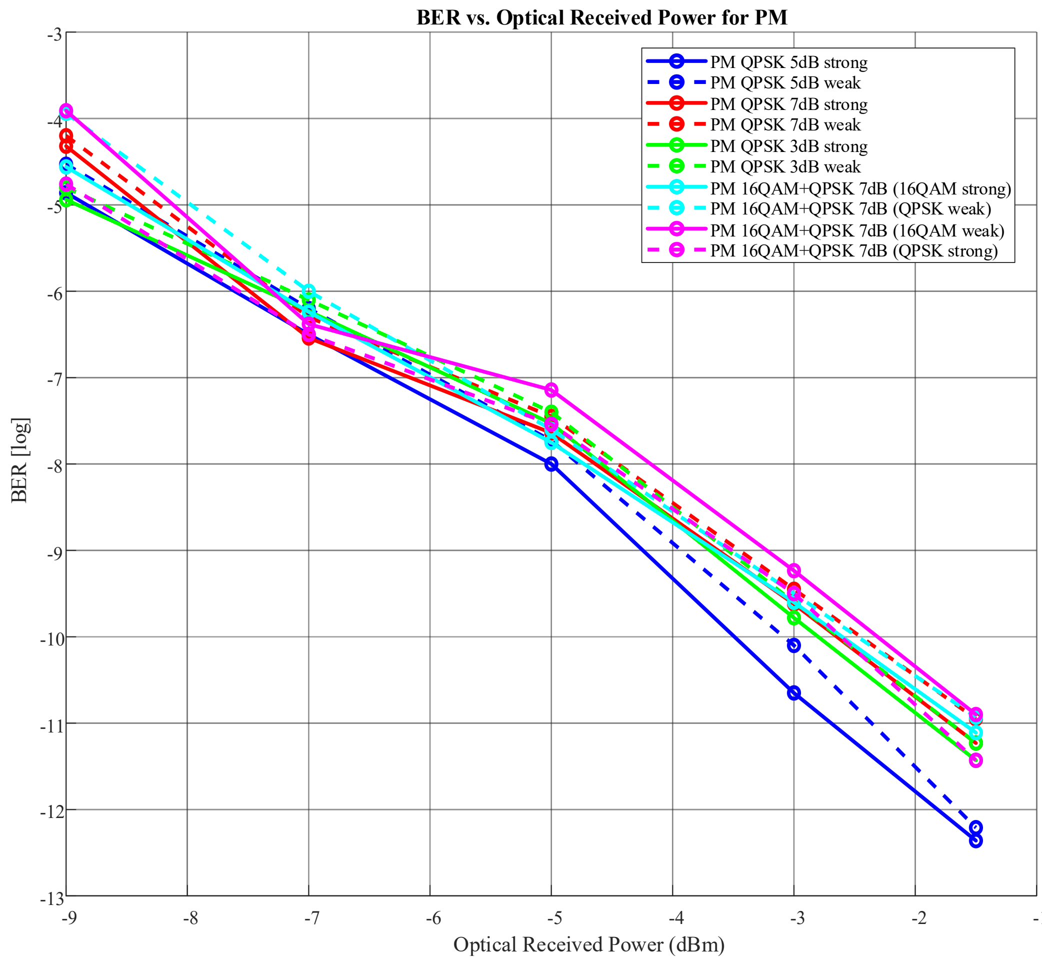

Fig 3.10 Calculated BER of PM signals.

The Error Vector Magnitude (EVM) measured for the AM constellation of 0.16×16QAM+0.84×QPSK (power ratio of 7 dB) was 2.41% for the strong QPSK and 2.53% for the weak 16QAM, with corresponding Bit Error Rates (BERs) of $10^{-16.38}$ and $10^{-15.53}$, respectively. For the PM signals, the EVMs were 3.84% for the strong QPSK and 4.5% for the weak 16QAM, with corresponding BERs of $10^{-11.43}$ and $10^{-10.9}$, respectively, at an optical received power of -1.5 dBm. Additionally, at an optical received power of -9 dBm, the EVMs for the AM and PM weak 16QAM reached 8.59% and 10.12%, respectively, and for the AM and PM strong QPSK, they were 7.96% and 9.34%. The BERs for the AM and PM weak 16QAM were $10^{-5.18}$ and $10^{-3.91}$, and for the AM and PM strong QPSK, they were $10^{-6.43}$ and $10^{-4.76}$, respectively. These values are well below the forward error correction (FEC) threshold of 3.8×10^{-3}, indicating that error-free transmission is achievable.

3.2.3 **Discussion**

In this study, we have successfully demonstrated a coherent MPL that employs high spectral efficiency power multiplexing, achieving significant improvements in data transmission rates. By integrating advanced amplitude and phase modulation techniques with digital phase noise cancellation. After transmission over an SMF, the optical signals were detected at a coherent receiver, to which an LO light wave from a free-running laser source was applied. Using the developed DSP algorithm, recovery of the two power multiplexed microwave vector signals, free from joint phase noise and unstable offset frequency, was achieved. An experiment was conducted, demonstrating the transmission of four independent microwave vector signals, each at a microwave frequency of 5 GHz, and a baud rate of 0.5 Gbaud/s, over a 10 km SMF. The EVMs for the recovered weak AM 16QAM signal were measured to be 2.59%, and for the strong AM QPSK signal, 2.36% at a received optical power of -1.5 dBm, and 8.59% and 7.96%, at a received optical power of -9 dBm and for the PM microwave signals, measured EVMs were 3.67% and 3.54% at optical received power of -1 dBm and 9.34% and 8.59% at optical received power of -9 dBm, respectively. These values are sufficient to achieve error-free transmission without and with forward error correction (FEC).

3.3 System Architecture (DD-MZM system)

3.3.1 Introduction

While the orthogonal polarization approach demonstrated in our first experimental work successfully implemented power multiplexing in coherent microwave photonic links, it faced a significant challenge in the requirement for precise channel length matching. To address this limitation, we developed an alternative approach that utilizes digital filtering techniques to extract the beat note after detection, eliminating the need for precise optical path length matching between channels.

3.3.2 System Architecture

The digital filter approach employs a DD-MZM to modulate the optical carrier with power-multiplexed microwave signals. Fig 3.11 illustrates the schematic diagram of this system, which consists of a transmitter and a coherent receiver connected by an SMF.

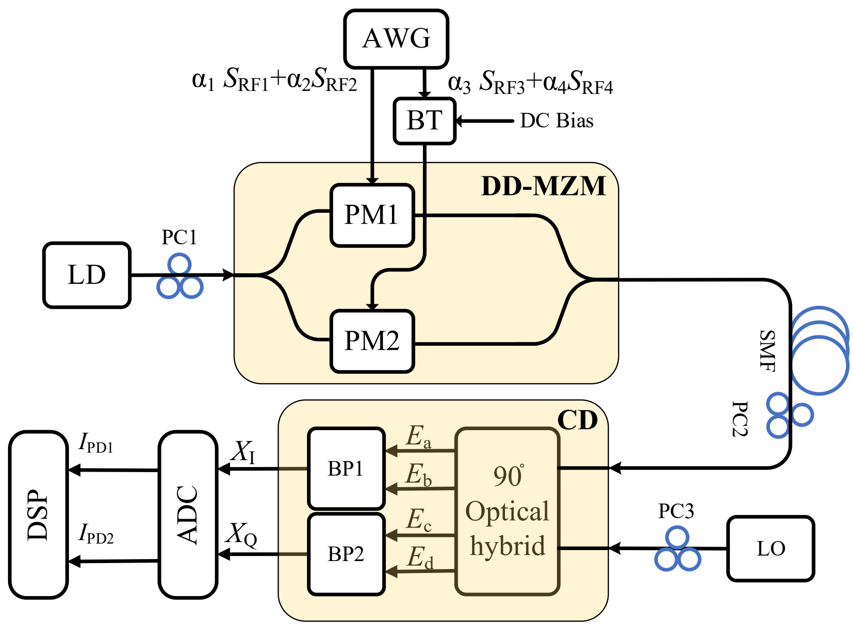

Fig 3.11 The schematic of the proposed MWP link: ADC: analog-to-digital converter (implemented by the built-in ADCs of the DSO used for waveform acquisition), AWG: arbitrary wave generator, BP: balanced photodetector, BT: Bias Tee, CD: coherent detector, DD-MZM: dual-drive Mach-Zehnder modulator, LO: local oscillator, OC: optical coupler, PC: polarization controller, SMF: single-mode fiber.

At the transmitter, an LD generates a CW light, which is sent via a PC to a DD-MZM. Unlike the previous approach that used separate modulators for amplitude and phase modulation, the DD-MZM integrates two PMs in its two arms, allowing for more compact and efficient modulation.

Two pairs of power-multiplexed microwave vector signals are applied to the DD-MZM via the two RF ports, generating two phase-modulated optical signals. The DD-MZM is biased to operate at the quadrature transmission point, which is achieved by applying a DC voltage through a bias tee. This quadrature biasing is crucial as it introduces a 90° phase shift between the signals in the two arms, allowing the receiver to differentiate between the power-multiplexed signals based on their phase difference.

The modulated optical signal is then transmitted over an SMF to a coherent receiver. At the receiver, a free-running laser serves as the local oscillator (LO), generating a CW light that is combined with the received signal in a 90° optical hybrid. The optical hybrid outputs four optical signals that are detected by balanced photodetectors, producing two electrical signals (XI and XQ) that contain both the desired microwave signals and the beat note between the transmitter laser and the LO. In the experimental implementation, XI and XQ are digitized by the built-in ADC of a real-time/digital storage oscilloscope, and the recorded samples are saved and processed offline by the DSP algorithm; therefore, the "ADC" block in Fig. 3.11 represents the oscilloscope sampling function and not a separate standalone device.

When the DD-MZM is biased at the quadrature transmission point, under small-signal modulation, the optical field at the output of the DD-MZM can be approximately expressed as

$$\begin{aligned} E_s(t) &= \frac{\sqrt{2P_sL}}{2}\exp\left[j\left(\omega_c t+\varphi_c(t)\right)\right]\times\begin{bmatrix} \exp\left[j\left(\dfrac{\pi}{V_\pi}\left(\alpha_1 s_{RF1}(t)+\alpha_2 s_{RF2}(t)\right)\right)\right] \\ +\exp\left[j\left(\dfrac{\pi}{V_\pi}\left(\alpha_3 s_{RF3}(t)+\alpha_4 s_{RF4}(t)\right)+\dfrac{\pi}{2}\right)\right]\end{bmatrix} \\ &\approx \frac{\sqrt{2P_sL}}{2}\exp\left[j\left(\omega_c t+\varphi_c(t)\right)\right]\times\left\{\frac{\pi}{V_\pi}\begin{bmatrix}\alpha_1 s_{RF1}(t)+\alpha_2 s_{RF2}(t) \\ +j\left(\alpha_3 s_{RF3}(t)+\alpha_4 s_{RF4}(t)\right)\end{bmatrix}+1+j\right\} \end{aligned} \tag{3-11}$$

where P_s is the power of the light at the output of the LD, ω_c is the angular frequency of the optical wave, S_{RF1} to S_{RF4} *are the RF signals*, L is the link loss between the LD and the DD-MZM, $\varphi_c(t)$ is the phase noise induced by the LD, V_π is the half-wave voltage of the DD-MZM, and $\alpha_1 - \alpha_4$are the allocated power ratios of the microwave vector signals. Note that $\alpha_1 + \alpha_2 = 1$ and $\alpha_3 + \alpha_4 = 1$. As can be seen from (1), the two power-multiplexed microwave signals are linearly mapped to the optical domain with a 90° phase shift between them introduced by the bias voltage, to make it operate at the quadrature transmission point. After transmission over the SMF, the optical signals are coherently detected at the coherent receiver. The coherent receiver consists of a 90° optical hybrid (OH) and two balanced photodetectors (BPDs).

For LO, a free-running light source is used, and the optical field at its output is given by

$$E_{LO}(t) = \sqrt{P_{LO}} \exp\left[j\left(\omega_{LO} t + \varphi_{LO}(t)\right)\right] \tag{3-12}$$

where P_{LO} is the optical power of the light at the output of the LO laser source, ω_{LO} is the angular frequency of the light, and $\varphi_{LO}(t)$ is its phase noise. After the 90° OH, four optical signals are obtained, which are given by

$$\left[E_a(t) \quad E_b(t) \quad E_c(t) \quad E_d(t)\right] = \left[E_x(t) \quad E_{LO}(t)\right] \begin{bmatrix} 1 & 1 & 1 & 1 \\ 1 & e^{j\pi} & e^{j\frac{\pi}{2}} & e^{-j\frac{\pi}{2}} \end{bmatrix} \tag{3-13}$$

and after photodetection, we have:

$$\begin{aligned} X_I(t) &= \frac{1}{2} R\left[E_a(t) E_a^*(t) - E_b(t) E_b^*(t)\right] \\ &= \frac{R\sqrt{2P_s L P_{LO}}}{2} \begin{Bmatrix} \cos\left[\Delta\omega t + \varphi(t)\right] \\ -\sin\left[\Delta\omega t + \varphi(t)\right] \end{Bmatrix} + \frac{R\pi\sqrt{2P_s L P_{LO}}}{2V_\pi} \begin{Bmatrix} (\alpha_1 s_{RF1}(t) + \alpha_2 s_{RF2}(t)) \cos\left[\Delta\omega t + \varphi(t)\right] \\ -(\alpha_3 s_{RF3}(t) + \alpha_4 s_{RF4}(t)) \sin\left[\Delta\omega t + \varphi(t)\right] \end{Bmatrix} \end{aligned}$$

(3-14)

$$X_Q(t) = \frac{1}{2}R\left[E_c(t)E_c^*(t) - E_d(t)E_d^*(t)\right]$$
$$= \frac{R\sqrt{2P_sLP_{LO}}}{2}\begin{Bmatrix} \sin\left[\Delta\omega t + \varphi(t)\right] \\ +\cos\left[\Delta\omega t + \varphi(t)\right] \end{Bmatrix} + \frac{R\pi\sqrt{2P_sLP_{LO}}}{2V_\pi}\begin{Bmatrix} (\alpha_1 s_{RF1}(t) + \alpha_2 s_{RF2}(t))\sin\left[\Delta\omega t + \varphi(t)\right] \\ +(\alpha_3 s_{RF3}(t) + \alpha_4 s_{RF4}(t))\cos\left[\Delta\omega t + \varphi(t)\right] \end{Bmatrix}$$

(3-15)

where $\Delta\omega$ is the offset frequency between the LD and the LO ($\Delta\omega = \omega_s - \omega_{LO}$), also $\varphi(t)$ is $\varphi_c(t) - \varphi_{LO}(t)$.

3.3.3 Digital Signal Processing Algorithm

The key innovation in this approach lies in the DSP algorithm used to extract the beat note and recover the transmitted signals. Unlike the orthogonal polarization approach, which required precise channel length matching to maintain the phase relationship between beat notes, the digital filter approach captures the beat note directly from the detected signals using digital filters.

When the transmitter laser and the LO are not phase-locked, the detected signals at the coherent receiver contain the joint phase noise from both lasers, as well as an unstable frequency offset due to the slight difference in wavelength between the two lasers. These impairments can severely degrade the quality of the recovered signals if not properly addressed.

The DSP algorithm developed for this system effectively mitigates these impairments through a series of filtering operations. The algorithm first separates the beat note from the modulated signals using a combination of lowpass filters (LPFs) and bandpass filters (BPFs). The LPFs extract the beat note, which contains the joint phase noise and frequency offset information, while the BPFs isolate the modulated signals without the beat note.

Mathematically, the DSP algorithm can be expressed as:

$$
\begin{aligned}
\alpha_1 s_{RF1}(t)+\alpha_2 s_{RF2}(t) &\propto \begin{bmatrix} \left(LPF\left(X_I\right)+LPF\left(X_Q\right)\right)\times BPF\left(X_I(t)\right) \\ +\left(LPF\left(X_Q\right)-LPF\left(X_I\right)\right)\times BPF\left(X_Q(t)\right) \end{bmatrix} \\
&= P_s L P_{LO} R^2 \left(\frac{\pi}{V_\pi}\right)\left[\alpha_1 s_{RF1}(t)+\alpha_2 s_{RF2}(t)\right]
\end{aligned}
\qquad (3\text{-}16)
$$

$$
\begin{aligned}
\alpha_3 s_{RF3}(t)+\alpha_4 s_{RF4}(t) &\propto \begin{bmatrix} \left(LPF\left(X_I\right)+LPF\left(X_Q\right)\right)\times BPF\left(X_Q(t)\right) \\ -\left(LPF\left(X_Q\right)-LPF\left(X_I\right)\right)\times BPF\left(X_I(t)\right) \end{bmatrix} \\
&= P_s L P_{LO} R^2 \left(\frac{\pi}{V_\pi}\right)\left[\alpha_3 s_{RF3}(t)+\alpha_4 s_{RF4}(t)\right]
\end{aligned}
\qquad (3\text{-}17)
$$

where LPF denotes a low-pass filtering operation, and BPF denotes a band-pass filtering operation.

Fig 3.12 illustrates the flow chart of this algorithm, showing how the beat note is extracted using LPFs and then combined with the filtered signals to recover the original microwave vector signals.

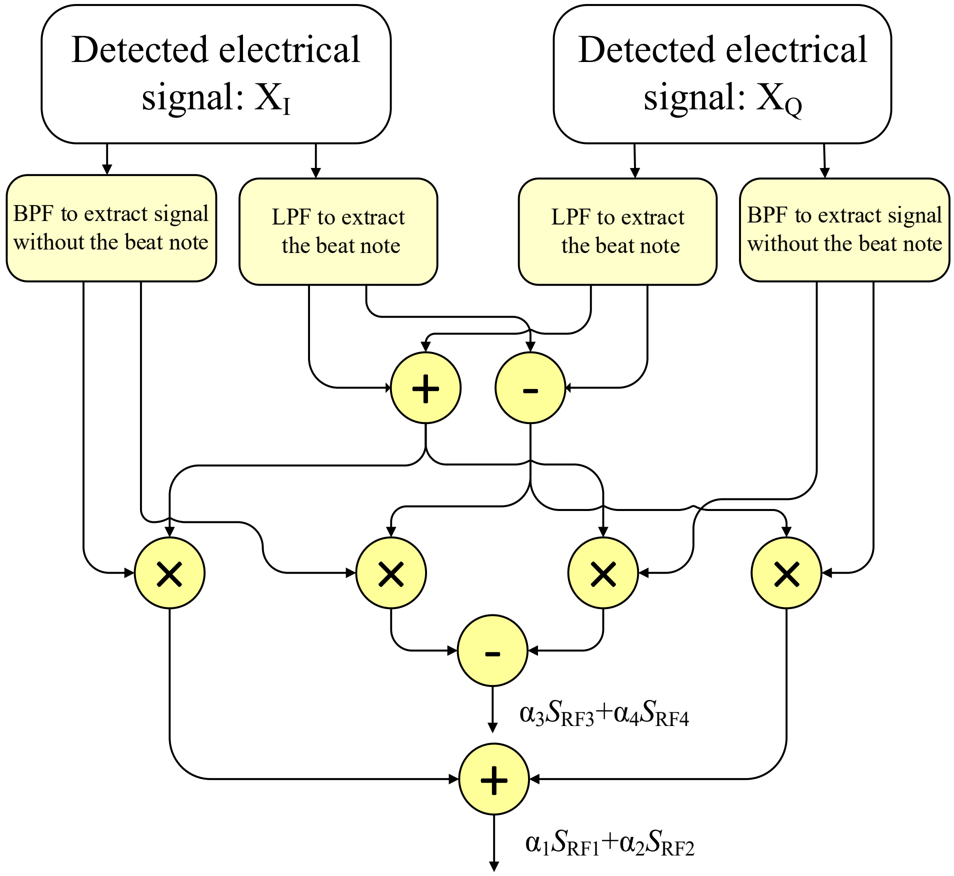

Fig 3.12 Flow chart of the algorithm to cancel the joint phase noise and the unstable offset frequency and recovery of the two power-multiplexed microwave vector signals. LPF: low-pass filter; BPF: bandpass filter.

Advantages of the Digital Filter Approach: The digital filter approach offers several significant advantages over the orthogonal polarization approach:

1. **Elimination of Channel Length Matching Requirement**: By extracting the beat note directly from the detected signals using digital filters, this approach eliminates the need for precise optical path length matching between channels. This simplifies the system design and improves robustness against environmental variations.

2. **Improved Flexibility**: The digital filter approach can adapt to different beat note frequencies and phase relationships through software adjustments, without requiring hardware modifications. This flexibility makes the system more versatile and easier to optimize for different operating conditions.

3. **Enhanced Scalability**: The digital filter approach can be more easily scaled to accommodate additional signals or higher modulation formats, as it does not face the physical constraints associated with maintaining precise optical path lengths.

4. **Reduced Hardware Complexity**: By using a single DD-MZM instead of separate modulators for amplitude and phase modulation, and by eliminating the need for polarization multiplexing and demultiplexing components, the digital filter approach reduces the hardware complexity and cost of the system.

3.3.4 Experimental results

To validate the proposed scheme, an experiment is conducted based on the setup shown in Fig. 3.11 CW optical wave at 1550 nm, generated by the transmitter laser source (Agilent N7714A) with an output power of 16 dBm, is directed to the DD-MZM (Fujitsu, FTM7821ER) via PC1. The DD-MZM, which has a half-wave voltage of 4 V, a 3 dB bandwidth of 10 GHz, and an insertion loss of 6 dB, consists of two PMs in its two arms. Two independent pairs of power-multiplexed microwave vector signals, generated by an arbitrary waveform generator (AWG, Keysight M8195A) with a sampling rate of 65 GSa/s and a bandwidth of 25 GHz, are applied to the PMs in the DD-MZM through the two RF input ports. Each power-multiplexed signal consisted of a weak 16QAM signal and a strong QPSK signal, each with a center frequency of 4 GHz and a baud rate of 0.5 Gbaud/s. The DD-MZM is biased at the quadrature transmission point. Two phase-modulated optical signals are generated and transmitted over a 10 km SMF to the coherent receiver (Keysight N4391A) via PC2.

Another CW optical wave at 1550.01 nm with a power of 16 dBm, obtained from another channel of Agilent N7714A, is used as the LO source and sent to the coherent receiver through PC3. The slight wavelength difference between the transmitter laser source and the LO laser source introduced an offset frequency of 1.25 GHz. Following coherent detection, two electrical signals are obtained, which are sampled by an oscilloscope (Keysight DSOZ504A) with a sampling rate of 80 GSa/s and a bandwidth of 32 GHz. The sampled signals are processed by a DSP unit, and based on the algorithm given in (3-16) and (3-17), the joint phase noise and unstable frequency offset are mitigated. The two power-multiplexed microwave signals are then demultiplexed to recover the four microwave vector signals.

Fig 3.13 (a) shows the spectrums of the two power-multiplexed signals at the output of the coherent receiver, denoted as X_I and X_Q, where the carrier frequency of the microwave signals at 4 GHz is down- and up-converted to 2.75 GHz and 5.25 GHz due to the 1.25 GHz beat note. For each power-multiplexed signal, a digital BPF is applied to extract the desired signal, as shown in Fig. 3.13 (b). The 1.25 GHz beat note is selected using an LPF with its spectrum shown in Fig. 3.13 (c). The four multiplexed microwave vector signals are recovered at the output of the DSP unit, with the spectrum shown in Fig. 3.13 (d). Fig 3.14 displays the measured constellations of the recovered power-multiplexed signals for two different power multiplexing ratios: (0.1 × 16QAM + 0.9 × QPSK) and (0.2 × QPSK + 0.8 × QPSK). SIC is used to separate the power-multiplexed signals, where the stronger signal is decoded first and subtracted from the power-multiplexed signal, and the procedure is repeated for the second stronger signal.

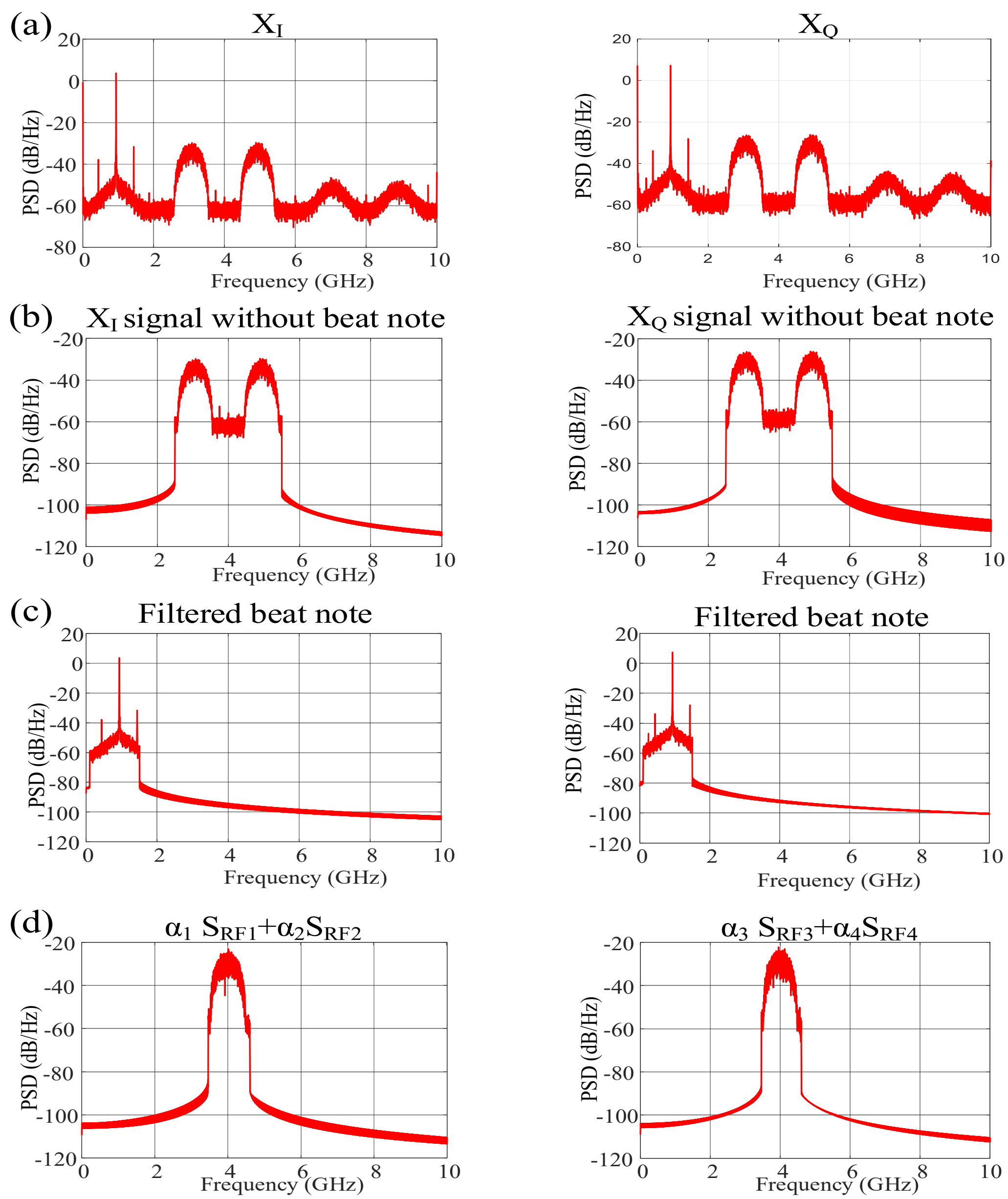

Fig 3.13 a) XI and XQ. b) Filtered signals without the beat note. c) Filtered beat notes, d) Signals after the DSP.

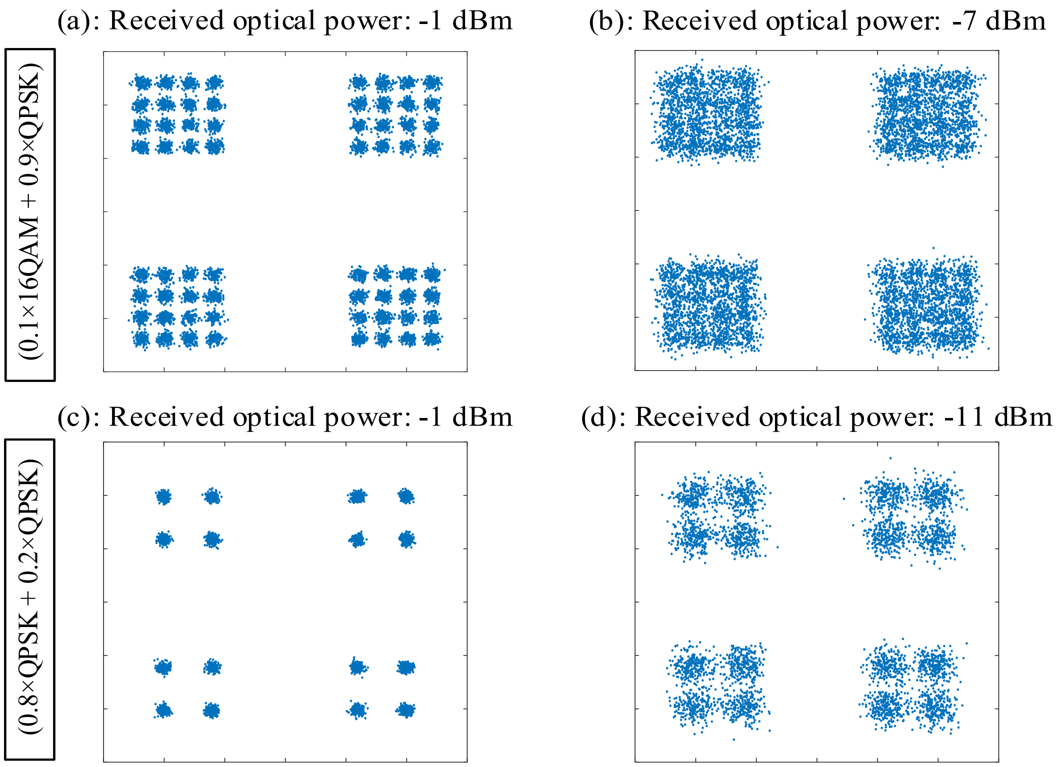

Fig 3.14 Constellation diagram of the recovered power-multiplexed microwave vector signals. 0.1×16QAM + 0.9×QPSK (power ratio:9.5dB) when the received optical power is (a) -1 dBm and (b) -7 dBm. 0.2×QPSK + 0.8×QPSK (power ratio: 6dB) when the received optical power is (c) -1dBm and (d) -7 dBm.

The measured EVMs of the recovered microwave vector signals at different received optical power levels are shown in Fig. 3.15. For the power multiplexing scheme (0.1×16QAM + 0.9×QPSK), the EVMs are measured to be 3.7% for the weak 16QAM signal and 2.5% for the strong QPSK signal at a received optical power of -1 dBm.

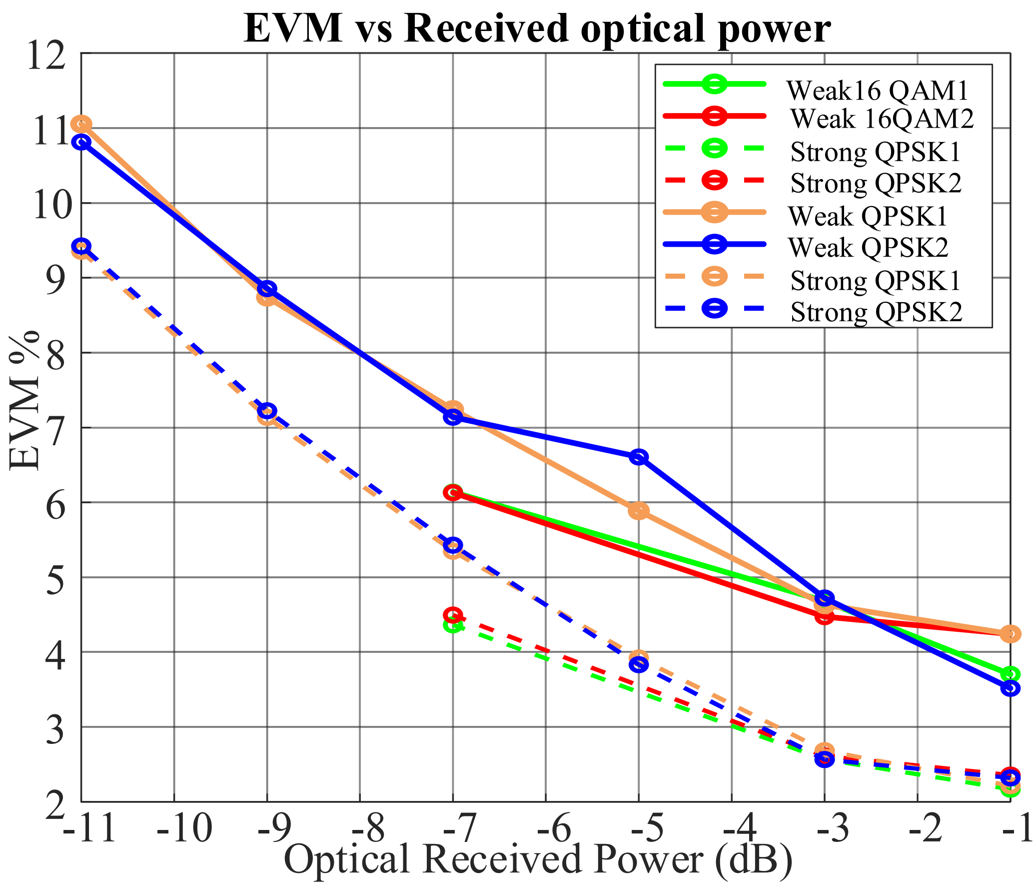

Fig 3.15 Measured EVMs of the received microwave vector signals.

The BERs of the recovered microwave vector signals are also calculated, which are depicted in Fig. 3.16 for both the strong QPSK and weak 16QAM signals. At a received optical power of -11 dBm, the EVMs for the two 16QAM microwave signals reach 11%, and for the strong QPSK microwave signals, the EVMs reach 9.3%, with the corresponding BERs of 10-4.5 and 10-6.1, respectively, which are well below the forward error correction (FEC) threshold of 3.8×10-3. However, increasing the optical power to -1 dBm results in BERs of 10-9.3 and 10-11, respectively, and error-free transmission can be achieved.

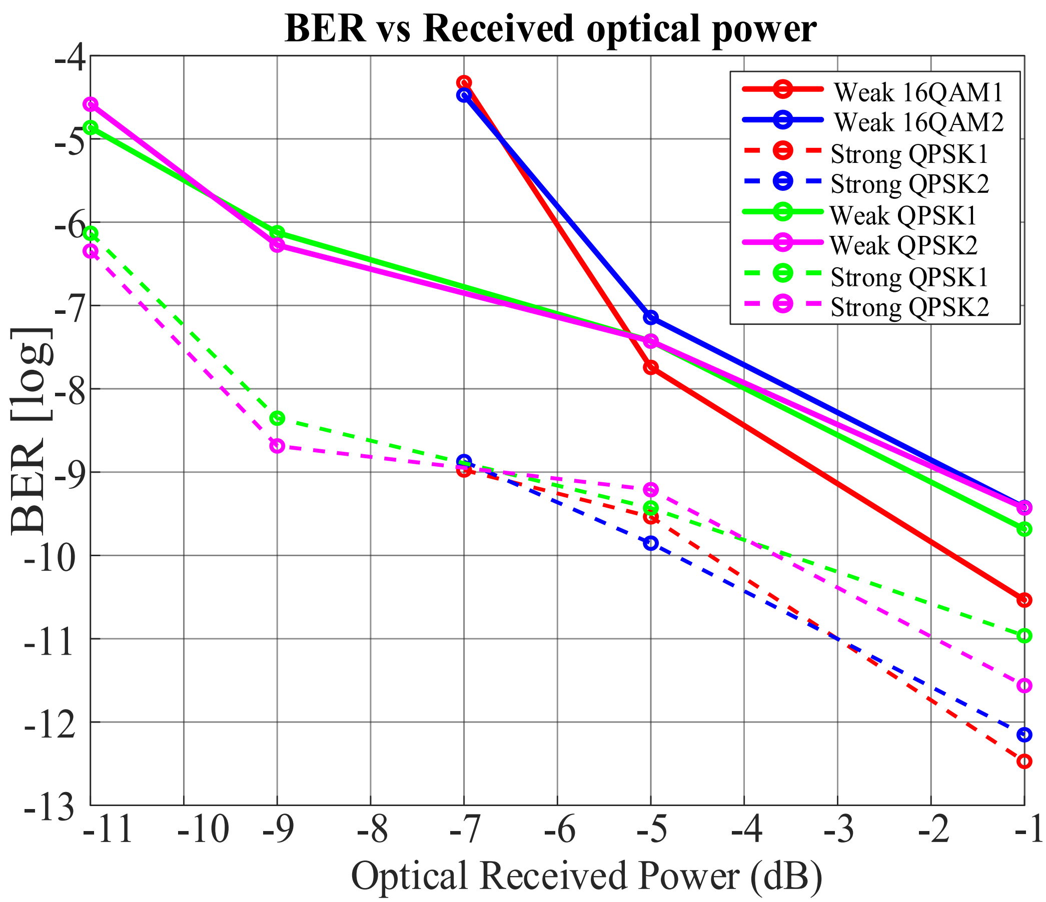

Fig 3.16 Calculated BERs of the received microwave vector signals.

3.3.5 Discussion

We have successfully demonstrated a coherent microwave photonic link incorporating power multiplexing to increase spectral efficiency and enhance data transmission capacity. At the transmitter, a DD-MZM was used at which two independent pairs of power-multiplexed microwave vector signals were phase-modulated on an optical carrier, to generate two phase-modulated optical signals. After transmission over an SMF, the optical signals were detected at a coherent receiver, to which an LO light wave from a free-running laser source was applied. Using the developed DSP algorithm, recovery of the two power-multiplexed microwave vector signals, free from joint phase noise and unstable offset frequency, was achieved. An experiment was conducted, demonstrating the transmission of four independent microwave vector signals, each at a microwave frequency of 4 GHz, and a baud rate of 0.5 Gbaud/s, over a 10-km SMF. The EVMs for the recovered weak 16QAM signal were measured to be 3.7%, and for the strong QPSK signal, 2.5% at a received optical power of -1 dBm, and 11% and 9.3% at a received optical power of -11 dBm. These values are sufficient to achieve error-free transmission without and with FEC.

3.4 Summary

Comparison of Orthogonal Polarization and Digital Filter Approaches: Having examined both the orthogonal polarization and digital filter approaches for implementing coherent detection in power-multiplexed microwave photonic links, it is valuable to directly compare these two methods to understand their relative strengths, limitations, and application scenarios.

System Architecture Comparison: The orthogonal polarization approach utilizes a more complex transmitter architecture, requiring separate modulators for amplitude and phase modulation, as well as polarization multiplexing components to combine the modulated signal with an unmodulated reference. This approach also necessitates polarization demultiplexing at the receiver to separate the two orthogonally polarized signals before coherent detection.

In contrast, the digital filter approach employs a more streamlined transmitter architecture based on a single DD-MZM. This integration of modulation functions into a single component reduces the hardware complexity and footprint of the transmitter. The receiver architecture is also simpler, as it does not require polarization demultiplexing components.

Beat Note Extraction Mechanisms: The primary difference between the two approaches lies in their mechanisms for extracting beat notes. The orthogonal polarization approach relies on an unmodulated optical carrier transmitted in an orthogonal polarization state to serve as a reference for generating the beat note at the receiver. This approach physically separates the reference signal from the modulated signal, ensuring that the reference remains unaffected by the modulation process.

The digital filter approach, on the other hand, extracts the beat note directly from the detected signals using digital filtering techniques. By applying lowpass filters to the in-phase and quadrature components of the detected signal, this approach isolates the beat note, which contains the joint phase noise and frequency offset information. This beat note is then used to recover the original microwave vector signals through a series of digital signal processing operations.

Channel Length Matching Requirements: Perhaps the most significant distinction between the two approaches is their sensitivity to optical path length differences. The orthogonal polarization approach requires precise matching of the optical path lengths between the modulated signal channel and the unmodulated reference channel. This requirement stems from the need to maintain a specific phase relationship between the beat notes generated from the two channels at the receiver.

As discussed earlier, even minor path length differences can introduce significant phase offsets, potentially degrading the system performance. This sensitivity to path length differences necessitates careful system design and potentially the use of variable optical delay lines for phase adjustment, adding complexity and cost to the implementation.

In stark contrast, the digital filter approach eliminates this channel length matching requirement by extracting the beat note directly from the detected signals using digital filters. This approach is inherently robust against optical path length variations, as it does not rely on maintaining a specific phase relationship between physically separated optical paths. This robustness simplifies the system implementation and improves its stability under varying environmental conditions.

Performance Comparison: Both approaches demonstrated comparable performance in terms of EVM and BER. The orthogonal polarization approach achieved EVMs of 2.59% for the 16QAM signal and 2.36% for the QPSK signal at a received optical power of -1.5 dBm. Similarly, the digital filter approach achieved EVMs of 3.7% for the weak 16QAM signals and 2.5% for the strong QPSK signals at a received optical power of -1 dBm.

These results indicate that both approaches can effectively implement power multiplexing in coherent microwave photonic links with high signal quality. However, the slight performance advantage of the orthogonal polarization approach in terms of EVM must be weighed against its higher implementation complexity and stricter channel length matching requirements.

Scalability and Flexibility: The digital filter approach offers superior scalability and flexibility compared to the orthogonal polarization approach. By eliminating the physical constraints associated with maintaining precise optical path lengths, the digital filter approach can more easily accommodate additional signals or higher modulation formats through software adjustments, without requiring hardware modifications.

Additionally, the digital filter approach can adapt to different beat note frequencies and phase relationships through digital signal processing, making it more versatile and easier to optimize for various operating conditions. This adaptability is particularly valuable in dynamic environments where system parameters may change over time.

Implementation Complexity and Cost: From an implementation perspective, the digital filter approach offers significant advantages in terms of complexity and cost. By using a single DD-MZM instead of separate modulators for amplitude and phase modulation, and by eliminating the need for polarization multiplexing and demultiplexing components, this approach reduces the hardware complexity and cost of the system.

Furthermore, the elimination of the channel length matching requirement simplifies the system design and installation process, potentially reducing deployment costs and improving reliability. The digital filter approach also reduces the need for precise optical components and alignment, further contributing to cost savings.

Conclusion: This chapter has explored two innovative approaches for implementing power multiplexing in coherent microwave photonic links, with a particular focus on the critical role of beat notes in coherent detection systems. The beat note, which occurs when the incoming optical signal interferes with a local oscillator at the receiver, is the fundamental mechanism that enables phase-sensitive detection in coherent systems. Without this beat note, the phase information of the optical signal would be lost during photodetection, as conventional photodetectors respond only to the intensity of light, not its phase.

We have demonstrated that for coherent detection to function properly, the beat note must be correctly aligned with the signal components. This alignment is critical because the phase relationship between the beat note and the signal determines the accuracy of the recovered information. Any phase mismatch between the beat note and the signal components can lead to distortion or even complete loss of the transmitted information.

The orthogonal polarization approach, presented in our first experimental work, utilized an unmodulated optical carrier transmitted in an orthogonal polarization state to serve as a reference for generating the beat note at the receiver. This approach physically separated the reference signal from the modulated signal, ensuring that the reference remained unaffected by the modulation process. However, it required precise matching of the optical path lengths between the modulated signal channel and the unmodulated reference channel to maintain the proper phase relationship between the beat notes.

The digital filter approach, introduced in our second experimental work, addressed this limitation by extracting the beat note directly from the detected signals using digital filtering techniques. By applying lowpass filters to the in-phase and quadrature components of the detected signal, this approach isolated the beat note, which contained the joint phase noise and frequency offset information. This innovation eliminated the need for precise optical path length matching, simplifying the system implementation and improving its stability under varying environmental conditions.

Both approaches successfully demonstrated the concept of power multiplexing in coherent microwave photonic links, achieving comparable performance in terms of EVM and BER. The orthogonal polarization approach achieved EVMs of 2.59% for the 16QAM signal and 2.36% for the QPSK signal at a received optical power of -1.5 dBm, while the digital filter approach achieved EVMs of 3.7% for the weak 16QAM signals and 2.5% for the strong QPSK signals at a received optical power of -1 dBm.

The progression from the orthogonal polarization approach to the digital filter approach represents a significant advancement in the practical implementation of coherent detection for power-multiplexed microwave photonic links. By addressing the channel length matching requirement, the digital filter approach made the technology more accessible and robust for real-world applications, while maintaining high performance.

In conclusion, the power multiplexing techniques presented in this chapter, combined with coherent detection and advanced digital signal processing, offer a promising solution for increasing the spectral efficiency and data transmission capacity of microwave photonic links. These innovations pave the way for high-capacity, spectrally efficient communication systems that can meet the growing bandwidth demands of next-generation networks.

Chapter 4 Self-Coherent Detection for High Spectral Efficiency RoF Links

4.1 Overview of Self-Coherent Detection

The relentless growth in data traffic and the increasing demand for high-speed wireless communication systems have driven researchers to explore innovative techniques to enhance spectral efficiency in RoF systems. While traditional intensity modulation with direct detection (IM/DD) systems offer simplicity in implementation, they suffer from limited spectral efficiency as they can only detect intensity-modulated signals [13],[51],[75]. Coherent detection systems, which utilize a local oscillator at the receiver to detect both amplitude and phase information, offer significantly higher spectral efficiency and improved receiver sensitivity [22],[86]. However, these advantages come at the cost of increased system complexity, higher power consumption, and greater expense due to the need for a local oscillator, optical hybrids, and balanced photodetectors [114].

Self-coherent detection has emerged as a promising alternative that bridges the gap between the simplicity of direct detection and the spectral efficiency of coherent detection. By eliminating the need for a separate local oscillator at the receiver, self-coherent detection systems offer a more cost-effective and energy-efficient solution for high-capacity next-generation RoF networks [88],[117]. The fundamental principle of self-coherent detection involves transmitting a reference signal [148],[149], often referred to as a pilot carrier or pilot tone, along with the data-carrying signals on the same optical carrier. This pilot carrier, generated from the same laser source as the data signals, serves as a self-reference that enables the recovery of both amplitude and phase information at the receiver through direct detection followed by appropriate digital signal processing [40],[148].

The concept of self-coherent detection represents a significant advancement in microwave photonic links, offering several key advantages over traditional coherent detection systems. First, by eliminating the need for a separate local oscillator at the receiver, self-coherent detection systems reduce hardware complexity, power consumption, and cost. Second, since the pilot carrier and data signals are generated from the same laser source, the phase noise correlation between them can be exploited to achieve effective phase noise cancellation through digital signal processing. Third, self-coherent detection systems can achieve spectral efficiencies comparable to those of traditional coherent systems while maintaining the simplicity of direct detection at the receiver.

In recent years, various approaches to self-coherent detection have been proposed and demonstrated, each with its own unique characteristics and performance trade-offs. These include Stokes Vector Receivers, which transmit the pilot carrier on an orthogonal polarization state relative to the modulated optical signal, and KK detection methods, which utilize a pilot tone transmitted along with an SSB microwave signal. While these approaches have shown promising results, they still face challenges in terms of implementation complexity, spectral efficiency, and carrier-to-signal power ratio requirements [40],[41],[148].

This chapter presents a novel self-coherent detection technique that addresses these challenges by modulating two independent microwave vector signals, along with a single-sideband pilot carrier, on a single optical carrier using a DD-MZM. This approach enables the transmission of multiple data streams with high spectral efficiency while maintaining the simplicity of direct detection at the receiver. Through a combination of innovative system architecture and advanced digital signal processing algorithms, this self-coherent detection technique achieves error-free transmission of complex modulation formats with minimal hardware complexity.

The remainder of this chapter is organized as follows: Section 4.1.1 provides an overview of various types of self-coherent detection techniques, highlighting their principles, advantages, and limitations. Section 4.2 describes the system architecture of the proposed DD-MZM-based self-coherent detection system, including the transmitter design, receiver configuration, and mathematical model. Section 4.3 details the digital signal processing algorithms used for signal recovery and phase noise cancellation. Section 4.4 presents the experimental results, demonstrating the performance of the proposed system in terms of EVM, BER, and constellation quality. Finally, Section 4.5 summarizes the key findings and contributions of this work, highlighting the potential of self-coherent detection for high-capacity next-generation RoF networks.

4.1.1 Various Types of Self-Coherent Detection

Stokes Vector Receivers [44],[89],[151]: Stokes Vector Receivers (SVRs) represent one of the earliest and most widely studied approaches to self-coherent detection. In SVR systems, the pilot carrier is transmitted on an orthogonal polarization state relative to the modulated optical signal from the transmitter to the receiver. This approach enables the detection of both the intensity and phase of the optical carrier without requiring a separate local oscillator at the receiver.

The basic principle of SVR operation involves dividing the light generated at the transmission site into two branches: one remains unmodulated and serves as a reference, while the other undergoes modulation with the data signals. These two branches are then polarization-multiplexed for transmission over a single fiber. At the receiver, the polarization states are separated, and the unmodulated reference is used to recover the phase information of the modulated signal.

SVR systems offer several advantages, including improved receiver sensitivity compared to traditional direct detection systems and the ability to compensate for linear impairments such as chromatic dispersion and polarization mode dispersion. However, they still require polarization-diversity components at the receiver, which adds to the system complexity and cost. Recent advancements in SVR technology have focused on miniaturization and integration, with researchers developing compact implementations using technologies such as spin-dependent optical gratings and dielectric metasurfaces.

For example, researchers have demonstrated high-speed Stokes vector receivers enabled by spin-dependent liquid crystal gratings that can separate the circular and linear components of incident light, allowing polarization states to be resolved with high accuracy. These systems have achieved Stokes vector direct detection of quadrature phase-shift keying (QPSK), and 16QAM signals with data rates of up to 32 GBd. Other implementations have utilized silicon photonic platforms to create monolithically integrated SVR receivers, demonstrating transmission rates of up to 128 Gb/s over distances of 100 km.

KK Detection: KK detection represents another important approach to self-coherent detection. This method is based on the famous KK relations, which establish a mathematical relationship between the real and imaginary parts of a complex function that is analytic in the upper half of the complex plane. In the context of optical communications, the KK relations can be used to recover the phase of a minimum-phase signal from its amplitude, enabling the reconstruction of the complex-valued optical field from intensity measurements alone [38]-[42].

The KK detection method involves transmitting a strong carrier tone at one edge of the signal spectrum, ensuring that the received signal satisfies the minimum-phase condition. At the receiver, the intensity of the optical signal is detected using a single photodiode, and the KK relations are applied to recover the phase information. This approach allows for the digital compensation of linear propagation impairments, such as chromatic dispersion and polarization mode dispersion, without requiring the complex optical front-end of traditional coherent receivers.

KK detection offers several advantages, including simplified receiver hardware (requiring only a single photodiode instead of multiple balanced photodetectors and optical hybrids) and improved spectral efficiency compared to other self-coherent approaches. However, it also has some limitations, including a more stringent requirement on the power of the transmitted carrier tone and the need for high-speed analog-to-digital converters with sufficient resolution to capture the large dynamic range of the received signal.

Recent research in KK detection has focused on optimizing the trade-off between carrier-to-signal power ratio and system performance, as well as developing efficient digital signal processing algorithms for phase recovery and impairment compensation. Experimental demonstrations have shown that KK detection can achieve performance comparable to traditional coherent detection in terms of reach and spectral efficiency, while significantly reducing receiver complexity and cost.

Single-Sideband Pilot Carrier Technique [150]-[152]: The SSB pilot carrier technique represents a more recent advancement in self-coherent detection, offering a balance between implementation simplicity and spectral efficiency [36],[37],[150]. This approach, which is the focus of our current work, involves modulating two independent microwave vector signals, along with a single-sideband pilot carrier, on a single optical carrier using a DD-MZM [153].

In this technique, the SSB pilot carrier is generated by applying an RF carrier and its Hilbert transform to each arm of a biased DD-MZM, which helps in the detection of both intensity and phase information of the transmitted light. The modulated optical signals are then transmitted over a single-mode fiber to a photodetector at the receiver, where direct detection is performed. A digital signal processing algorithm is employed to recover the transmitted microwave signals and cancel the phase noise introduced by the system.

The SSB pilot carrier technique offers several key advantages over other self-coherent detection approaches. First, it eliminates the need for polarization-diversity components at the receiver, as both the pilot carrier and data signals are transmitted in a single polarization state. This significantly reduces the hardware complexity and cost of the receiver. Second, it achieves higher spectral efficiency compared to traditional self-coherent approaches, as it does not require a frequency gap between the pilot carrier and the data signals. Third, it enables effective phase noise cancellation through digital signal processing, as the pilot carrier and data signals experience the same phase noise from the laser source.

Our experimental results, which will be discussed in detail in Section 4.4, demonstrate that the SSB pilot carrier technique can achieve error-free transmission of complex modulation formats, such as 16QAM and QPSK, with error vector magnitudes (EVMs) of less than 3% at optical powers as low as -5 dBm. This performance is comparable to that of traditional coherent detection systems, but with significantly reduced hardware complexity and cost.

In summary, self-coherent detection offers a promising approach for high spectral efficiency RoF links, combining the advantages of coherent detection with the simplicity of direct detection. Among the various self-coherent detection techniques, the SSB pilot carrier approach stands out for its balance of spectral efficiency, implementation simplicity, and performance, making it particularly well-suited for next-generation high-capacity RoF networks.

4.2 System Architecture of a DD-MZM System

The proposed self-coherent detection system employs a DD-MZM architecture that enables the transmission of two independent microwave vector signals on a single optical carrier, along with a single-sideband (SSB) pilot carrier. This innovative approach achieves high spectral efficiency while maintaining the simplicity of direct detection at the receiver. This section provides a detailed description of the system architecture, including the transmitter design, receiver configuration, and the mathematical model that governs the system operation.

4.2.1 Transmitter Design

Fig 4.1 illustrates the schematic diagram of the proposed microwave photonic link based on self-coherent detection with a DD-MZM system.

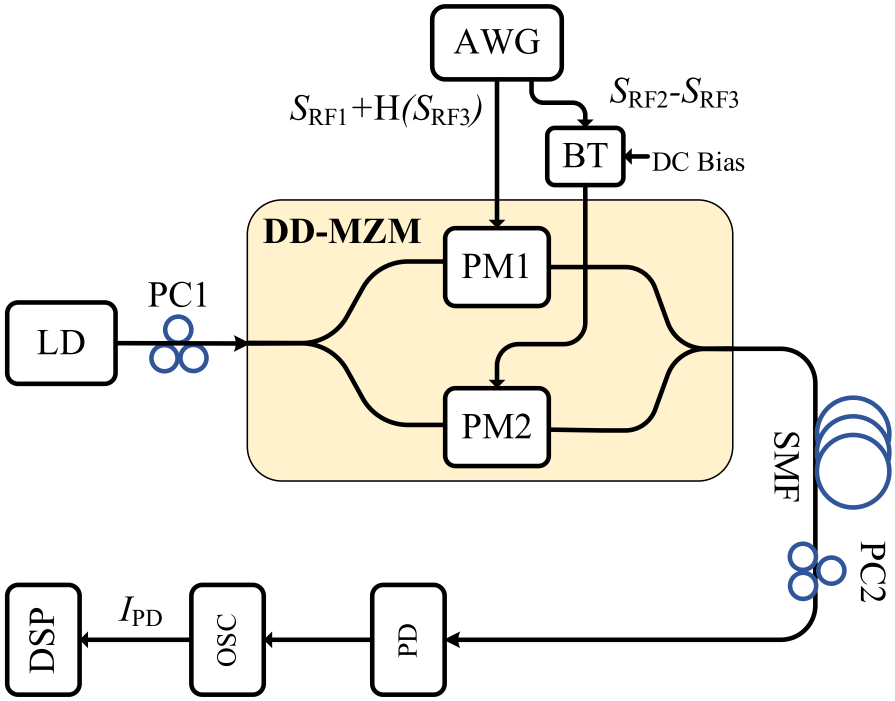

Fig 4.1 The schematic of the proposed MWP link: AWG: Arbitrary wave generator, BT: Bias Tee, DD-MZM: Dual-drive Mach-Zehnder modulator, DSP: Digital signal processing unit, H: Hilbert-transform, LD: Laser diode, OSC: Oscilloscope, PC: Polarization controller, PD: Photodetector, PM: Phase modulator, SMF: Single-mode fiber.

At the transmitter, a laser diode (LD) generates a continuous wave (CW) optical carrier at a wavelength of 1550 nm. This optical carrier is directed through a polarization controller (PC1) to ensure proper alignment with the input of the DD-MZM. The DD-MZM is the key component in the transmitter architecture, featuring two phase modulators (PMs), one in each arm of the interferometric structure.

The DD-MZM is biased to operate at the quadrature transmission point, which is achieved by applying a DC voltage through a bias tee. This bias point is critical as it introduces a 90° phase shift between the two arms of the modulator, enabling the differentiation of the RF signals by their phase difference. This phase relationship is essential for the subsequent signal recovery process at the receiver.

Two independent microwave vector signals ($S_{RF1}$and S_{RF2}) and one single-sideband pilot carrier (S_{RF3}) are applied to the DD-MZM via its two radio-frequency (RF) ports. The SSB pilot carrier is generated by applying an RF carrier and its Hilbert transform to each arm of the biased DD-MZM. This approach ensures that the pilot carrier is transmitted as a single sideband, which is crucial for the detection of both intensity and phase information of the transmitted light.

The mathematical representation of the optical field at the output of the DD-MZM can be expressed as:

$$E_s(t) \propto \exp\left[j\left(\omega_c t + \varphi_c(t)\right)\right] \times \begin{bmatrix} \exp\left[j\left(\frac{\pi}{V_\pi}\left(S_{RF1}(t) + \mathrm{H}\left(S_{RF3}(t)\right)\right)\right)\right] \\ +\exp\left[j\left(\frac{\pi}{V_\pi}\left(S_{RF2}(t) - S_{RF3}(t)\right) + \frac{\pi}{2}\right)\right] \end{bmatrix} \quad (4\text{-}1)$$

where ω_c is the angular frequency of the optical wave, $\varphi_c(t)$ is the phase noise induced by the LD, V_π is the half-wave voltage of the DD-MZM, S_{RF1} and S_{RF2} are the independent microwave signals and H is the Hilbert transform that is used to make the SSB pilot carrier.

Since $S_{RF3} = \cos\left(\omega_{pc} t + \varphi_{pc}(t)\right)$ where ω_{pc} is the angular frequency of the pilot carrier and $\varphi_{pc}(t)$ is the phase noise induced by the AWG, the electric field at the output of the transmitter will be:

$$E_s(t) \propto \exp\left[j\left(\omega_c t + \varphi_c(t)\right)\right] \times \begin{bmatrix} \exp\left[j\left(\frac{\pi}{V_\pi}\left(S_{RF1}(t) + \mathrm{H}\left(\cos\left(\omega_{pc} t + \varphi_{pc}(t)\right)\right)\right)\right)\right] \\ +\exp\left[j\left(\frac{\pi}{V_\pi}\left(S_{RF2}(t) - \cos\left(\omega_{pc} t + \varphi_{pc}(t)\right)\right) + \frac{\pi}{2}\right)\right] \end{bmatrix} \quad (4\text{-}2)$$

By small signal analysis, the field can be estimated as

$$E_s(t) \propto \exp\left[j\left(\omega_c t+\varphi_c(t)\right)\right]\times\left\{\begin{array}{l}\left[\frac{\pi}{V_\pi}\times\left[jS_{RF1}(t)-S_{RF2}(t)\right]+1+j\right]\\+\frac{\pi}{V_\pi}\left(j.\mathrm{H}\left(S_{RF3}(t)\right)+S_{RF3}(t)\right)\end{array}\right\}$$

$$=\exp\left[j\left(\omega_c t+\varphi_c(t)\right)\right]\times\left\{\begin{array}{l}\left[\frac{\pi}{V_\pi}\times\left[jS_{RF1}(t)-S_{RF2}(t)\right]+1+j\right]\\+\frac{\pi}{V_\pi}\left(\begin{array}{c}j.\sin\left(\omega_{pc}t+\varphi_{pc}\right)+\\\cos\left(\omega_{pc}t+\varphi_{pc}\right)\end{array}\right)\end{array}\right\}$$

$$=\exp\left[j\left(\omega_c t+\varphi_c(t)\right)\right]\times\left\{\begin{array}{l}\left[\frac{\pi}{V_\pi}\times\left[jS_{RF1}(t)-S_{RF2}(t)\right]+1+j\right]\\+\frac{\pi}{V_\pi}.\exp\left(j\left(\omega_{pc}t+\varphi_{pc}(t)\right)\right)\end{array}\right\} \quad (4\text{-}3)$$

This expression shows that the two microwave signals are linearly mapped onto the optical domain with a 90° phase shift introduced by the bias voltage. The SSB pilot carrier is realized through the combination of the Hilbert transform and the quadrature bias point of the DD-MZM.

In this experimental demonstration, the system is evaluated in an offline (post-processing) manner rather than in real time. Specifically, the receiver electrical waveforms are digitized by the built-in ADCs of the DSO used for acquisition, saved to disk, and subsequently transferred to the DSP unit for signal recovery and phase-noise cancellation.

4.2.2 Fiber Transmission

After modulation, the optical signal, containing both the data signals and the SSB pilot carrier, is transmitted over a single-mode fiber (SMF). During transmission, the optical signal may experience various impairments, including chromatic dispersion, polarization mode dispersion, and fiber nonlinearities. However, one of the key advantages of the proposed self-coherent detection scheme is its ability to compensate for these impairments through digital signal processing at the receiver.

The use of a single polarization state for both the data signals and the pilot carrier simplifies the transmission system and eliminates the need for polarization tracking or demultiplexing at the receiver. This approach also makes the system inherently scalable to dual-polarization multiplexing, which could potentially double the data rate without significantly increasing the system complexity.

4.2.3 Receiver Configuration

At the receiver, the optical signal is directed through another polarization controller (PC2) to optimize the polarization state for detection. The signal is then directly detected by a single photodetector (PD), which converts the optical signal into an electrical current proportional to the optical power.

The direct detection process follows the square-law principle, where the photocurrent is proportional to the square of the optical field magnitude. The resulting electrical signal after photodetection can be expressed as:

$$I_{PD}(t) = \left|E_s\right|^2 = \left[\left[\begin{matrix}\left(\frac{\pi}{V_\pi}S_{RF1}(t)\right)^2 + \\ \left(\frac{\pi}{V_\pi}S_{RF2}(t)\right)^2\end{matrix}\right] + \left[\begin{matrix}\left(\frac{2\pi}{V_\pi}S_{RF1}(t)\right) \\ -\left(\frac{2\pi}{V_\pi}S_{RF2}(t)\right)\end{matrix}\right] + DC\right]$$
$$+\left[\left[2\sqrt{2}.\cos\left(\omega_{pc}t + \varphi_{pc} - \frac{\pi}{4}\right)\right] + \left[\begin{matrix}-\frac{2\pi}{V_\pi}S_{RF2}(t)\cos\left(\omega_{pc}t + \varphi_{pc}\right) \\ +\frac{2\pi}{V_\pi}S_{RF1}(t)\sin\left(\omega_{pc}t + \varphi_{pc}\right)\end{matrix}\right]\right] \qquad (4\text{-}4)$$

The square law detected signal has been separated into two brackets, as can be seen in (4-4), the first bracket has components at DC frequency and ω_{RF} and $2 \times \omega_{RF}$ where ω_{RF} is the angular frequency of the independent microwave signals, and the second bracket has components at ω_{LO} and $\omega_{pc} \pm \omega_{RF}$.

It is worth noting that the simplicity of the receiver configuration is one of the key advantages of the proposed self-coherent detection scheme. Unlike traditional coherent detection systems that require complex optical front-ends with multiple optical hybrids and balanced photodetectors, the proposed system uses only a single photodetector, significantly reducing the hardware complexity, cost, and power consumption of the receiver.

4.3 Digital Signal Processing Algorithms

The DSP algorithms play a crucial role in the proposed self-coherent detection system, enabling the recovery of the transmitted microwave vector signals and the cancellation of phase noise introduced by both the laser source and the arbitrary waveform generator. This section provides a detailed description of the DSP algorithms employed in the system, including the mathematical principles, implementation details, and their role in enhancing system performance.

4.3.1 Signal Recovery Algorithm

The DSP algorithm for signal recovery and phase noise cancellation is illustrated in Fig. 4.2, which shows the flow chart of the processing steps applied to the detected signal.

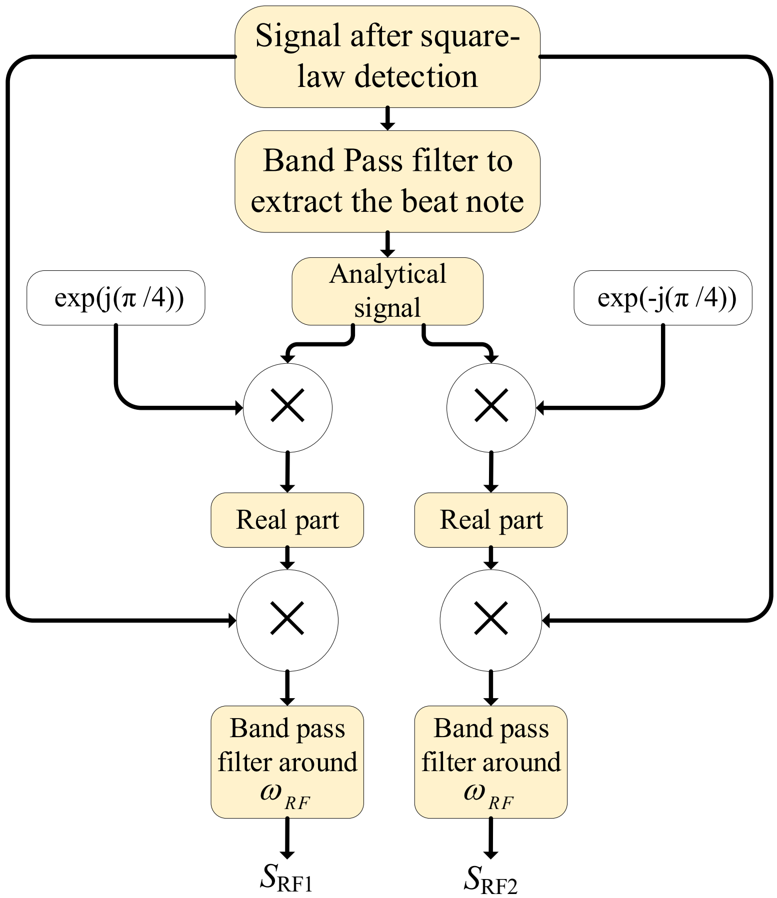

Fig 4.2 Flow chart of the algorithm to cancel the phase noise and recover the two microwave vector signals.

For signal recovery, only the second bracket is needed, as it contains the beat notes between the pilot carrier and the data signals. The first step in the DSP algorithm is to apply a bandpass filter (BPF) to extract these beat note components, which are centered around the frequency of the pilot carrier (ω_LO). This filtering operation can be represented as:

$$I'_{PD}(t)=\left[2\sqrt{2}.\cos\left(\omega_{pc}t+\varphi_{pc}-\frac{\pi}{4}\right)\right]+\left[\begin{matrix}-\frac{2\pi}{V_\pi}S_{RF2}(t)\cos\left(\omega_{pc}t+\varphi_{pc}\right)\\+\frac{2\pi}{V_\pi}S_{RF1}(t)\sin\left(\omega_{pc}t+\varphi_{pc}\right)\end{matrix}\right] \tag{4-5}$$

For the next step of the DSP algorithm, the beat note component (which is at ω_{LO}) should be extracted by a BPF,

$$I_c(t) = 2\sqrt{2}.\cos\left(\omega_{pc}t + \varphi_{pc} - \frac{\pi}{4}\right) \tag{4-6}$$

To recover the two independent microwave signals, the algorithm introduces a phase shift to the beat note. Specifically, the beat note is given a +45° phase shift to recover S_{RF2} and a -45° phase shift to recoverS_{RF1}. This results in:

$$\begin{aligned} I_{c1}(t) &= 2\sqrt{2}\cos\left[\omega_{pc}t + \varphi_{pc}\right] \\ I_{c2}(t) &= 2\sqrt{2}\sin\left[\omega_{pc}t + \varphi_{pc}\right] \end{aligned} \tag{4-7}$$

The algorithm then multiplies the filtered signal $I'_{PD}(t)$ by the phase-shifted beat notes $I_{c1}(t)$ and $I_{c2}(t)$:

$$\begin{aligned} I_1(t) = I'_{PD}(t)I_{c1}(t) = 4\Big[&\cos(-\pi/4) + \cos\left[2\left(\omega_{pc}t + \varphi_{pc}\right) - \pi/4\right]\Big] \\ &- 2\sqrt{2}\frac{\pi}{V_\pi}S_{RF2}(t)\left\{1 + \cos\left[2\left(\omega_{pc}t + \varphi_{pc}\right)\right]\right\} \\ &+ 2\sqrt{2}\frac{\pi}{V_\pi}S_{RF1}(t).\sin\left[2\left(\omega_{pc}t + \varphi_{pc}\right)\right] \end{aligned} \tag{4-8}$$

as can be seen in (4-8), only S_{RF2} has a component that has not been upconverted or downconverted by ω_{LO} or $2 \times \omega_{pc}$, and the other components are at DC frequency or $2 \times \omega_{pc}$, so we can use a digital BPF, as shown in the algorithm, to recover S_{RF2} and cancel the phase noise

$$I'_1(t) = -2\sqrt{2}\frac{\pi}{V_\pi}S_{RF2}(t) \tag{4-9}$$

The same procedure recovers the S_{RF1}. So, by using the proposed algorithm, we can recover the microwave vector signals and cancel the phase noise.

4.3.2 Phase Noise Cancellation

One of the key advantages of the proposed self-coherent detection scheme is its ability to cancel phase noise introduced by both the arbitrary waveform generator. This is achieved through the correlation between the phase noise experienced by the pilot carrier and the data signals.

In traditional coherent detection systems, phase noise from the transmitter laser and the local oscillator can significantly degrade system performance, especially for higher-order modulation formats. In the proposed self-coherent detection system, the pilot carrier and data signals are generated from the same laser source and experience the same phase noise during transmission. This correlation is exploited in the DSP algorithm to achieve effective phase noise cancellation.

The phase noise cancellation process can be understood by examining the mathematical expressions for the recovered signals. The phase term $\varphi_{pc}(t)$, which represents the phase noise from the arbitrary waveform generator, appears in both the beat note and the data signal terms in $I'_{PD}(t)$. When the beat note is multiplied by $I'_{PD}(t)$, the phase terms cancel out, resulting in recovered signals that are free from the phase noise $\varphi_{pc}(t)$.

4.4 Experimental Results

To validate the proposed self-coherent detection system, a comprehensive experimental demonstration was conducted. This section presents the experimental setup, measurement results, and performance analysis of the system, demonstrating its capability to achieve high spectral efficiency in RoF links.

4.4.1 Experimental Setup

A proof-of-concept experiment was conducted based on the setup shown in Fig 4.1. At the transmitter, a CW optical carrier at 1550 nm was generated by a laser source (Yokogawa AQ2201) with an output power of 12 dBm. The optical carrier was directed to a DD-MZM (Fujitsu FTM7821ER) via PC1. The DD-MZM, which has a half-wave voltage of 4 V and a 3 dB bandwidth of 10 GHz, was biased at the quadrature transmission point.

Two independent microwave vector signals and the SSB pilot carrier were generated by an arbitrary waveform generator (AWG, Keysight M8195A) and applied to the phase modulators in the DD-MZM through the two RF input ports. The RF carrier frequency for each microwave signal was set at 2 GHz with a symbol rate of 0.5 Gbaud/s, while the frequency of the SSB pilot carrier (ω_{pc}) was set at 10 GHz.

After modulation, the optical signal was transmitted over a 10 km single-mode fiber (SMF) to the self-coherent receiver. At the receiver, the optical signal was directed through another polarization controller (PC2) and directly detected by a photodetector (New Focus 1014). The resulting electrical signal was sampled by an oscilloscope (Agilent DSO-X 93204A) with a sampling rate of 80 GSa/s and a bandwidth of 32 GHz. The sampled signals were then processed using the digital signal processing (DSP) algorithm described in Section 4.3 to recover the original microwave vector signals and cancel the phase noise.

4.4.2 Signal Processing and Recovery

Fig. 4.3 illustrates the signal processing and recovery process. Fig. 4.3(a) shows one of the electrical signals applied to the RF ports of the DD-MZM, consisting of an independent microwave signal and the pilot carrier. Fig 4.3(b) displays the electrical signal at the output of the photodetector (I_{pd}), where both the first and second brackets of I_{pd}, as defined in Section 4.3, are visible. As explained previously, only the second bracket is needed for recovering the microwave signals, and this component is depicted in Fig. 4.3(c) after bandpass filtering. Finally, Fig. 4.3(d) shows the recovered microwave signal (S_{RF2}) after the complete DSP algorithm has been applied.

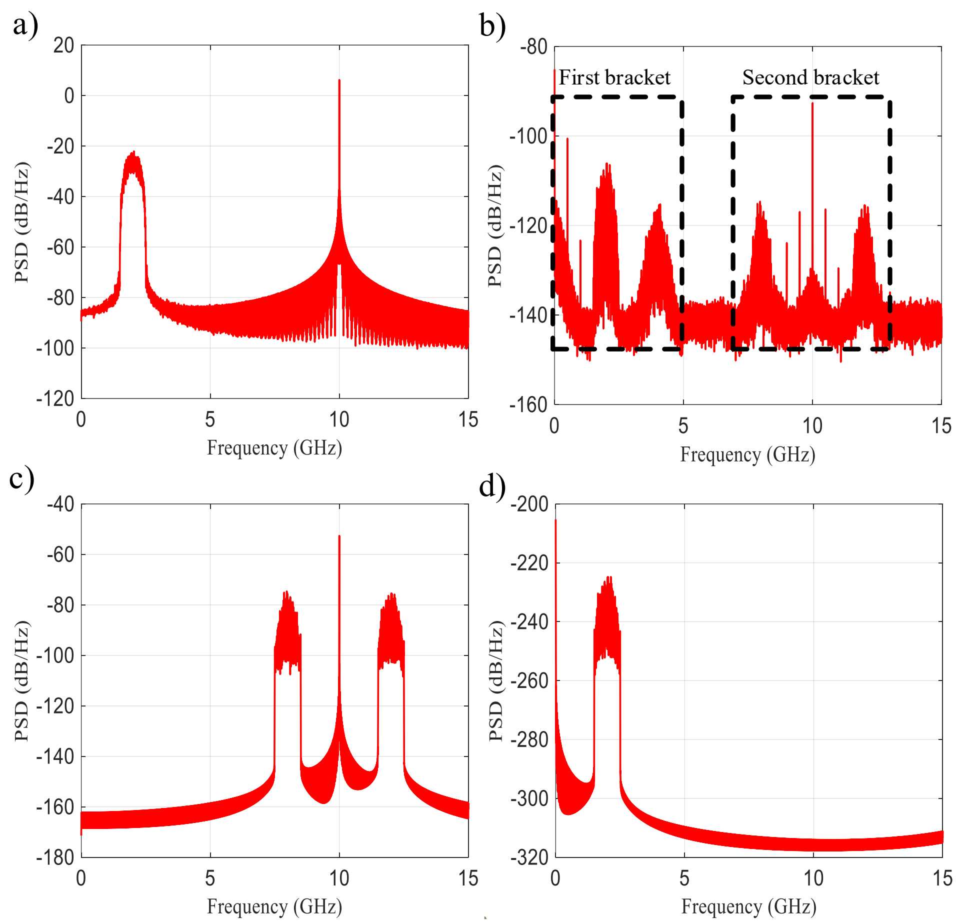

Fig 4.3 a) One of the electrical signals generated at the AWG ($\boldsymbol{S_{RF2} - S_{RF3}}$). b) The electrical signal at the output of the photodetector ($\boldsymbol{I_{pd}}$). c) Filtered $\boldsymbol{I_{pd}}$ which is needed to recover the independent microwave signals. d) Recovered $\boldsymbol{S_{RF2}}$.

The successful recovery of the original microwave signals demonstrates the effectiveness of the proposed self-coherent detection scheme and the associated DSP algorithm. The clear separation of the signal components and the clean recovery of the microwave signals indicate that the system is capable of accurately transmitting and recovering complex modulation formats with minimal distortion.

4.4.3 Performance Evaluation

The performance of the proposed self-coherent detection system was evaluated in terms of EVM and BER at different received optical power levels. Fig. 4.4 presents the measured EVMs of the recovered microwave vector signals as a function of the received optical power.

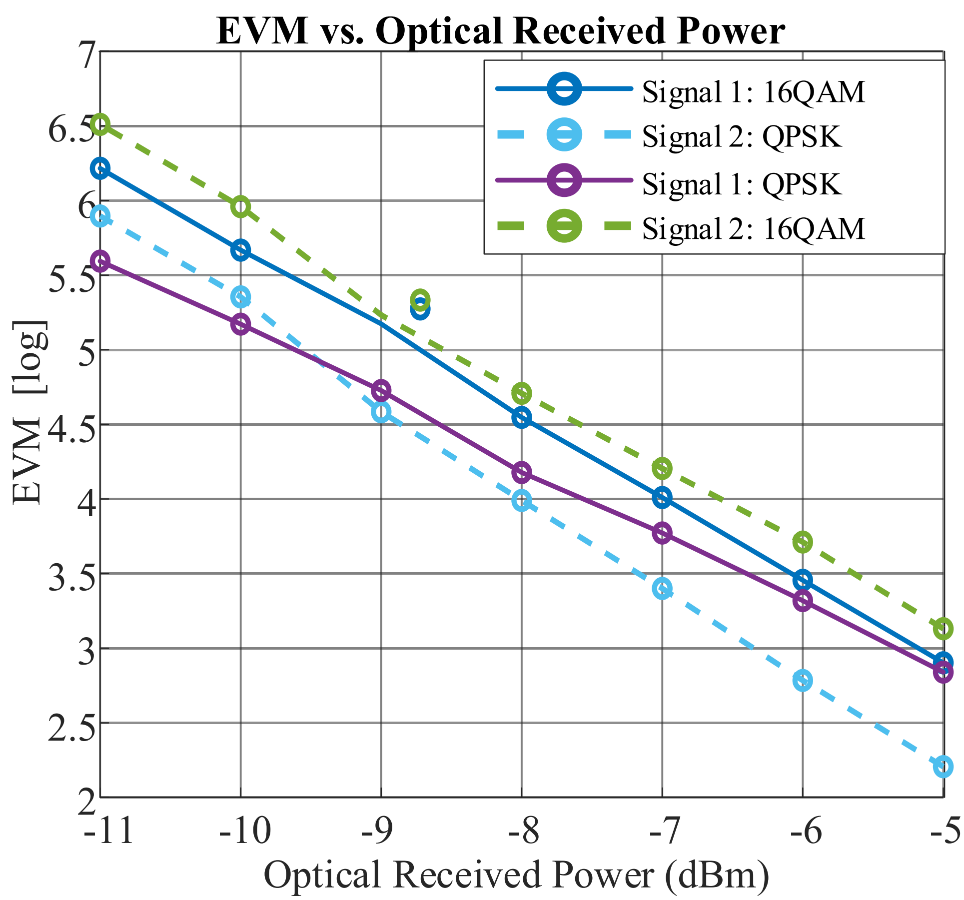

Fig 4.4 Measured EVMs of the received microwave vector signals.

At a received optical power of -5 dBm, the system achieved EVMs of 2.90% for the 16QAM signal and 2.70% for the QPSK signal. These EVM values are well below the threshold required for error-free transmission, indicating excellent signal quality. As the received optical power decreased, the EVM values increased gradually, but remained within acceptable limits even at lower power levels. This demonstrates the robustness of the proposed system against variations in received optical power.

The BERs of the recovered microwave vector signals were also calculated and are shown in Fig. 4.5. At a received optical power of -5 dBm, the system achieved BERs of $10^{-13.60}$ for the 16QAM signal and $10^{-13.66}$ for the QPSK signal, which are well below the FEC threshold of 3.8×10^{-3}. Even at a reduced optical power of -11 dBm, the system maintained BERs of $10^{-10.74}$ and $10^{-10.88}$ for the 16QAM and QPSK signals, respectively, still enabling error-free transmission after FEC.

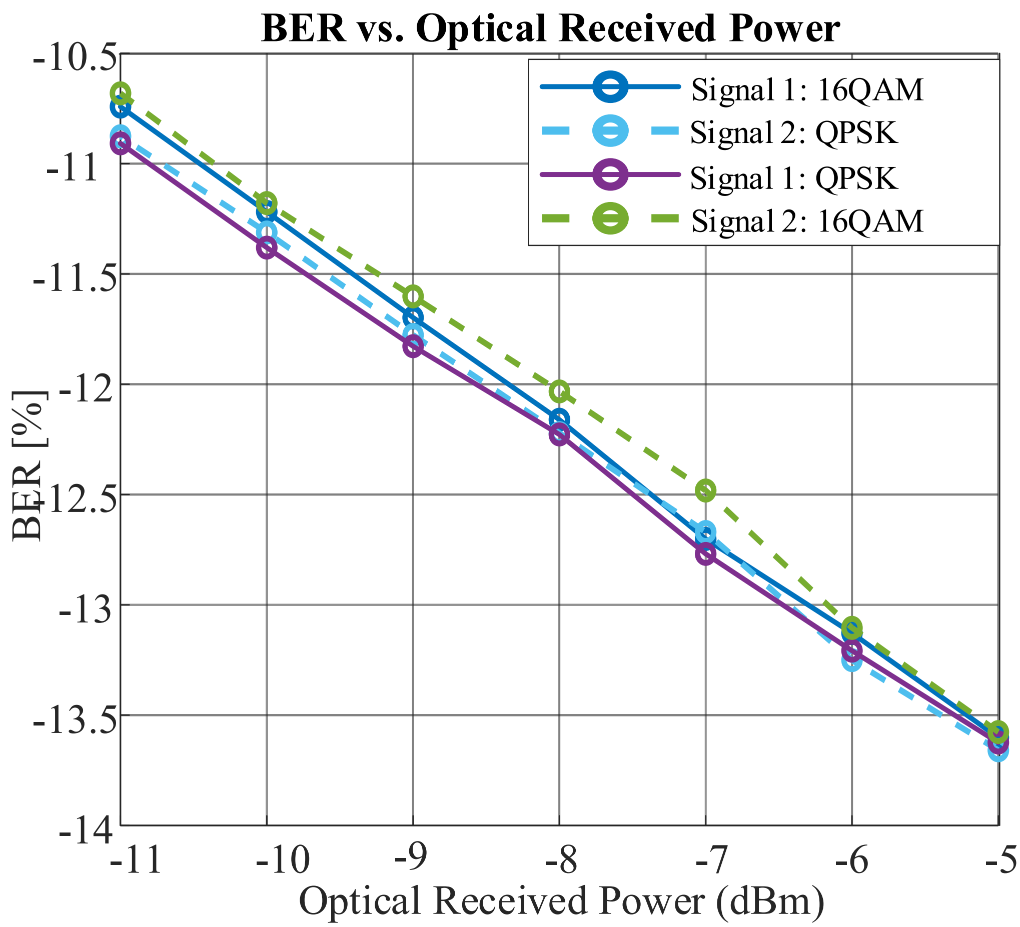

Fig 4.5 Calculated BERs of the received microwave vector signals.

4.4.4 Constellation and Eye Diagram Analysis

The constellation diagrams of the reconstructed 16QAM and QPSK signals at various received optical power levels offer further insight into the system's performance. Fig 4.6 shows the constellation diagrams at received optical powers of -5 dBm and -11 dBm.

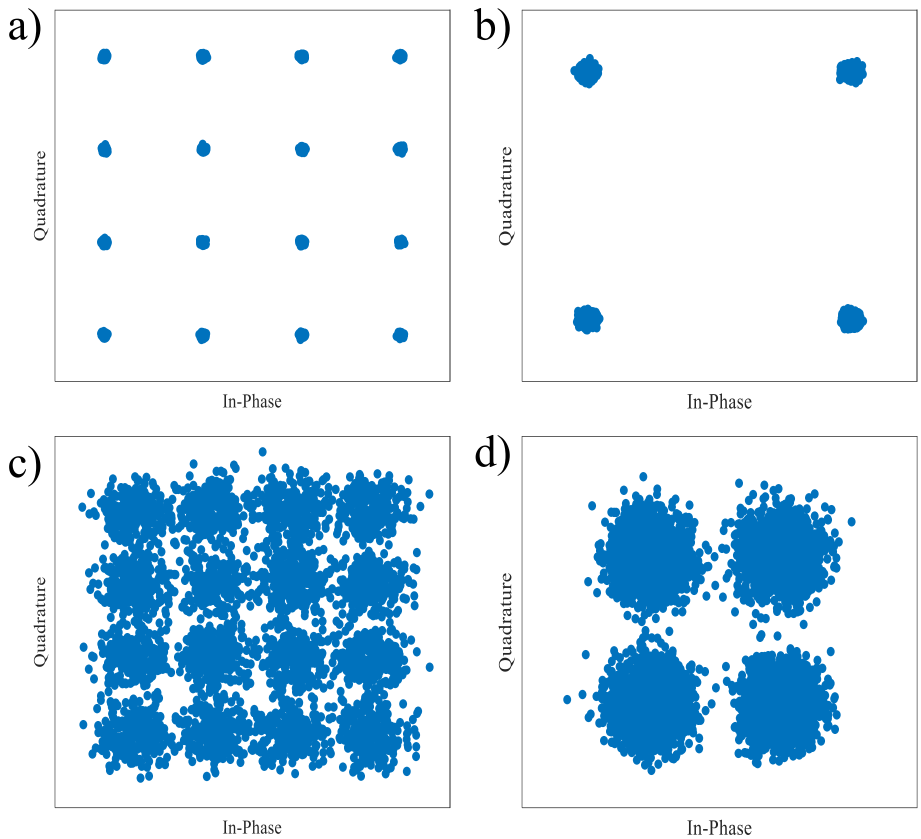

Fig 4.6 a,c) Constellation diagram of the 16QAM signal recovered as $\boldsymbol{S_{RF1}}$ at -5 dBm and -11 dBm. b,d) Constellation diagram of the QPSK signal recovered as $\boldsymbol{S_{RF2}}$ at -5 dBm and -11 dBm.

At -5 dBm (Fig. 4.6(a) and 4.6(b)), the constellation points for both the 16QAM and QPSK signals are tightly clustered, indicating low noise and distortion. The clear separation between constellation points ensures reliable symbol detection and low bit error rates. Even at the reduced optical power of -11 dBm (Fig 4.6(c) and 4.6(d)), the constellation diagrams maintain their structure, although with slightly increased spreading of the constellation points due to the lower signal-to-noise ratio.

The eye diagrams of the recovered signals, shown in Fig. 4.7, provide additional confirmation of the system's performance. At the highest received optical power (-5 dBm), the eye diagrams (Fig.

4.7(a) and 4.7(b)) are well-defined, with clear and open "eyes," indicating minimal ISI and low noise levels. This demonstrates the system's capability to recover both 16QAM and QPSK signals with high fidelity under optimal conditions.

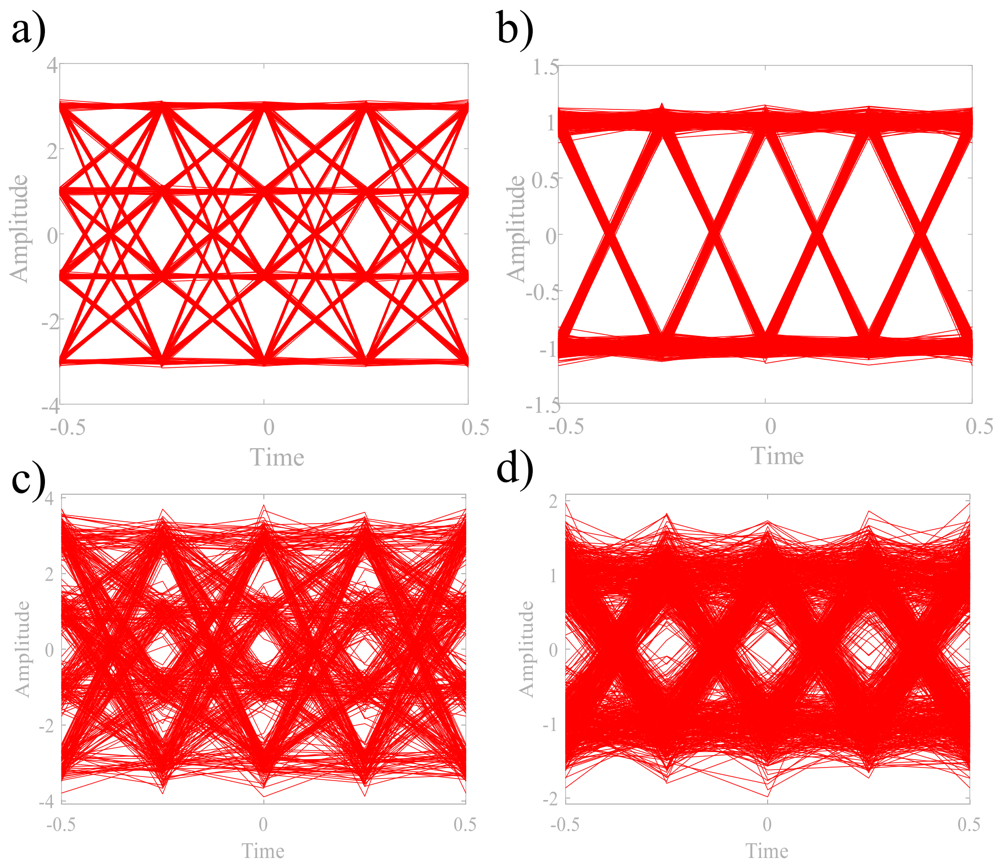

Fig 4.7 a,c) Eye diagram of the 16QAM signal recovered as $\boldsymbol{S_{RF1}}$ at -5 dBm and -11 dBm. b,d) Eye diagram of the QPSK signal recovered as $\boldsymbol{S_{RF2}}$ at -5 dBm and -11 dBm.

As the optical power decreases to -11 dBm, the eye diagrams (Fig. 4.7(c) and 4.7(d)) show some degradation due to increased phase noise and reduced signal-to-noise ratio. However, the recovered signals still maintain sufficient integrity, as corroborated by the measured EVMs and BERs, which remain below the FEC threshold. These results confirm the robustness of the proposed self-coherent detection scheme for practical RoF systems.

4.5 Summary

This chapter has presented a novel high spectral efficiency microwave photonic link based on self-coherent detection. The proposed system enables the transmission of two independent microwave vector signals on a single optical carrier, modulated via a DD-MZM, along with an SSB pilot carrier that facilitates both intensity and phase recovery. This approach offers a cost-effective and energy-efficient solution for high-capacity next-generation RoF networks.

The self-coherent detection technique presented in this chapter addresses several key challenges in RoF systems. By eliminating the need for a separate local oscillator at the receiver, the proposed system significantly reduces hardware complexity, cost, and power consumption compared to traditional coherent detection systems. At the same time, it achieves spectral efficiencies comparable to those of coherent systems by enabling the transmission of complex modulation formats such as 16QAM and QPSK.

A comprehensive overview of self-coherent detection was provided, including a detailed discussion of various approaches such as SVRs, KK detection, and the proposed SSB pilot carrier technique. Each approach offers unique advantages and trade-offs in terms of spectral efficiency, implementation complexity, and performance. The SSB pilot carrier technique stands out for its balance of spectral efficiency, implementation simplicity, and performance, making it particularly well-suited for next-generation high-capacity RoF networks.

The system architecture of the proposed DD-MZM-based self-coherent detection system was described in detail, including the transmitter design, fiber transmission, and receiver configuration. The mathematical model governing the system operation was presented, providing insight into the modulation and detection processes. The key advantages of the system, including high spectral efficiency, reduced hardware complexity, phase noise cancellation, scalability, and compatibility with advanced modulation formats, were highlighted.

A novel DSP algorithm was developed to recover the transmitted microwave signals and cancel the phase noise introduced by the system. The algorithm exploits the correlation between the phase noise experienced by the pilot carrier and the data signals to achieve effective phase noise cancellation. The mathematical principles, implementation details, and practical considerations of the DSP algorithm were discussed, demonstrating its effectiveness in signal recovery and noise suppression.

Experimental results validated the performance of the proposed self-coherent detection system. At an RF frequency of 2 GHz and a symbol rate of 0.5 Gbaud/s, the system achieved error-free transmission of two independent signals, with EVMs of 2.90% for a 16QAM signal and 2.69% for a QPSK signal at an optical power of -5 dBm. The corresponding bit error rates (BERs) were well below the FEC threshold, indicating excellent signal quality. Even at reduced optical power levels, the system maintained acceptable performance, demonstrating its robustness against variations in received optical power.

The constellation diagrams and eye patterns of the recovered signals provided further confirmation of the system's performance, showing clear and well-defined structures at optimal conditions and maintaining sufficient integrity even at lower optical power levels. A comparison with other approaches to high spectral efficiency RoF links highlighted the advantages of the proposed system in terms of spectral efficiency, hardware complexity, and performance.

In conclusion, the self-coherent detection technique presented in this chapter offers a promising solution for high spectral efficiency RoF links. By combining the advantages of coherent detection with the simplicity of direct detection, this approach addresses the growing demand for high-capacity, cost-effective optical communication systems. The experimental demonstration confirms the feasibility and effectiveness of the proposed system, paving the way for its application in next-generation communication networks.

Future research directions in this area may include extending the system to dual-polarization multiplexing to further increase the data rate, investigating the performance of the system with higher-order modulation formats and at higher symbol rates, and exploring the integration of the proposed approach with other advanced techniques such as WDM to achieve even higher capacity and spectral efficiency.

Chapter 5 Conclusion and Future Work

5.1 Research Contributions

This thesis introduced and demonstrated a novel coherent microwave photonic link architecture that combines multiple multiplexing techniques with advanced DSP to achieve high performance. The key contributions of this work can be summarized as follows:

Integration of Amplitude and Phase Modulation with Polarization Multiplexing: The link simultaneously carried two independent vector-modulated signals (one on the optical intensity and one on the optical phase) on the same optical wavelength. This was achieved using cascaded modulators, specifically an MZM followed by a PM, to impose separate amplitude- and phase-modulated data streams. The modulated optical wave was then polarization-multiplexed with an unmodulated optical carrier acting as a reference and sent through the single-mode fiber. This dual-polarization scheme effectively provided an orthogonal channel for a reference or additional signal, doubling the link capacity and enabling polarization-based demultiplexing at the receiver. Compared to a conventional single-signal RoF link, our approach significantly enhances spectral efficiency by transmitting multiple overlapping signals on a single RF channel.

DSP-Based Joint Phase Noise Cancellation and Signal Demultiplexing: We developed an offline DSP algorithm that recovers both the amplitude-modulated and phase-modulated microwave signals and cancels the combined phase noise from the free-running lasers at the transmitter and local oscillator. The coherent receiver detected the optical signal with a separate local oscillator laser, and the DSP synchronized the carrier phase and frequency between transmitter and receiver. By processing the received I/Q waveforms, the algorithm removed the joint phase fluctuations of the two lasers and separated the superimposed signals (including polarization demultiplexing of the orthogonal components). This digital phase noise cancellation technique eliminates the need for optical phase-locked loops, allowing the use of inexpensive, free-running lasers. The successful recovery of both the phase-modulated and intensity-modulated vectors demonstrates the effectiveness of the DSP in mitigating impairments and isolating the amplitude and phase information of each signal.

5.2 Limitations and Challenges

Although the proposed power-multiplexed, coherent microwave-photonic link with DSP-based phase-noise cancellation is experimentally validated, several practical issues merit explicit discussion. Below, we group the key challenges and articulate why they arise, how they manifested in our experiments, and what design/operational mitigations are appropriate.

5.2.1 Phase noise and frequency-offset planning:

In a free-running coherent link, both the transmitter and LO lasers contribute phase noise and an unstable frequency difference. Without careful planning, the combined process produces constellation rotation, cycle slips, and residual phase drift that can overwhelm higher-order constellations and SIC.

Also, in the self-coherent MWP link that was explained in Chapters 3 and 4's experiments, the offset frequency between the pilot note and the laser's wavelength or the LO's wavelength and the LD's wavelength should be chosen properly so that the information from both sidebands does not fold on each other or interfere with other components in the signal.

Also, in the experiments discussed in Chapters 3 and 4, it is important to carefully select the offset frequency. Here, the offset frequency refers to the difference between the pilot tone, a reference frequency inserted into the signal, and the wavelength of the main laser, or between the LO and the LD in the transmitter. Choosing this offset appropriately ensures that information carried on both optical sidebands remains distinct. This prevents the sidebands from overlapping or interfering with each other or other parts of the signal.

For PNC schemes that do not phase-lock the LO, the offset frequency is typically selected two to three times the RF bandwidth so that the beat note and its sidebands are spectrally separable in DSP. This imposes a concrete planning rule on allowable RF bandwidths and IF selection. In our experiments, we set the offset frequency to 1.25 GHz, which up-converted and down-converted 4–5 GHz carriers into well-separated bands before digital filtering.

In Chapter 4, the PNC chain explicitly extracts the beat note at ω_{LO} With a BPF, it applies ±45° phase rotations to form analytic references and then multiplies and filters to recover the RF streams while rejecting phase noise and the frequency offset component. The method relies on a clean selection of the ω_{LO} line and accurate quadrature rotation.

5.2.2 Optical power budget and dynamic range

The end-to-end optical SNR and linear headroom determine the highest reliable power-multiplexing ratio and the maximum useful modulation order. In our cascaded MZM and PM implementation, each modulator contributes ~4–5 dB of insertion loss. We also dedicate part of the optical power to an unmodulated reference channel (e.g., a 90:10 or 95:5 split) to facilitate beat-note extraction. Both choices tighten the OSNR budget for payload channels. Nowadays, with advancements in silicon photonics and MWP devices, we can utilize lower-loss components (e.g., modulators, optical couplers) for reliable beat-note recovery and apply gain/attenuation planning at the receiver for improved detection with reduced loss.

5.2.3 SIC sensitivity to power ratios and ordering

Power-domain multiplexing assumes stable alpha-ratios between co-carried data streams. SIC performance depends on decoding the stronger stream first and subtracting it; drifts in α_n Or mis-ordering increases residual interference and propagates errors to weaker streams. Additionally, there is a problem within the coefficients themselves, where if the coefficients are not chosen properly, data streams will interfere with each other, as illustrated in Fig. 5.1.

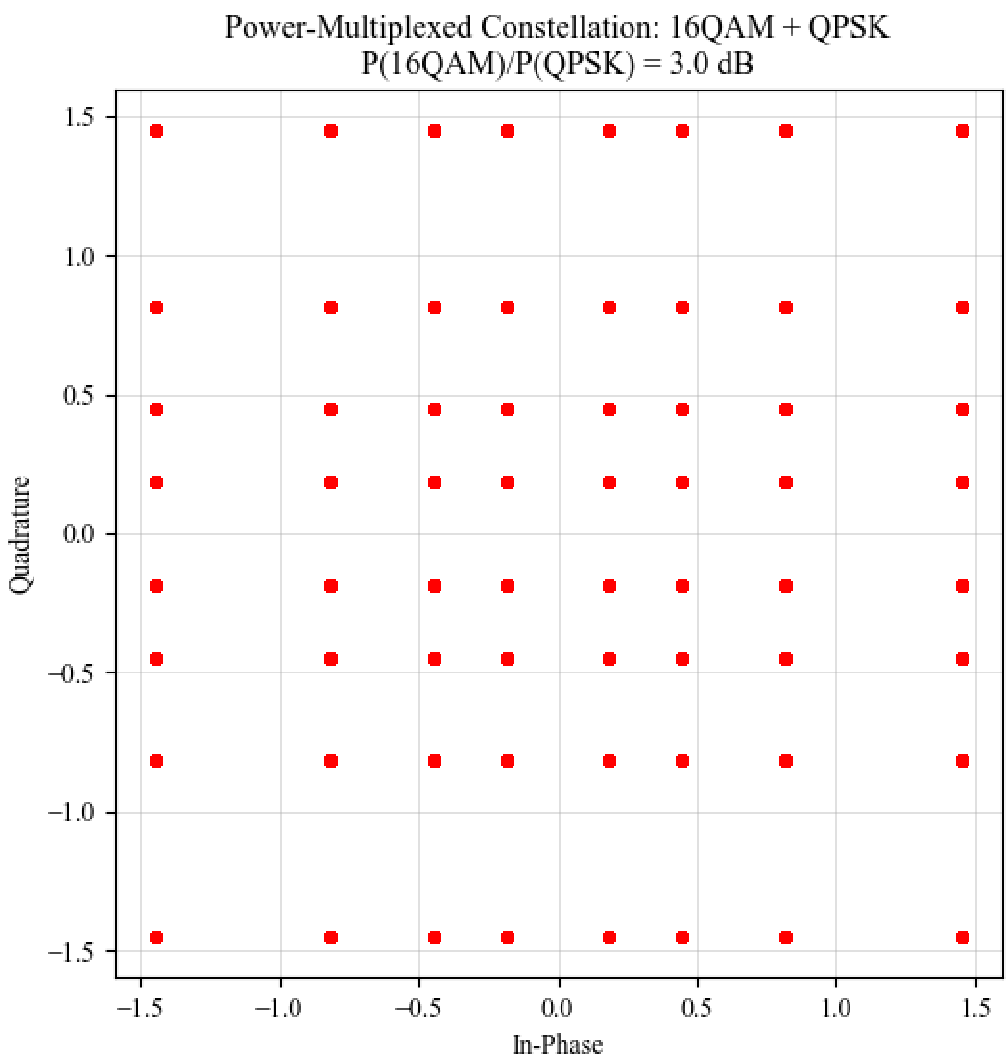

Fig 5.1 Interference observed in the constellation diagram of power-multiplexed QAM signals within an optical communication system, caused by incorrect power allocation coefficients.

5.3 Future Research Directions

Building on the successful demonstration of a coherent, multi-multiplexed microwave photonic link, several future research directions are envisioned to further enhance and extend this work. The following are forward-looking ideas and potential improvements that could be explored:

5.3.1 Machine Learning in Communication Systems

One promising avenue is the integration of machine learning (ML) and deep learning techniques into the signal processing pipeline of microwave photonic links. As communication systems become more complex, data-driven algorithms can offer adaptive and efficient solutions beyond what traditional DSP can achieve. For example, neural network-based algorithms can be developed to enhance signal recovery, channel estimation, and adaptive filtering in real-time. Machine learning models can learn to invert channel impairments or optimize performance metrics by training on experimental data. In the context of our system, an ML-enhanced receiver could dynamically adjust to changing fiber or laser conditions and perform tasks such as noise reduction, nonlinearity compensation, and adaptive modulation selection autonomously. A concrete scenario is using a deep neural network to demultiplex overlapping power-multiplexed signals. Instead of the sequential interference cancellation approach (which subtracts the stronger signal and then decodes the weaker), a neural network could parallelize this process. Recent research has proposed neural-network-based NOMA demultiplexing for RoF systems, where each overlapped signal is separated in parallel without relying on iterative cancellation. This approach drastically reduces decoding latency and increases flexibility compared to conventional SIC. Applying such ML techniques, the receiver DSP could simultaneously recover multiple superimposed signals with a trained model that accounts for fiber dispersion, laser phase noise, and other nonlinearities all at once. It is a new type of estimator that has an equalizer within itself. Moreover, machine learning can aid in adaptive modulation and coding: the transmitter could use reinforcement learning to switch modulation formats or power ratios on the fly based on link conditions predicted by the receiver. This kind of cognitive adaptation would ensure the link always operates at the optimal trade-off between data rate and reliability. In summary, incorporating ML/DL in future coherent MWP links could yield smarter transceivers that self-optimize and achieve better performance (lower error rates, higher capacity) under dynamic conditions. This is a fertile area of research, bridging advanced communication theory with artificial intelligence to push beyond the limits of manual DSP design. There are papers, such as [156]-[163], that have initiated research on implementing ML into RoF; however, a significant path remains for commercializing this area.

5.3.2 Photonic Neural Networks and Hardware Acceleration for DSP

As data rates and channel counts increase, the DSP workload in coherent links, especially for real-time operations, becomes computationally intensive. A forward-looking solution is to employ photonic hardware acceleration, which performs certain signal processing functions in the optical domain or via optical computing elements, thereby achieving ultrafast, parallel computation. One emerging technology is the use of integrated photonic neural networks to equalize and process optical communication signals. Photonic neural networks (PNNs) implement neural network models using optical components (lasers, modulators, waveguides) and have demonstrated the potential for sub-nanosecond latency and high-throughput processing, thanks to the fast propagation of light and inherent parallelism. For instance, researchers have successfully applied photonic neural networks to compensate for fiber nonlinearities and dispersion in 10–40 Gb/s optical signals, demonstrating that these optical processors can effectively equalize distorted signals across a range of modulation formats. In the context of our MWP link, one could imagine a photonic neural network module integrated into the receiver that takes the raw photodetector outputs and optically computes the inverse channel response or demodulates the signals, thereby offloading the digital DSP. This would enable real-time correction of impairments at speeds beyond electronic processing limits, potentially allowing our system to scale to much higher bandwidths or symbol rates. Additionally, photonic hardware could accelerate specific DSP operations, such as optical Fourier transform units for fast spectrum processing or all-optical matrix multipliers for MIMO signal mixing. There is ongoing progress in analog optical computing; one recent demonstration utilized an optical deep learning processor to directly process RF signals in the analog domain at speeds limited only by the bandwidth of photonic devices. Such approaches could be leveraged to implement parts of the microwave photonic link's processing (like fast interference cancellation or adaptive filtering) in hardware, drastically reducing latency. Another promising direction is the use of optical neuromorphic processors for decision tasks: an optical neural network could, for instance, classify the modulation format or detect anomalies in the link (for performance monitoring) almost instantly. Overall, exploring photonic DSP acceleration and optical neural-network-based equalizers could break the bottleneck of digital processing, enabling our coherent link architecture to operate in real-time, even as data rates reach the multi-gigabit or even terabit-per-second regime. This interdisciplinary direction combines photonics with AI (artificial intelligence) hardware, paving the way for fully integrated microwave photonic transceivers with built-in intelligence and ultrafast processing.

5.3.3 **Integrated Silicon Photonics for RoF Systems**

The first opportunity is a monolithically integrated, self-coherent RoF transceiver in which the carrier reference is generated, routed, and stabilized entirely on-chip. Instead of relying on discrete LOs or external pilot tones, an on-chip optical frequency synthesizer and distribution network could feed coherent mixers and balanced detectors with sub-pico-second skew, while integrated phase-noise-shaping loops suppress LO noise before digitization. The key research questions are how to co-design the optical synthesizer, optical hybrids, and low-latency control loops to meet EVM at mm-wave/low-THz carriers without the power overheads of today's DSP-heavy solutions.

Future RoF front-ends should be genuinely programmable. Beyond today's heater-tuned Mach-Zehnder Interferometer meshes, investigate a "photonic Field Programmable Gate Arrays" fabric that combines low-loss interferometer primitives with non-volatile trim elements to eliminate static bias power. Embedding dense monitor photodiodes and on-chip calibration engines could enable background self-calibration (gain/phase/bias) and closed-loop linearization, turning the PIC into a software-defined microwave-photonic platform whose filtering, mixing, and beamforming graphs are compiled at run time.

Scalable true-time-delay beamforming on silicon remains an open systems problem. A promising path is a hierarchical delay network that shares broadband delay banks across many antenna ports via wavelength- or mode-space multiplexing, dramatically reducing area and tuning power per port. Research tasks include co-synthesizing delay-error budgets, heater granularity, and packaging parasitics to achieve wide-angle, wideband beam steering with deterministic phase coherence among dozens to hundreds of radiating elements.

Silicon photonics also enables new RoF linearization strategies that are difficult to implement electronically at mm-wave. Explore "photonic digital predistortion" where a small, high-rate optical auxiliary path implements adaptive predistorters (memory polynomial/Volterra kernels) that pre-compensate the combined electro-optic chain, including modulators, drivers, and photomixers. The open questions are the best partitioning of kernels between optics and electronics, convergence under temperature drift, and how to sense error signals optically without incurring large tap losses.

Another underexplored area is co-packaged RF-photonic front-ends that bring optical frequency conversion within a few millimeters of the antenna feed. Co-designing the PIC with SiGe/CMOS RF integrated circuits and the antenna substrate (interposer or organic package) can minimize electrical intermediate-frequency runs, improve impedance control at frequencies above 100 GHz, and reduce EMI. Research should quantify the EVM/phase-noise benefits of such co-packaging, along with thermal-mechanical strategies (athermal waveguide structures, distributed heaters) to maintain stable frequency responses without the Use of Thermoelectric Coolers.

Transporting carriers beyond 100 GHz on fiber using on-chip photomixing remains an open field for silicon photonics. Investigate heterodyne generation with narrow-spacing on-chip lasers or frequency-divided optical carriers, followed by uni-traveling-carrier-class photodiodes engineered in silicon-compatible stacks or plasmonic-enhanced junctions. The research challenge is joint optimization of optical beat-note linewidth, photodiode saturation/thermal handling, and broadband matching to extract >10 dBm at sub-THz with acceptable linearity.

Spatial scaling is another frontier: integrate compact mode- or core-multiplexers on silicon to realize spatial-division-multiplexed RoF links over few-mode or multicore fiber. A PIC that simultaneously modulates several orthogonal spatial channels and performs optical MIMO pre- and post-processing could increase fronthaul capacity without requiring an increase in fiber count. Open questions include mode-dependent loss equalization on-chip and the extent to which optical MIMO can replace electronic MIMO in radio access networks.

Each of these directions lends itself to concrete, novel milestones: a first-of-its-kind fully on-chip self-coherent link; watt-class reduction via photonic KK; a non-volatile, programmable beamformer with background calibration; a co-packaged photonic integrated circuit with RF integrated circuit “fiber-to-antenna” module; sub-THz photomixing with link-level EVM targets; optical physically unclonable function-secured provisioning; and spatially multiplexed RoF on a single silicon die. Together, they sketch a research agenda where silicon photonics does not just shrink today’s RoF boxes, but changes the architectural playbook for how fiber and radio meet.

REFERENCES

[1] J. G. Proakis and M. Salehi, Digital Communications, 5th ed. New York, NY, USA: McGraw-Hill, 2008.

[2] A. Lapidoth, A Foundation in Digital Communication. Cambridge, U.K.: Cambridge Univ. Press, 2009.

[3] G. P. Agrawal, Fiber-Optic Communication Systems, 4th ed. Hoboken, NJ, USA: Wiley, 2010.

[4] L. N. Binh, Optical Fiber Communication Systems with MATLAB® and Simulink® Models, 2nd ed. Boca Raton, FL, USA: CRC Press, 2014.

[5] K. C. Kao and G. A. Hockham, “Dielectric-fibre surface waveguides for optical frequencies,” Proc. IEE, vol. 113, no. 7, pp. 1151–1158, Jul. 1966.

[6] M.-J. Li and D. A. Nolan, “Optical Transmission Fiber Design Evolution,” J. Lightwave Technol., vol. 26, no. 9, pp. 1079–1092, 2008.

[7] R. J. Mears, L. Reekie, I. M. Jauncey, and D. N. Payne, “Low-noise erbium-doped fibre amplifier operating at 1.54 μm,” Electron. Lett., vol. 23, no. 19, pp. 1026–1028, 1987.

[8] C. A. Brackett, “Dense wavelength division multiplexing networks: Principles and applications,” IEEE J. Sel. Areas Commun., vol. 8, no. 6, pp. 948–964, 1990.

[9] T. Okoshi and K. Kikuchi, Coherent Optical Fiber Communications. Dordrecht, Netherlands: Springer, 1988.

[10] C. Papapavlou et al., “Toward SDM-Based Submarine Optical Networks: A Review of Their Evolution and Upcoming Trends,” Telecom, vol. 3, no. 2, art. 15, 2022.

[11] P. J. Winzer, D. T. Neilson, and A. R. Chraplyvy, “Fiber-optic transmission and networking: the previous 20 and the next 20 years [Invited],” Opt. Express., vol. 26, no. 18, pp. 24190–24239, 2018.

[12] G. Rademacher, B. J. Puttnam, R. S. Luís, et al., “Peta-bit-per-second optical communications system using a standard-cladding-diameter 15-mode fiber,” Nat. Commun., vol. 12, art. 4238, 2021.

[13] J. Yao, “Microwave Photonics,” J. Lightwave Technol., vol. 27, no. 3, pp. 314–335, 2009.

[14] J. Capmany and D. Novak, “Microwave photonics combines two worlds,” Nat. Photon., vol. 1, no. 6, pp. 319–330, 2007.

[15] A. J. Seeds and K. J. Williams, “Microwave Photonics,” J. Lightwave Technol., vol. 24, no. 12, pp. 4628–4641, 2006.

[16] G. H. Smith, D. Novak, and Z. Ahmed, “Overcoming chromatic-dispersion effects in fiber-wireless systems incorporating external modulators,” IEEE Trans. on Microw. Theory and Techniques, vol. 45, no. 8, pp. 1410–1415, 1997.

[17] G. H. Smith, D. Novak, and Z. Ahmed, “Technique for optical SSB generation to overcome dispersion penalties in fibre-radio systems,” Electron. Lett., vol. 33, no. 1, pp. 74–75, 1997.

[18] H. Kim et al., “Reconfigurable WDM Millimeter-Waveband RoF and Baseband System for Broadband Wireless Access,” J. Lightwave Technol., vol. 26, no. 15, pp. 2486–2496, 2008.

[19] Z. Tang and S. Pan, “A Full-Duplex Radio-Over-Fiber Link Based on a Dual-Polarization Mach–Zehnder Modulator,” IEEE Photon. Tech. Lett., vol. 28, no. 8, pp. 852–855, 2016.

[20] A. Tarighat, R. C. J. Hsu, A. H. Sayed, and B. Jalali, “Digital adaptive phase noise reduction in coherent optical links,” J. Lightwave Technol., vol. 24, no. 3, pp. 1269–1276, Mar. 2006.

[21] T. Xu, C. Jin, S. Zhang, G. Jacobsen, S. Popov, M. Leeson, and T. Liu, “Phase noise cancellation in coherent communication systems using a radio frequency pilot tone,” Appl. Sci., vol. 9, no. 21, Art. 4717, Nov. 2019.

[22] S. J. Savory, “Digital Coherent Optical Receivers: Algorithms and Subsystems,” IEEE J. Sel. Topics Quantum Electron., vol. 16, no. 5, pp. 1164–1179, 2010.

[23] K. Kikuchi, “Fundamentals of Coherent Optical Fiber Communications,” J. Lightwave Technol., vol. 34, no. 1, pp. 157–179, Jan. 2016.

[24] X. Chen, T. Shao, and J. Yao, "Digital Phase Noise Cancellation for a Coherent-Detection Microwave Photonic Link," IEEE Photon. Technol. Lett., vol. 26, no. 8, pp. 805-808, Apr. 2014.

[25] P. Li, Z. Dai, L. Yan, and J. Yao, "A microwave photonic link with quadrupled capacity based on coherent detection and digital phase noise cancellation," J. Lightwave Technol., vol. 40, no. 20, pp. 6845–6851, Oct. 15, 2022.

[26] P. Li, Z. Dai, L. Yan, and J. Yao, "Radio over fiber links with increased spectral efficiency based on coherent detection and digital processing," in Proc. International Topical Meeting on Microwave Photonics (MWP), Pisa, Italy, 2021, pp. 1–4.

[27] P. Li, R. Xu, Z. Dai, Z. Lu, L. Yan, and J. Yao, "A high spectral efficiency radio over fiber link based on coherent detection and digital phase noise cancellation," J. Lightwave Technol., vol. 39, no. 20, pp. 6443–6449, Oct. 15, 2021.

[28] X. Chen and J. Yao, "Data rate quadrupled coherent microwave photonic link," IEEE Photon. Tech. Lett., vol. 29, no. 13, pp. 1071–1074, July 1, 2017.

[29] X. Chen and J. Yao, "A high spectral efficiency coherent microwave photonic link employing both amplitude and phase modulation with digital phase noise cancellation," J. Lightwave Technol., vol. 33, no. 14, pp. 3091–3097, July 15, 2015.

[30] X. Chen and J. Yao, "A coherent microwave photonic link with digital phase noise cancellation," in Proc. 2014 International Topical Meeting on Microwave Photonics (MWP) & 9th Asia-Pacific Microwave Photonics Conference (APMP), Hokkaido, Japan, 2014.

[31] S. M. R. Islam, N. Avazov, O. A. Dobre, and K.-S. Kwak, "Power-Domain Non-Orthogonal Multiple Access (NOMA) in 5G Systems: Potentials and Challenges," IEEE Commun. Surveys & Tutorials, vol. 19, no. 2, pp. 721–742, 2017.

[32] L. Dai, B. Wang, Z. Ding, Z. Wang, S. Chen, and L. Hanzo, "A Survey of Non-Orthogonal Multiple Access for 5G," IEEE Commun. Surveys & Tutorials, vol. 20, no. 3, pp. 2294–2323, 2018.

[33] J. A. Altabas et al., "Nonorthogonal multiple access and carrierless amplitude phase modulation for flexible multiuser provisioning in 5G mobile networks," J. Lightwave Technol., vol. 35, no. 24, pp. 5456–5463, Dec. 15, 2017.

[34] S. Sarmiento Hernández et al., "High-Capacity Converged Passive Optical Network and RoF-Based 5G+ Fronthaul Using 4-PAM and NOMA-CAP Signals," J. Lightwave Technol., vol. 39, pp. 372–380, 2021.

[35] C. Lim, Y. Tao, and A. Nirmalathas, "Investigation on NOMA-Based 60-GHz Radio-over-Fiber Fronthaul Links," Proc. ONDM 2021, pp. 1–3.

[36] H. Ji et al., "Complementary polarization-diversity coherent receiver for self-coherent homodyne detection with rapid polarization tracking," J. Lightwave Technol., vol. 40, no. 9, pp. 2773–2779, May 1, 2022.

[37] H. Ji et al., "Photonic-Integrated Self-Coherent Homodyne Receiver Without Optical Polarization Control for Polarization-Multiplexing Short-Reach Optical Interconnects," J. Lightwave Technol., vol. 41, no. 3, pp. 911–918, Feb. 2023.

[38] T. Bo and H. Kim, "Toward practical Kramers–Kronig receiver: Resampling, performance, and implementation," J. Lightwave Technol., vol. 37, no. 2, pp. 461–469**,** Jan. 15, 2019.

[39] Z. Li, W.-R. Peng, A. Li, X. Chen, and K. Kikuchi, "SSBI mitigation and the Kramers–Kronig scheme in single-sideband direct-detection transmission with receiver-based electronic dispersion compensation," J. Lightwave Technol., vol. 35, no. 10, pp. 1887–1893, May 15, 2017.

[40] T. Harter et al., "Generalized Kramers–Kronig receiver for coherent terahertz communications," Nature Photon., vol. 14, pp. 601–606, Oct. 2020.

[41] C. Antonelli, A. Mecozzi, and M. Shtaif, "Kramers–Kronig PAM transceiver and two-sided polarization-multiplexed Kramers–Kronig transceiver," J. Lightwave Technol., vol. 36, no. 2, pp. 468–475, Jan. 15, 2018.

[42] M. van den Hout, S. van der Heide, and C. Okonkwo, "Kramers–Kronig receiver with digitally added carrier combined with digital resolution enhancer," J. Lightwave Technol., vol. 40, no. 5, pp. 1400–1406**,** Mar. 1, 2022.

[43] D. Che, C. Sun, and W. Shieh, "Optical field recovery in Stokes space," J. Lightwave Technol., vol. 37, no. 2, pp. 451–460, Jan. 15, 2019.

[44] D. Che, A. Li, X. Chen, Q. Hu, Y. Wang, and W. Shieh, "Stokes vector direct detection for linear complex optical channels," J. Lightwave Technol., vol. 33, no. 3, pp. 678–684, Feb. 1, 2015.

[45] P. Zhu, Y. Yoshida, A. Kanno, and K.-i. Kitayama, "DSP-enhanced radio-over-fiber technologies for 5G-and-beyond wired–wireless convergence," J. of Opt. Commun. and Netw., vol. 14, no. 8, pp. 595–605, Aug. 2022.

[46] P. Li, Z. Dai, L. Huang, and J. Yao, "Non-orthogonal multiple access in a radio over fiber link based on optical-domain power allocation," Opt. Lett., vol. 48, pp. 6204–6207, 2023.

[47] K. Xu, R. Wang, Y. Dai, F. Yin, J. Li, Y. Ji, and J. Lin, "Microwave photonics: radio-over-fiber links, systems, and applications [Invited]," Photon. Res., 2(4), B54–B63, 2014.

[48] D. Wake, A. Nkansah, and N. J. Gomes, "Radio Over Fiber Link Design for Next Generation Wireless Systems," J. Lightwave Technol., 28(16), 2456–2464, 2010.

[49] M. Zhu, L. Zhang, J. Wang, L. Cheng, C. Liu, and G.-K. Chang, "Radio-over-fiber access architecture for integrated broadband wireless services," J. Lightwave Technol., vol. 31, no. 23, pp. 3614–3620, Dec. 1, 2013.

[50] Y.-Y. Won, H.-S. Kim, Y.-H. Son, and S.-K. Han, "Full colorless WDM–radio-over-fiber access network supporting simultaneous transmission of millimeter-wave band and baseband gigabit signals by sideband routing," J. Lightwave Technol., vol. 28, no. 16, pp. 2213–2218, Aug. 15, 2010.

[51] J. Yao, "Microwave photonic systems," J. Lightwave Technol., vol. 40, no. 20, pp. 6595–6607, Oct. 15, 2022.

[52] G.-L. Li and P. K. L. Yu, "Optical Intensity Modulators for Digital and Analog Applications," J. Lightwave Technol., vol. 21, no. 9, pp. 2010–2030, Sep. 2003.

[53] R. C. Alferness, "Waveguide Electrooptic Modulators," IEEE Trans. on Microwave Theory and Techniques, vol. 30, no. 8, pp. 1121–1137, Aug. 1982.

[54] R. Sabella and P. Lugli, High Speed Optical Communications. New York, NY, USA: Springer, 1999.

[55] J. Capmany and C. R. Fernández-Pousa, “Quantum modelling of electro-optic modulators,” Laser & Photon. Rev., vol. 5, pp. 750–772, 2011.

[56] X. N. Fernando, Radio over Fiber for Wireless Communications: From Fundamentals to Advanced Topics. 1st ed. Wiley-IEEE Press, 2014, sec. 2.3, “Optical Receiver,” pp. 72-79.

[57] D. Zibar, X. Yu, C. Peucheret, P. Jeppesen, and I. T. Monroy, “Digital coherent receiver for phase-modulated radio-over-fiber optical links,” IEEE Photon. Techn. Lett., vol. 21, no. 3, pp. 155–157, Feb. 1, 2009.

[58] R. Li, X. Han, X. Chen, X. Chen, and J. Yao, “A phase-modulated microwave photonic link with an extended transmission distance,” IEEE Photon. Tech. Lett., vol. 27, no. 24, pp. 2563–2566, Dec. 15, 2015.

[59] E. L. Wooten et al., “A Review of Lithium Niobate Modulators for Fiber-Optic Communications Systems,” IEEE J. of Sel. Top. in Quantum Electron., vol. 6, no. 1, pp. 69–82, Jan./Feb. 2000.

[60] R. B. Welstand, J. T. Zhu, W. X. Chen, A. R. Clawson, P. K. L. Yu, and S. A. Pappert, “Combined Franz–Keldysh and Quantum-Confined Stark Effect Waveguide Modulator for Analog Signal Transmission,” J. Lightwave Technol., vol. 17, no. 3, pp. 497–502, Mar. 1999.

[61] P. Chaisakul et al., “23 GHz Ge/SiGe Multiple Quantum Well Electro-Absorption Modulator,” Opt. Exp., vol. 20, no. 3, pp. 3219–3224, Jan. 2012.

[62] Y. Tang et al., “Over 67 GHz Bandwidth Hybrid Silicon Electroabsorption Modulator,” Opt. Exp., vol. 20, no. 10, pp. 11529–11535, May 2012.

[63] C. G. Lim, “Electro-Absorption Modulator Integrated Lasers With Enhanced Signal Injection Efficiency,” J. Lightwave Technol., vol. 26, no. 6, pp. 685–691, Mar. 2008.

[64] G. J. Foschini and C. D. Poole, “Statistical Theory of Polarization Dispersion in Single Mode Fibers,” J. Lightwave Technol., vol. 9, no. 11, pp. 1439–1456, Nov. 1991.

[65] C. R. Menyuk and B. S. Marks, "Interaction of Polarization Mode Dispersion and Nonlinearity in Optical Fiber Transmission Systems," J. Lightwave Technol., vol. 24, no. 7, pp. 2806–2826, Jul. 2006.

[66] P. Ciprut, B. Gisin, N. Gisin, R. Passy, J.-P. von der Weid, F. Prieto, and C. W. Zimmer, "Second-Order Polarization Mode Dispersion: Impact on Analog and Digital Transmissions," J. Lightwave Technol., vol. 16, no. 5, pp. 757–771, May 1998.

[67] R.-J. Essiambre and R. W. Tkach, "Capacity Trends and Limits of Optical Communication Networks," Proceedings of the IEEE, vol. 100, no. 5, pp. 1035–1055, May 2012.

[68] K. Inoue, "Four-Wave Mixing in an Optical Fiber in the Zero-Dispersion Wavelength Region," J. Lightwave Technol., vol. 10, no. 11, pp. 1553–1561, Nov. 1992.

[69] R. Hui, K. Demarest, and C. Allen, "Cross-Phase Modulation in Multispan WDM Optical Fiber Systems," J. Lightwave Technol., vol. 17, no. 6, pp. 1018–1026, Jun. 1999.

[70] A. Kobyakov, M. Sauer, and D. Chowdhury, "Stimulated Brillouin Scattering in Optical Fibers," Adv. in Opt. Photon., vol. 2, no. 1, pp. 1–59, 2009.

[71] J. Bromage, "Raman Amplification for Fiber Communication Systems," J. Lightwave Technol., vol. 22, no. 1, pp. 79–93, Jan. 2004.

[72] A. D. Ellis, J. Zhao, and D. Cotter, "Performance Limits in Optical Communications Due to Fiber Nonlinearity," Adv. in Opt. Photon., vol. 9, no. 3, pp. 429–503, 2017.

[73] R. W. Tkach, A. R. Chraplyvy, F. Forghieri, A. H. Gnauck, and R. M. Derosier, "Four-Photon Mixing and High-Speed WDM Systems," J. Lightwave Technol., vol. 13, no. 5, pp. 841–849, May 1995.

[74] E. Desurvire, "Analysis of noise figure spectral distribution in erbium-doped fiber amplifiers pumped near 980 and 1480 nm," Applied Opt., vol. 29, no. 21, pp. 3118–3125, 1990.

[75] C. H. Cox III, E. I. Ackerman, R. A. Helkey, and G. E. Betts, "Techniques and Performance of Intensity-Modulation Direct-Detection Analog Optical Links," IEEE Trans. on Microw. Theory and Techn., vol. 45, no. 8, pp. 1375–1383, Aug. 1997.

[76] F.-L. Wang, X.-W. Ma, Y.-Z. Huang, Y.-D. Yang, J.-Y. Han, and J.-L. Xiao, "Relative intensity noise in high-speed hybrid square-rectangular lasers," Photon. Res., vol. 6, no. 3, pp. 193–197, 2018.

[77] C. R. Giles and E. Desurvire, "Modeling erbium-doped fiber amplifiers," J. Lightwave Technol., vol. 9, no. 2, pp. 271–283, 1991.

[78] C. H. Henry, "Theory of the linewidth of semiconductor lasers," IEEE J. of Quantum Electron., vol. 18, no. 2, pp. 259–264, Feb. 1982.

[79] G. Colavolpe, T. Foggi, E. Forestieri and M. Secondini, "Impact of Phase Noise and Compensation Techniques in Coherent Optical Systems," in J. Lightwave Technol., vol. 29, no. 18, pp. 2790-2800, Sept.15, 2011.

[80] H. Zhang, A. Wen, W. Zhang, W. Zhang, and W. Li, "A simplified coherent-detected radio-over-fiber link with intensity and phase modulation and simple digital phase noise cancellation," Opt. Comm., vol. 484, art. no. 126700, 2021.

[81] A. A. Sardarzadeh, P. Li, and J. Yao, "Investigating power multiplexing for coherent microwave photonic links," in Proc. International Topical Meeting on Microwave Photonics (MWP), Pisa, Italy, 2024, pp. 1–4.

[82] B. Zhang, C. Malouin, and T. J. Schmidt, "Design of coherent receiver optical front end for unamplified applications," Opt. Exp., vol. 20, pp. 3225–3234, 2012.

[83] T. Pfau, S. Hoffmann, and R. Noé, "Hardware-Efficient Coherent Digital Receiver Concept With Feedforward Carrier Recovery for M-QAM Constellations," J. Lightwave Technol., vol. 27, no. 8, pp. 989–999, 2009.

[84] P. J. Winzer and R.-J. Essiambre, "Advanced Modulation Formats for High-Capacity Optical Transport Networks," J. Lightwave Technol., vol. 24, no. 12, pp. 4711–4728, Dec. 2006.

[85] E. Ip and J. M. Kahn, "Compensation of Dispersion and Nonlinear Impairments Using Digital Backpropagation," J. Lightwave Technol., vol. 26, no. 20, pp. 3416–3425, Oct. 2008.

[86] P. J. Winzer, "High-Spectral-Efficiency Optical Modulation Formats," J. Lightwave Technol., vol. 30, no. 24, pp. 3824–3835, Dec. 2012.

[87] M. Mazur, A. Lorences-Riesgo, J. Schröder, P. A. Andrekson, and M. Karlsson, "10 Tb/s PM-64QAM Self-Homodyne Comb-Based Superchannel Transmission with 4% Shared Pilot Tone Overhead," J. Lightwave Technol., vol. 36, no. 16, pp. 3176–3184, 2018.

[88] W. Shieh, "Carrier-assisted differential detection," Light: Science & Applications, vol. 9, no. 1, 2020.

[89] D. Che, C. Sun, and W. Shieh, "Maximizing the spectral efficiency of Stokes vector receiver with optical field recovery," Opt. Exp., vol. 26, no. 22, pp. 28976–28981, 2018.

[90] M. Kuschnerov, F. N. Hauske, K. Piyawanno, M. S. Alfiad, B. Spinnler, and B. Lankl, "DSP for Coherent Single-Carrier Receivers," J. Lightwave Technol., vol. 27, no. 16, pp. 3614–3622, 2009.

[91] G. Li, "Recent advances in coherent optical communication," Adv. in Opt. and Photon., vol. 1, no. 2, pp. 279–307, 2009.

[92] E. P. da Silva and D. Zibar, "Widely Linear Equalization for IQ Imbalance and Skew Compensation in Optical Coherent Receivers," J. Lightwave Technol., vol. 34, no. 15, pp. 3577–3586, 2016.

[93] M. S. Faruk and K. Kikuchi, "Adaptive frequency-domain equalization in digital coherent optical receivers," Opt. Exp., vol. 19, no. 13, pp. 12789–12798, 2011.

[94] R. Kudo, T. Kobayashi, K. Ishihara, Y. Takatori, A. Sano, and Y. Miyamoto, "Coherent Optical Single-Carrier Transmission Using Overlap Frequency Domain Equalization for Long-Haul Optical Systems," J. Lightwave Technol., vol. 27, no. 16, pp. 3721–3728, 2009.

[95] L. Huang, Z. Lu, K. Wu, and J. Yao, "Simple polarization-insensitive coherent RoF link with increased capacity," Opt. Lett., vol. 48, pp. 3179–3182, 2023.

[96] K. Kikuchi, "Performance analyses of polarization demultiplexing based on constant-modulus algorithm in digital coherent optical receivers," Opt. Exp., 19(10), 9868–9877, 2011.

[97] D. N. Godard, “Self-recovering equalization and carrier tracking in two-dimensional data communication systems,” IEEE Trans. on Commun., 28(11), 1867–1875, 1980.

[98] I. Roudas et al., “Optimal polarization demultiplexing for coherent optical communication systems,” J. Lightwave Technol., vol. 28, no. 7, pp. 1121–1134, Apr. 1, 2010.

[99] D. Zhao, L. Xi, X. Tang, W. Zhang, Y. Qiao, and X. Zhang, “Digital pilot-aided carrier frequency offset estimation for coherent optical transmission systems,” Opt. Exp., vol. 23, pp. 24822–24832, 2015.

[100] A. J. Viterbi and A. M. Viterbi, “Nonlinear estimation of PSK-modulated carrier phase with application to burst digital transmission,” IEEE Trans. on Inf. Theory, vol. 29, no. 4, pp. 543–551, Jul. 1983.

[101] F. Chang, K. Onohara, and T. Mizuochi, “Forward error correction for 100 G transport networks,” IEEE Commun. Mag., vol. 48, no. 3, pp. S48–S55, Mar. 2010.

[102] I. B. Djordjevic, M. Arabaci, and L. L. Minkov, “Next Generation FEC for High-Capacity Communication in Optical Transport Networks,” J. Lightwave Technol., 27(16), 3518–3530, Aug. 2009.

[103] E. Ip and J. M. Kahn, “Feedforward Carrier Recovery for Coherent Optical Communications,” J. Lightwave Technol., vol. 25, no. 9, pp. 2675–2692, Sep. 2007.

[104] A. Meiyappan, P.-Y. Kam, and H. Kim, “On Decision Aided Carrier Phase and Frequency Offset Estimation in Coherent Optical Receivers,” J. Lightwave Technol., vol. 31, no. 13, pp. 2055–2063, Jul. 2013.

[105] Q. Zhuge, J. Hu, S. Kamran, A. P. T. Lau, and C. Lu, “Pilot-aided carrier phase recovery for M-QAM using superscalar parallelization-based PLL,” Opt. Exp., vol. 20, no. 17, pp. 19599–19609, 2012.

[106] H. Cheng, L. Yan, A. P. T. Lau, and C. Lu, “Pilot-symbols-aided cycle slip mitigation for DP-16QAM optical communication systems,” Opt. Exp., vol. 21, no. 19, pp. 22166–22178, 2013.

[107] L. Gonzalez-Guerrero, H. Shams, I. Fatadin, J. E. Wu, M. J. Fice, M. Naftaly, A. J. Seeds, and C. C. Renaud, "Pilot-Tone Assisted 16-QAM Photonic Wireless Bridge Operating at 250 GHz," J. Lightwave Technol., vol. 39, no. 9, pp. 2725–2736, 2021.

[108] F. Tian, F. Li, C. Wang, J. Zhang, F. Li, and J. Wang, "1.06 Tbit/s space-division-multiplexing self-homodyne coherent detection with multi-core fiber for short-reach networks," Opt. Exp., vol. 32, no. 24, pp. 42500–42513, 2024.

[109] M. S. Erkılınç, D. Lavery, K. Shi, B. C. Thomsen, P. Bayvel, R. I. Killey, and S. J. Savory, "Polarization-Insensitive Single-Balanced Photodiode Coherent Receiver for Long-Reach WDM-PONs," J. Lightwave Technol., vol. 34, no. 8, pp. 2034–2041, 2016.

[110] Q. Yang, S. Chen, and W. Shieh, "428-Gb/s single-channel coherent optical OFDM transmission," Opt. Exp., vol. 18, no. 16, pp. 16883–16888, 2010.

[111] H. Li et al., "Microwave photonic link enabling transmission of multiple microwave vector signals over fiber," Opt. Exp., vol. 30, no. 5, pp. 6690–6704, 2022.

[112] J. Pfeifle et al., "Coherent terabit communications with microresonator Kerr frequency combs," Nat. Photon., vol. 8, pp. 375–380, 2014.

[113] S. J. Savory, G. Gavioli, R. I. Killey, and P. Bayvel, "Electronic compensation of chromatic dispersion using a digital coherent receiver," Opt. Exp., vol. 15, no. 5, pp. 2120–2126, 2007.

[114] D. A. Morero, M. A. Castrillón, A. Aguirre, M. R. Hueda, and O. E. Agazzi, "Design Tradeoffs and Challenges in Practical Coherent Optical Transceiver Implementations," J. Lightwave Technol., vol. 34, no. 1, pp. 121–136, 2016.

[115] L. Liu et al., "DSP-free coherent receivers in frequency-synchronous optical networks for low-cost interconnects," Advanced Photonics Nexus, vol. 4, no. 3, 036013, 2025.

[116] E. Börjeson and P. Larsson-Edefors, "Cycle-slip rate analysis of blind phase search DSP circuit implementations," in Proc. Optical Fiber Communication Conference and Exhibition (OFC), San Diego, CA, USA, 2020, pp. 1–3.

[117] H. Ji et al., "Photonic Integrated Self-Coherent Homodyne Receiver," J. Lightwave Technol., vol. 41, no. 18, pp. 5806–5815, 2023.

[118] C. Doerr et al., "Single-chip silicon photonics 100-Gb/s coherent transceiver," in Proc. Optical Fiber Communication Conference (OFC), San Francisco, CA, USA, 2014, pp. 1-3.

[119] K.-i. Kitayama, A. Maruta, and Y. Yoshida, "Digital coherent technology for optical fiber and radio-over-fiber transmission systems," J. Lightwave Technol., vol. 32, no. 20, pp. 3411–3420, Oct. 15, 2014.

[120] B. Mukherjee, "WDM Optical Communication Networks: Progress and Challenges," IEEE J. on Sel. Areas in Commun., vol. 18, no. 10, pp. 1810–1824, Oct. 2000.

[121] R. Ramaswami, "Multiwavelength Lightwave Networks for Computer Communication," IEEE Commun. Mag., vol. 31, no. 2, pp. 78–88, Feb. 1993.

[122] L. Dai, B. Wang, Y. Yuan, S. Han, C.-L. I, and Z. Wang, "Non-Orthogonal Multiple Access for 5G: Solutions, Challenges, Opportunities, and Future Research Trends," IEEE Comm. Mag., vol. 53, no. 9, pp. 74–81, Sept. 2015.

[123] Z. Ding, Y. Liu, J. Choi, Q. Sun, M. Elkashlan, C.-L. I, and H. V. Poor, "Application of Non-Orthogonal Multiple Access in LTE and 5G Networks," IEEE Comm. Mag., vol. 55, no. 2, pp. 185–191, Feb. 2017.

[124] K. Miyamoto, R. Kudo, K. Yashiki, T. Katayama, and T. Kawanishi, "Transmission Performance Investigation of RF Signal in RoF–DAS over a WDM-PON with MIMO," J. Lightwave Technol., vol. 31, no. 22, pp. 3477–3483, 2013.

[125] Y. Zhu, J. Luo, K. Wang, J. Yu, J. Zhang, and G.-K. Chang, "Experimental Demonstration of a WDM-RoF Based Mobile Fronthaul With a Directly Modulated 3-Section DBR Laser," J. Lightwave Technol., vol. 37, no. 16, pp. 3875–3883, 2019.

[126] P. T. Dat, A. Kanno, K. Inagaki, F. Rottenberg, N. Yamamoto, and T. Kawanishi, "High-Speed and Uninterrupted Communication for High-Speed Trains by Ultrafast WDM Fiber–Wireless Backhaul System," J. Lightwave Technol., vol. 37, no. 1, pp. 205–217, 2019.

[127] J. Xia et al., "A future-proof reconfigurable wireless and fixed converged optical fronthaul network using silicon photonic switching strategies," J. Lightwave Technol., vol. 41, no. 6, pp. 1610–1618, Mar. 15, 2023.

[128] N. Cheng, C. W. Chow, C. H. Yeh, C. H. Wang, S. Chi, and H. K. Tsang, "Reflective Crosstalk Cancellation in Self-Seeded WDM-PON for Mobile Fronthaul/Backhaul," J. Lightwave Technol., vol. 34, no. 8, pp. 2056–2062, 2016.

[129] H. Yang, J. Zhou, W. Hu, J. Yu, and X. Li, "Optically Powered 5G WDM Fronthaul Network With Weakly-Coupled Multicore Fiber," Opt. Exp., vol. 30, no. 11, pp. 19795–19806, 2022.

[130] Y. Han and G. Li, "Coherent optical communication using polarization multiple-input–multiple-output," Optics Express, vol. 13, pp. 7527–7534, 2005.

[131] W. Shieh, H. Bao, and Y. Tang, "Coherent optical OFDM: Theory and design," Opt. Exp., vol. 16, pp. 841–859, 2008.

[132] W. Wang, D. Zou, X. Feng, Q. Sui, R. Lu, Z. Cao, and F. Li, "Optical polarization-division multiplexing fiber–wireless integration system at Ka-band based on a low-cost dual-drive MZM," Opt. Exp., vol. 29, pp. 37453–37463, 2021.

[133] P. Serena, C. Lasagni, and A. Bononi, "The enhanced Gaussian noise model extended to polarization-dependent loss," J. Lightwave Technol., vol. 38, no. 20, pp. 5685–5694, Oct. 15, 2020.

[134] Z. Ding, Z. Yang, P. Fan, and H. V. Poor, "On the Performance of Non-Orthogonal Multiple Access in 5G Systems with Randomly Deployed Users," IEEE Signal Processing Lett., vol. 21, no. 12, pp. 1501–1505, Dec. 2014.

[135] J. Choi, "Power Allocation for Max-Sum Rate and Max-Min Rate Proportional Fairness in NOMA," IEEE Comm. Lett., vol. 20, no. 10, pp. 2055–2058, Oct. 2016.

[136] P. Patel and J. Holtzman, "Analysis of a Simple Successive Interference Cancellation Scheme in a DS/CDMA System," IEEE J. on Selected Areas in Communications, vol. 12, no. 5, pp. 796–807, Jun. 1994.

[137] T. M. Cover, “Broadcast Channels,” IEEE Trans. on Inf. Theory, vol. 18, no. 1, pp. 2–14, Jan. 1972.

[138] P. P. Bergmans, “Random Coding Theorem for Broadcast Channels with Degraded Components,” IEEE Trans. on Inf. Theory, vol. 19, no. 2, pp. 197–207, Mar. 1973.

[139] P. P. Bergmans, “A Simple Converse for Broadcast Channels with Additive White Gaussian Noise,” IEEE Trans. on Inf. Theory, vol. 20, no. 2, pp. 279–280, Mar. 1974.

[140] H. Weingarten, Y. Steinberg, and S. Shamai (Shitz), “The Capacity Region of the Gaussian Multiple-Input Multiple-Output Broadcast Channel,” IEEE Trans. on Inf. Theory, vol. 52, no. 9, pp. 3936–3964, Sept. 2006.

[141] Y. Liu, Z. Qin, M. Elkashlan, Z. Ding, A. Nallanathan, and L. Hanzo, “Nonorthogonal multiple access for 5G and beyond,” Proceedings of the IEEE, vol. 105, no. 12, pp. 2347–2381, Dec. 2017.

[142] Y. Tian, C. Lim, A. Nirmalathas, and K.-L. Lee, “Multi-cell coordination for 60 GHz RoF fronthaul enabled by a non-orthogonal multiple access scheme without successive interference cancellation,” Opt. Lett., vol. 43, pp. 4236–4239, 2018.

[143] S. Sarmiento et al., “High-capacity converged passive optical network and RoF-based 5G+ fronthaul using 4-PAM and NOMA-CAP signals,” J. Lightwave Technol., vol. 39, no. 2, pp. 372–380, Jan. 15, 2021.

[144] I. Fatadin, D. Ives, and S. J. Savory, “Blind equalization and carrier phase recovery in a 16-QAM optical coherent system,” J. Lightwave Technol., vol. 27, no. 15, pp. 3042–3049, Aug. 1, 2009.

[145] E. S. Chou and J. M. Kahn, “Successive interference cancellation on frequency-selective channels with mode-dependent gain,” J. Lightwave Technol., vol. 40, no. 12, pp. 3729–3738, Jun. 15, 2022.

[146] B. Lin, J. Xu, Z. Ghassemlooy, and X. Tang, “Power-code division non-orthogonal multiple access scheme for next-generation passive optical networks,” Opt. Express, vol. 27, pp. 35740–35749, 2019.

[147] K. Suzuoki, D. Hisano, K. Mishina, K. Maruta, and A. Maruta, "Demonstration of Asynchronous Successive Interference Canceller for Uplink NOMA-PON," 2021 Optical Fiber Communications Conference and Exhibition (OFC), San Francisco, CA, USA, 2021, pp. 1-3.

[148] E. S. Chou, H. Srinivas, and J. M. Kahn, “Phase retrieval-based coherent receivers: Signal design and degrees of freedom,” J. Lightwave Technol., vol. 40, no. 5, pp. 1296–1307, Mar. 1, 2022.

[149] C. Zhang, Y. Zhu, J. Lin, et al., “High-fidelity sub-petabit-per-second self-homodyne fronthaul using broadband electro-optic combs,” Nature Comm., vol. 15, art. no. 6621, 2024.

[150] F. Liu, P. Li, N. Zhong, X. Deng, L. Yan, W. Pan, and X. Zou, “Millimeter-wave over fiber integrated sensing and communication system using self-coherent OFDM,” Opt. Express, vol. 32, pp. 15493–15506, 2024.

[151] D. Che, A. Li, X. Chen, Q. Hu, Y. Wang, and W. Shieh, “Stokes vector direct detection for short-reach optical communication,” Opt. Lett., vol. 39, pp. 3110–3113, 2014.

[152] M. Xue, S. Pan, and Y. Zhao, “Optical single-sideband modulation based on a dual-drive MZM and a 120° hybrid coupler,” J. Lightwave Technol., vol. 32, no. 19, pp. 3317–3323, Oct. 1, 2014.

[153] D. Pérez-Galacho et al., “QPSK modulation in the O-band using a single dual-drive Mach–Zehnder silicon modulator,” J. Lightwave Technol., vol. 36, no. 18, pp. 3935–3940, Sept. 15, 2018.

[154] X. Fang, Y. Zhu, X. Cai, W. Hu, Z. He, S. Yu, and F. Zhang, “Overcoming laser phase noise for low-cost coherent optical communication,” Nat. Comm., vol. 15, art. no. 6339, Jul. 27, 2024.

[155] Y. Zhu and W. Hu, “Optical access networks for fixed and mobile applications [Invited Tutorial],” J. of Optical Communications and Networking, vol. 16, no. 2, pp. A118–A135, Feb. 2024.

[156] F. N. Khan, Q. Fan, C. Lu, and A. P. T. Lau, “An optical communication’s perspective on machine learning and its applications,” J. Lightwave Technol., vol. 37, no. 2, pp. 493–516, Jan. 15, 2019.

[157] T. Koike-Akino, Y. Wang, D. S. Millar, K. Kojima, and K. Parsons, “Neural turbo equalization: Deep learning for fiber-optic nonlinearity compensation,” J. Lightwave Technol., vol. 38, no. 11, pp. 3059–3066, Jun. 1, 2020.

[158] B. Karanov et al., “End-to-end deep learning of optical fiber communications,” J. Lightwave Technol., vol. 36, no. 20, pp. 4843–4855, Oct. 15, 2018.

[159] Q. Fan, G. Zhou, T. Gui, et al., “Advancing theoretical understanding and practical performance of signal processing for nonlinear optical communications through machine learning,” Nature Comm., vol. 11, art. no. 3694, 2020.

[160] D. Rafique and L. Velasco, "Machine learning for network automation: overview, architecture, and applications [Invited Tutorial],” J. of Optical Communications and Networking, vol. 10, no. 10, pp. D126-D143, Oct. 2018.

[161] B. Lin, H. Yang, R. Wang, Z. Ghassemlooy, and X. Tang, “Convolutional neural network–based signal demodulation method for NOMA-PON,” Opt. Express, vol. 28, pp. 14357–14365, 2020.

[162] M. Liao, J. -S. Tseng, J. -H. Yan, H. -R. Chen, S. -H. Liou and K. -M. Feng, "Neural Network Based NOMA Demultiplexing with High Flexibility and Low Latency for 5G Radio-over-Fiber System," 2019 Asia Communications and Photonics Conf. (ACP), Chengdu, China, 2019, pp. 1-3.

[163] F. Musumeci et al., "An Overview on Application of Machine Learning Techniques in Optical Networks," IEEE Comm. Surveys & Tutorials, vol. 21, no. 2, pp. 1383-1408, Second quarter, 2019.